2020

Dissection of Neurons and Circuits Involved in Regulating Innate Behaviors, Movement and Higher Cognitive Functions in Mice

Luca Parolari

DISSECTION OF NEURONS AND CIRCUITS INVOLVED IN REGULATING INNATE BEHAVIORS, MOVEMENT AND HIGHER COGNITIVE FUNCTIONS IN MICE

A Thesis Presented to the Faculty of

The Rockefeller University

in Partial Fulfillment of the Requirements for

the degree of Doctor of Philosophy

by

Luca Parolari

June 2020

DISSECTION OF NEURONS AND CIRCUITS INVOLVED IN REGULATING INNATE BEHAVIORS, MOVEMENT AND HIGHER COGNITIVE FUNCTIONS IN MICE

Luca Parolari, M.D., Ph.D.

The Rockefeller University 2020

Elucidating the mechanisms through which brain circuits influence behavior is a fundamental tenet of Systems Neuroscience. Advancements in this field are critical to help us understand the inner workings of our brains, and eventually who we are as humans. Describing the physiologic functioning of neural circuits is also necessary to recognize their malfunctions, and to develop strategies to correct them. In many cases, however, alterations in the activity of brainwide circuits can be traced back to specific neuronal populations, and acting selectively upon these cells can restore the normal activity within the system, ultimately correcting the aberrant behavior. Thus, understanding how changes in gene expression and molecular profiles of neurons alter their function is critical to describe interneuronal dynamics within a circuit.

During my graduate studies in the Friedman Laboratory at Rockefeller I had the opportunity to combine both Systems and Molecular-Cellular approaches to dissect the circuits and identify the neuronal populations involved in regulating behaviors along the broadest spectrum: from subconscious and innate behaviors (ie, control of energy homeostasis) all the way to the highest order functions (ie, anxiety and compulsive

behaviors). To do so, I studied the interaction between cells, circuits and behavior in mice, an ideal model to test these conserved functions. This is because the mouse brain is evolutionarily close to the human brain, yet it is simpler and highly accessible to external manipulations with the molecular biology tools currently at our disposal.

The main focus of my graduate work has been to investigate the mechanisms underlying movement control, and regulation of emotions and higher cognitive functions. This project responded to my interest, originated during my medical training, in finding commonalities and differences in neural circuits and functions between brain disorders traditionally classified as pertaining to the sphere of Neurology and Psychiatry. I thus focused on a neural network of nuclei deeply involved in these behaviors, known as the basal ganglia, and in particular on the role of the Subthalamic Nucleus (STN) in Parkinson's Disease and Obsessive-Compulsive Disorder. I identified previously undescribed subpopulations of STN neurons, and tested their role in mediating motor, emotional and cognitive functions in mice, both in normal and pathologic state. This part of my graduate work is detailed in Chapter 1 to 6. The data I present here have important implications for the physiology and pathophysiology of movement and psychiatric disorders, with the potential for enabling further translational studies.

In addition to my main study, I was fascinated by the work conducted in the Friedman Laboratory to elucidate the metabolic and nervous mechanisms that regulate energy balance in the body. I therefore collaborated with a postdoctoral fellow in the laboratory and adopted the same experimental approaches to dissect a neural circuit involved in the maintenance of body temperature in mice. The anterior hypothalamus has been the main brain area associated with thermoregulation since the 1950s. With

our work, however, we found that a brainstem region known as the Dorsal Raphe Nucleus (DRN), and particularly a subpopulation of DRN neurons, can also respond selectively and powerfully to changes in external stimuli to maintain a constant body temperature. We also showed that this effect is achieved by inducing changes in both thermogenesis and locomotor activity, and mediated via projections to the anterior hypothalamus and to other brain areas known to be involved in thermoregulation. This part of my graduate work is detailed in the Appendix section. Taken together, these experiments reveal a circuit configuration that allows for the robust control of an innate homeostatic response.

ACKNOWLEDGMENTS

Graduate school has been an incredibly rewarding experience. I am thankful to have had the opportunity to work in a fun, stimulating environment that has allowed me to grow personally and professionally. First, I want to thank my advisor, Dr. Jeff Friedman, who has always been extremely supportive of my work, providing the resources and guidance needed for the successful execution of my project. I'm grateful to have had the opportunity to work with excellent scientists in his lab, and to have learnt how to be a better scientist from his example.

I also want to thank my Co-Advisor Dr. Nat Heintz, and my Faculty Advisory Committee, Dr. Mary-Beth Hatten and Dr. Winrich Freiwald. Nat, Mary-Beth and Winrich have been very supportive and provided valuable guidance at key moments during my project. Also, many thanks to Dr. Tamas Horvath from Yale University for serving as my external committee member.

I am indebted to former and current members of the Friedman lab. However, Dr. Marc Scheeberger, a postdoc in the lab, was instrumental in these years of work. He provided day-to-day help on experimental design and was a fantastic collaborator in all the projects I have been involved in since joining the lab. I also want to acknowledge the help of current and past lab members for technical assistance and useful discussions.

Finally, I want to thank my family and friends outside the lab, who accompanied my personal and professional growth in these past years. In particular, I want to acknowledge the support, guidance and mentorship of Dr. Joven Cuanang, a great source of inspiration and wisdom in these years, and a true friend. My parents Franca

and Giuseppe, and my brother Alessio, for their intelligence and foresight that made it possible for me to be here today, for the constant support, advice, and generosity.

TABLE OF CONTENTS

LIST OF FIGURES

LIST OF TABLES

CHAPTER 1

Introduction

Parkinson's Disease, Obsessive-Compulsive Disorder and the Basal Ganglia.

Parkinson's Disease (PD) is the 3rd most prevalent and disabling Neurologic disease in the U.S., affecting 1.7% of the population over 70, and it is characterized by progressive tremor, muscular rigidity, slowness of movement, and gait and balance impairments (Hirtz *et al.* 2007; Pringsheim *et al.* 2014). Obsessive-Compulsive Disorder (OCD) is the 4th most prevalent Psychiatric disorder, affecting 2.3% of the U.S. population, and is characterized by recurring, intrusive, anxiety-provoking thoughts (obsessions) and ritualistic behaviors performed to release such distress (compulsions), that highly impair daily function (Ruscio *et al.* 2010). Although they present very different clinical pictures, these highly prevalent diseases share several interesting features, including comorbidity, dysfunctions in the dopamine system, and electrical and metabolic activity in the basal ganglia circuitry (Nicoletti *et al,* 2013; Voon *et al,* 2010; Milad *et al,* 2012).

The **basal ganglia** are a group of subcortical nuclei crucially involved in the regulation of motor, cognitive and emotional functions (Alexander *et al*, 1990). The neural circuit interconnecting these nuclei is thought to be responsible for the execution of selected behaviors, such as a specific movement, and the simultaneous inhibition of others, such as the inhibition of competing and/or unwanted movements (DeLong *et al*, 1984). This selection is mediated by a dynamic balance between two parallel and opposed subcircuits, the direct and

indirect pathways (Figure 1). These pathways can respectively facilitate or block the transport of cortical signals to the thalamus, which in turn activates the cortex via glutamatergic projections. The net effect of the direct pathway is to disinhibit motor centers and release motor programs, facilitating the initiation and maintenance of a movement (“go” signal). The indirect pathway, on the opposite, antagonizes the direct pathway and suppresses motor activity (“no-go” signal). The balance between these pathways is finely regulated by changes in levels of neurotransmitter dopamine in the striatum, a crucial node in the circuit. If dopamine levels are higher than a threshold, the direct pathway overcomes the indirect’s antagonism, and the specific movement is executed. If dopamine is below the threshold, the indirect pathway prevails and the motor plan is interrupted, or not initiated (Kandel *et al.*, 2000, Lanciego *et al*, 2012, Parent *et al*, 1995). When the physiologic balance between direct and indirect pathways is altered, the underlying motor, cognitive and/or emotional functions are disrupted, resulting in Movement Disorders and/or Psychiatric Diseases.

In Movement Disorders where the direct pathway is pathologically hyperactive, patients show an overall increase in baseline motor activity characterized by abnormal and uncontrolled movements, such as those observed in the *hyperkinetic* disorders Huntington's Disease, dystonia and hemiballismus. Hyperactivation of the indirect pathway, on the opposite, induces *hypokinetic* movement disorders like PD (Kandel *et al.*, 2000, Lanciego *et al*, 2012, Parent *et al*, 1995). In PD degeneration of dopaminergic neurons of the brainstem causes dopamine levels in the striatum to drop, with subsequent

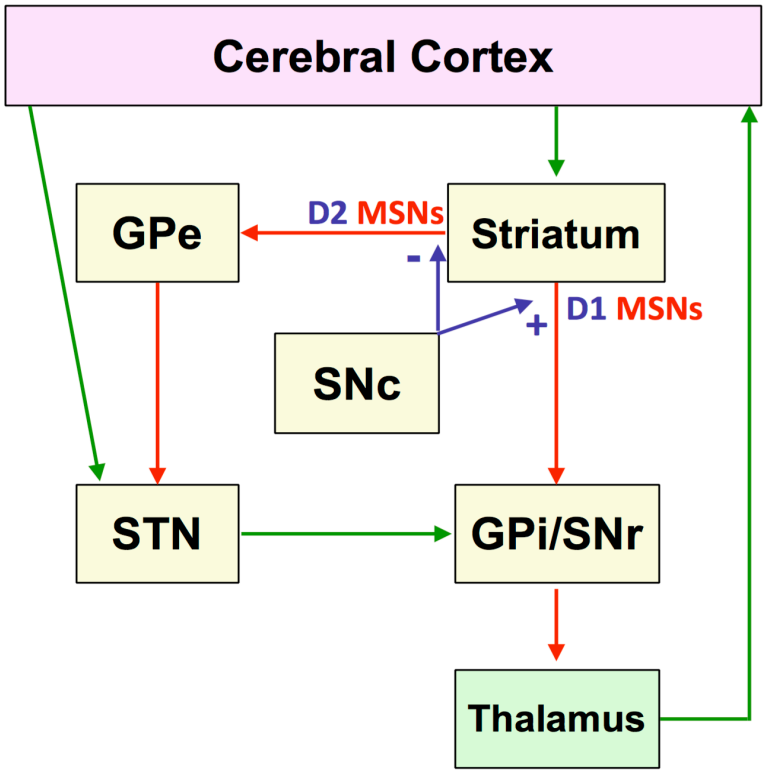

Figure 1. Schema of the basal ganglia circuitry.

Arrows: Green: excitatory glutamatergic projections; Red: inhibitory GABAergic; Blue: modulatory dopaminergic. *D1 MSNs: striatal GABAergic medium spiny neurons expressing excitatory dopamine receptor-1 (direct pathway); D2 MDNs: expressing inhibitory dopamine receptor 2 (indirect pathway). GPe/GPi: globus pallidus pars externa/interna; STN: subthalamic nucleus; SNc/r substantia nigra pars compacta/reticulata.*

inhibition of the direct and activation of the indirect pathways. The persistent hyperactivity of the “no-go” indirect pathway impairs the ability to initiate new motor plans, resulting in the slowness of movement and motor deficits observed in PD patients. Most pharmacological treatments of PD act by increasing dopamine levels in the brain, either via precursors (L-DOPA) or agonists of dopamine. While initially very effective and generally well-tolerated, in the long-term these drugs cause often debilitating side effects, such the insurgence of involuntary muscle contractions and movements known as dyskinesia. In these cases, patients may become candidates for second-line therapeutic alternatives, such as Deep Brain Stimulation (DBS). In PD patients, DBS is preferentially targeted to the Subthalamic Nucleus (STN) (Kringelbach *et al*, 2007; Follett *et al,* 2010, Odekerken *et al,* 2012).

Dysfunctions of the basal ganglia circuit are also associated with changes in limbic (eg, motivation, emotion, threat detection) and cognitive functions. These impairments are observed in several Psychiatric Diseases, including Addiction, Mood Disorders, Tourette Syndrome and OCD. All these conditions have also been associated with altered activity in basal ganglia circuits, and dysfunctions in the dopaminergic system (Ring *et al,* 2002; Yelnik *et al*, 2012). Interestingly, in some of these diseases, the impairment is not limited to limbic functions, but includes also motor symptoms. This is the case of Tourette Syndrome, a condition in which patients display involuntary and sudden impulses to execute specific movements or vocalizations, known as tics, that cannot be controlled (Leckman *et al*, 2002). However, differently from other uncontrollable

movements like chorea and hemiballismus, characterized by purposeless muscular contractions, tics most often consist of highly complex and directed motor plans and vocalizations (eg, complex gestures, fully formed sentences). Tourette Syndrome is also highly comorbid with OCD, a disorder characterized by recurring, intrusive, anxiety-provoking thoughts (obsessions) and ritualistic behaviors performed to release such distress (compulsions) (Ruscio *et al.* 2010). In both these conditions, therefore, alterations of the limbic and associative functions and motor control coexist. While the physiological changes in the interaction between direct and indirect pathways in these conditions are less well understood than in movement disorders, similar alterations in the basal ganglia circuit may be responsible for the observed cognitive, emotional and motor dysfunctions. In fact, patients with forms of OCD severe and refractory to multiple drug treatments can benefit from DBS of the STN, just like PD patients (Mallet *et al.* 2010; Blomstedt *et al.* 2010).

The Subthalamic Nucleus.

The Subthalamic Nucleus (STN) is the smallest nucleus of the basal ganglia, yet it plays a crucial role in regulating the circuits' dynamics. The STN is part of the indirect pathway, and the net effect of its activation is to inhibit the thalamo-cortical projection and interrupt movement (DeLong *et al*, 1984). In addition to receiving inputs from the globus pallidus externa as part of the indirect pathway, the STN is the target of afferents originating directly from the cortex. This cortico-subthalamic projection is also known as the "hyperdirect" pathway

(Nambu *et al,* 1996). Because of its unique connections to the cortex, and because it is the only excitatory glutamatergic node of the circuit, it is thought that the STN represents a relay for the cortex to assert its top-down executive control over the basal ganglia circuit, allowing the cortex to quickly act on the circuit while short-circuiting the striatum and dopaminergic regulation (Cavanagh *et al,* 2011). Via the STN, this circuit structure allows the cortex to sends a “no go” signal to the basal ganglia, inhibiting the thalamo-cortical activity and interrupting motor and limbic-associative stimuli, thus providing a high cognitive control in the face of conflict (Frank *et al,* 2007). In addition, it has been suggested that the cortico-subthalamic hyperdirect pathway may also play a role in facilitating the execution of specific motor plans: by discharging shortly before the activation of the direct pathway, it interrupts any other competing stimulus and prepares the circuit for the initiation of the next motor plan. Thus, the STN inhibits other competing programs and authorizes only the execution of the selected motor plan, and eventually stops it at the selected timing (Nambu *et al,* 2002). However, when the STN is hyperactive, like in PD, it permanently suppresses movement. DBS-STN is thought to improve PD symptoms by inhibiting the hyperactive STN (Benabid, 2003). While it is unclear if the nucleus is hyperactive in OCD, evidence suggests that OCD patients can benefit from inactivation of the STN with DBS (Mallet *et al.* 2010; Blomstedt *et al.* 2010).

Studies in human and non-human primates show that the STN, like all basal ganglia nuclei, is divided in different anatomical areas with distinct functions. Based on their connection to other basal ganglia nuclei and cortex, the

primate STN is thought to be divided in three areas: limbic, associative and sensorimotor (Alexander *et al.*, 1990; Karachi *et al*, 2005). Additionally, functional studies in monkeys show that pharmacological modulation of the activity of the sensorimotor area induces uncontrolled movements, while modulation of the limbic region induces impulsive behaviors and OCD-like stereotypies, such as repeated grooming, lip smacking, licking (Karachi *et al*, 2009). In patients, electrical modulation with DBS of the sensorimotor area of the STN helps the symptoms of PD, while modulation of the limbic-associative area is efficacious in OCD (Welter *et al.*, 2014; Mallet *et al.*, 2007).

Deep Brain Stimulation.

DBS is a neurosurgical treatment consisting of a permanent device implanted in specific brain regions to deliver a continuous electric current. Since its introduction in the clinic twenty years ago, DBS treatment has helped over 160.000 patients affected by several neurologic and psychiatric diseases, including PD, Dystonia, Tremor, Chronic Pain, OCD, Tourette Syndrome and Depression (Kringelbach *et al*, 2007). Many of the above diseases are characterized by dysfunctions in the basal ganglia circuit. By modulating the electrical activity of targeted nuclei, it is thought that DBS can restore the electrical balance within the circuit and improve the behavioral impairments. As previously mentioned, in PD and OCD this target is most frequently the STN (Follett *et al,* 2010, Odekerken *et al,* 2012).

In PD patients, DBS-STN improves parkinsonian tremor, rigidity and slowness of movement. This allows to control the symptoms with a lower dosage of dopaminergic drugs, therefore reducing the dyskinesia side effects associated with these pharmacotherapies and improving life quality. However, DBS of the STN is occasionally complicated by severe side effects, including most frequently cognitive decline, depression, hypomania and impulsivity (Welter *et al.*, 2014), signs of effects on limbic and/or associative functions as well. In addition, it is still unclear how DBS exerts its beneficial effects. While it is most commonly thought that high-frequency electrical current inactivates the neurons close to the electrode, it may also be affecting neurons in adjacent brain areas, or even in further brain region via fibers of passage or antidromic axonal transmission (Breysse *et al.*, 2015; Bourne *et al.*, 2012), and thus potentially contribute to DBS's undesired outcomes.

Goals of This Work

DBS is an extremely effective and useful therapeutic tool for certain Neurologic and Psychiatric diseases. However, it is a highly invasive treatment, whose efficacy can be blunted by off-target effects. This occurs because DBS is not cell-specific, thus the correct surgical placement of electrodes contributes greatly to the variability in efficacy and side effects observed between patients (Welter *et al.*, 2014). It is therefore of basic and potential clinical importance to define the neuronal populations responsible for DBS's function, which could enable the development of alternative cell-specific therapeutic approaches. However, the current tools in molecular and cellular biology do not allow researchers to identify specific neuronal populations *in vivo* and test their effect on behavior in human and non-human primates. Therefore, we set out to do so by translating these clinical observations "from bedside to bench", taking advantage of the invaluable molecular biology tools available in mice.

Because it regulates adaptive behaviors that are crucial for survival, the basal ganglia circuit is highly conserved throughout evolution. Phylogenetic studies suggest that some forms of the basal ganglia circuit can be found in the first vertebrate ancestor to mammals (Grillner *et al*, 2016). In rodents, the basal ganglia are anatomically and functionally analogous to primates, being involved in ancestral behaviors like emotion regulation and motor initiation, learning and automatization. For this reason, rodents, and specifically mice, are widely used as animal models to dissect and study this circuit and its related functions, in normal conditions and in disease. In particular, studies on mice and rats suggest

that also the rodent STN is involved in the control of both motor and emotion regulation functions. For example, reducing glutamatergic function of STN neurons increases locomotor activity (Schweizer *et al*, 2014), while DBS-STN decreases OCD-like behaviors in mice like excessive grooming (Chang *et al*, 2016) and compulsive lever pressing (Klavir *et al*, 2009).

In this context, we set out to adopt the mouse as a model to dissect at a cell-specific level the circuits underlying limbic and motor functions associated with PD and OCD. In order to develop cell-specific therapeutic options it is crucial to identify the neuronal populations that are responsible for mediating the positive effects of DBS in these diseases. Neuronal populations can be defined based on differences in morphology, gene-expression, connectivity, electrophysiological properties, and, most importantly, function. For our purpose, a helpful approach to define functionally relevant neuronal populations in the STN is to first identify genes expressed only in specific subgroups of neurons, and subsequently modulate their activity to assess their role in mediating different behaviors.

Therefore, with the current study we set out to:

1. Contribute to understanding the dynamics and mechanisms through which DBS asserts its effects: is modulation of STN neurons sufficient to elicit motor and limbic behaviors, and improve the symptoms of PD and OCD? Or DBS effects are mediated by other brain areas via fibers of passage, antidromic transmission, or off-target local stimulation?

2. Identify the STN neuronal populations responsible for mediating the beneficial effects of DBS in PD and OCD, and find potential approaches to modulate these cells in a less invasive and safe way.

CHAPTER 2

Neuronal Populations of the Mouse Subthalamic Nucleus

INTRODUCTION:

The subthalamic nucleus (STN) is the smallest structure in the basal ganglia, measuring just 3 x 5 x 12 mm in humans, and 0.3 x 0.6 x 0.8 mm in mice (Yelnik *et al*, 2007). Its limited size makes it extremely challenging to target surgically with high precision. In fact, the correct placement of electrodes during DBS-STN neurosurgery contributes greatly to the variability in efficacy and side effects observed between treated patients (Welter *et al*, 2014). In mice, in addition to the nucleus being 10-times smaller, the current tools for stereotaxic surgery don't allow the precision needed to consistently target the STN while sparing adjacent brain regions. Therefore, it it crucial to identify markers that are specific to STN neurons, which would help employ alternative therapeutic approaches of neural modulation with cell-specific accuracy.

Moreover, in the attempt to better understand the mechanisms through which DBS esserts its effect, and the circuit dynamics between local cells and with other nuclei of the basal ganglia, it is important to characterize the functional identity of STN cells. One initial question is whether these neurons are excitatory or inhibitory. Most histological studies in primates have reported that virtually all STN cells are excitatory glutamatergic projection neruons (Rafols *et al.*, 1976; Marani *et al.*, 2008). However, post-mortem analysis of human brains has suggested that a minority of STN cells may be inhibitory GABAergic interneurons (Levesque *et al*, 2005). In mice, recent studies have reported that virtually all STN cells express the glutamatergic marker *vGlut2*, which overlaps in 90% of cases with the gene Paired-Like Homeodomain 2 (*Pitx2*) (Schweizer *et al*, 2014;

Schweizer *et al*, 2016). However, whether there are inhibitory GABAergic cells in the mouse STN remains unknown. Additionally, it is important to identify more specific subpopulations of STN neurons, in the attempt to find cell populations to selectively target in the treatment of PD and OCD.

RESULTS:

Identification of Markers Specific to the Mouse STN.

To identify specific molecular subpopulations of neurons in the STN, we first scrutinized in-situ hybridization (ISH) studies from the Allen Brain Atlas (Lein *et al*, 2007) and the Gene Expression Nervous System Atlas (GENSAT) databases. STN-specific genes from these experiments were scored and ranked based on STN expression intensity, density, local specificity, as well as overall central nervous system specificity (Table 1). Intriguingly, four genes exhibited significantly high expression in the STN in comparison to neighboring areas and to the rest of the brain: Paired-Like Homeodomain 2 (*Pitx2*), Nitric Oxide Synthase 1 (*Nos1*), Neuron Derived Neurotrophic Factor (*Ndnf*), and Gamma-AminoButyric Acid Receptor Subunit Rho-3 (*Gabrr3*). To confirm their specificity to the STN we conducted brain-wide ISH studies in slices. These studies confirmed their expression in the STN, further suggesting that these markers might constitute specific molecular handles for STN neuromodulation (Figure 2A).

Table 1. Assessment of STN-Specificity of Candidate Marker Genes

Gene Name	Strength	Density (% cells)	Local Sp.	Global Sp.	Overall	Ranking	Notes
Pitx2	+++	60-70%; even	+++	+++	9	1	Posterior: transitions to SN, VTA
Gabrr3	+++	60-70%; even	+++	+++	9	2	Posterior: transitions to SN, VTA
Ndnf	+++	60-70%; postero-ventral	++	++	9	2	Posterior: transitions to SN
Nos1	++	50% post; 20% antero-dors	++	++	9	2	Post: SN sparse; Med: LH lots
Nov / CCN3	+++	70% postero-medio-ventral	++	++	8	3	Medial: few cells in LH; Dorsal: lots in ctx
C130021I20Rik	++	60% even	++	+++	8	3	Posterior: transitions to SN, VTA
Col24a1	++	30-40%; postero-ventral	++	+++	7	4	Dorsal: a few + cells in thalamus
Kcng4	++	60%; ventral	++	++	7	4	Dorsal/Posterior: very strong in ZI
Rapgef5	++	60-70% even	++	++	7	4	Ventral, dorsal: sparse background + ctx
Sema3d	+/++	30%; medio-ventral	+++	++	7	4	Weak signal/questionable background
Ttc6	+	40-50%; even	+++	++	6	5	
Sema3a	+/++	20-30%; medio-ventral	++	+	5	6	Dorsal in ctx, poterior very light in SN
Ankrd34b	++	50% even	+	+	5	6	Ventral: ZI, thalamus; Posterior: SN
Kcnab3	++	70% even	+	+	5	6	Dorsal: ZI + thalamus + ctx
Sema3f	+	30-40%; even	++	++	5	6	Medial, dorsal: ZI, LH, thalamus
Zfp618	+	30%; medio-ventral	++	+	4	7	
Stard5	+	60-70%; even	+	+	4	6	High background all around
Alox8	+	30-40% even	+	+	3	8	Heavy background
Kit / SCFR	+/++	30-40% even	+	+	3	8	Sparse background; heavy hippocampus

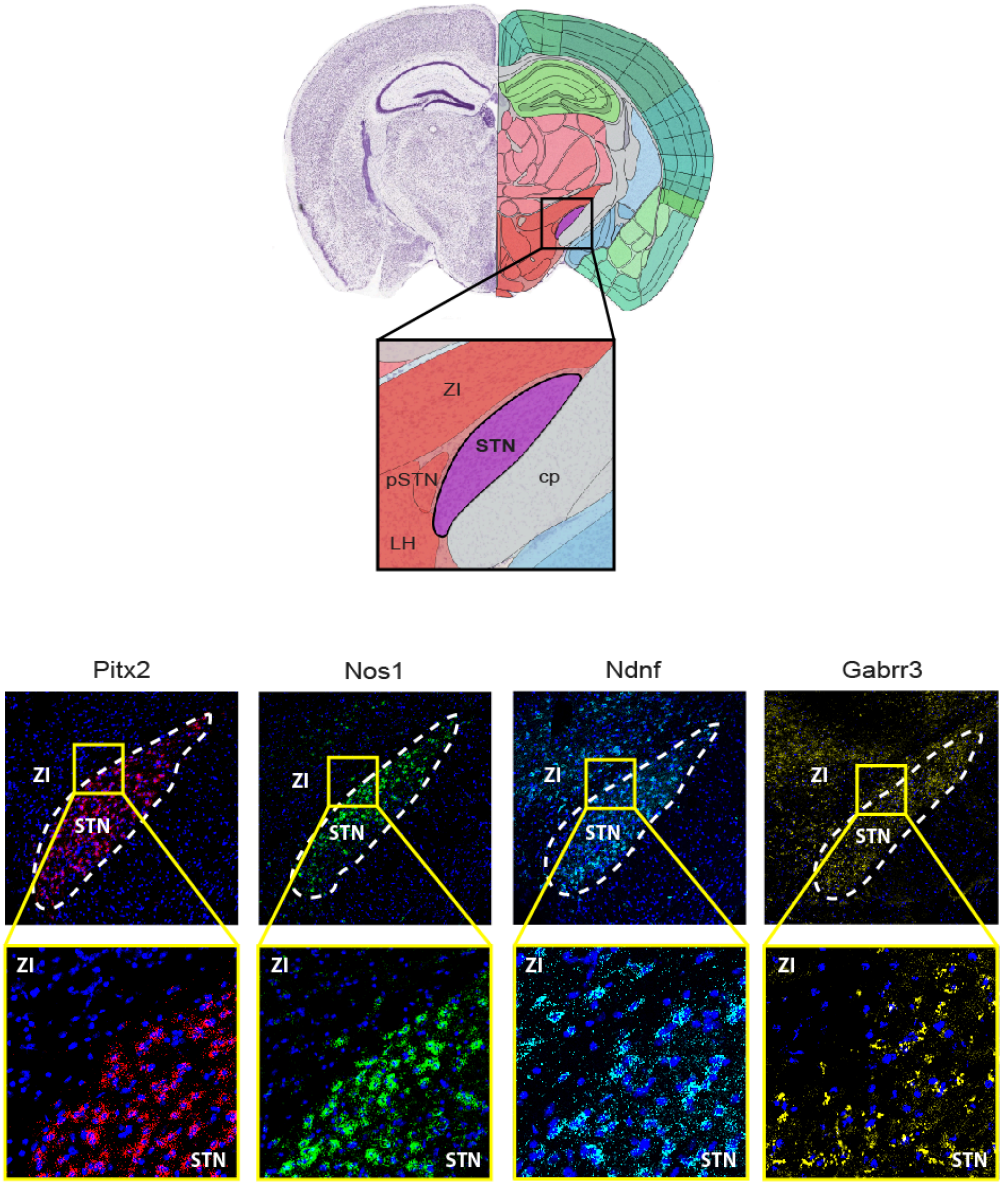

Figure 2A. ISH Studies Confirm Specificity to the STN of Candidate Markers.

Top: schema showing the location of the STN in the mouse brain (coronal view at AP: -2.0mm from bregma). Bottom: fluorescence *in situ* hybridization (FISH) of the STN confirming the expression of genes *Pitx2*, *Nos1*, *Ndnf*, *Gabrr3*. Top row: whole view. Bottom row: 20x magnification of border between STN and ZI. STN: Subthalamic Nucleus; pSTN: Para-Subthalamic Nucleus; ZI: Zona Incerta; LH: Lateral Hypothalamus; cp: Cerebral Peduncle.

Characterization of *Pitx2* as a Specific Marker for all STN neurons.

In addition, we conducted quantitative co-localization measurements from the ISH studies to further characterize the identified markers of STN subpopulations. Consistent with a recent report (Schweizer *et al*, 2016), ISH for *Pitx2* showed extensive co-localization with fluorescent microscopy nuclear counterstain 4',6-diamidino-2-phenylindole (DAPI) in the STN, suggesting that most STN cells express *Pitx2*. Furthermore, colocalization studies with the pan-neuronal marker neuronal-nuclei (*NeuN)* demonstrated that *Pitx2*-expressing cells are neurons (Figure 2B, left). Nearly all (>95%) *NeuN*-positive cells in the STN were co-labeled for *Pitx2*, thus *Pitx2* can be referred to as a marker for all STN neurons (hereafter referred to as STN^{Pitx2} neurons). Of note, a small number of cells were negative for both *NeuN* and *Pitx2* markers, suggesting the existence of a non-neuronal population of cells in the STN (Figure 2B, bottom left, white arrow). Next, we evaluated whether STN^{Pitx2} neurons are excitatory or inhibitory by coupling ISH studies for *Pitx2* and classical neurotransmitters. Importantly, ISH co-localization studies for *Pitx2* and either the glutamatergic marker *vGlut2* (*Slc17a7*) or the GABAergic marker *vGat* (*Slc32a1*) (Figure 2B, center and right) demonstrated that most STN^{Pitx2} neurons co-express *vGlut2*+, consistent with prior results (Schweizer *et al*, 2016), while none expressed *vGat.* However, we did note the presence of GABAergic neurons in the Zona Incerta (Z.I.), an adjacent structure, as previously established (Zhang *et al*, 2017). This observation proved that the absence of *vGat* staining in the STN was not due to technical limitations.

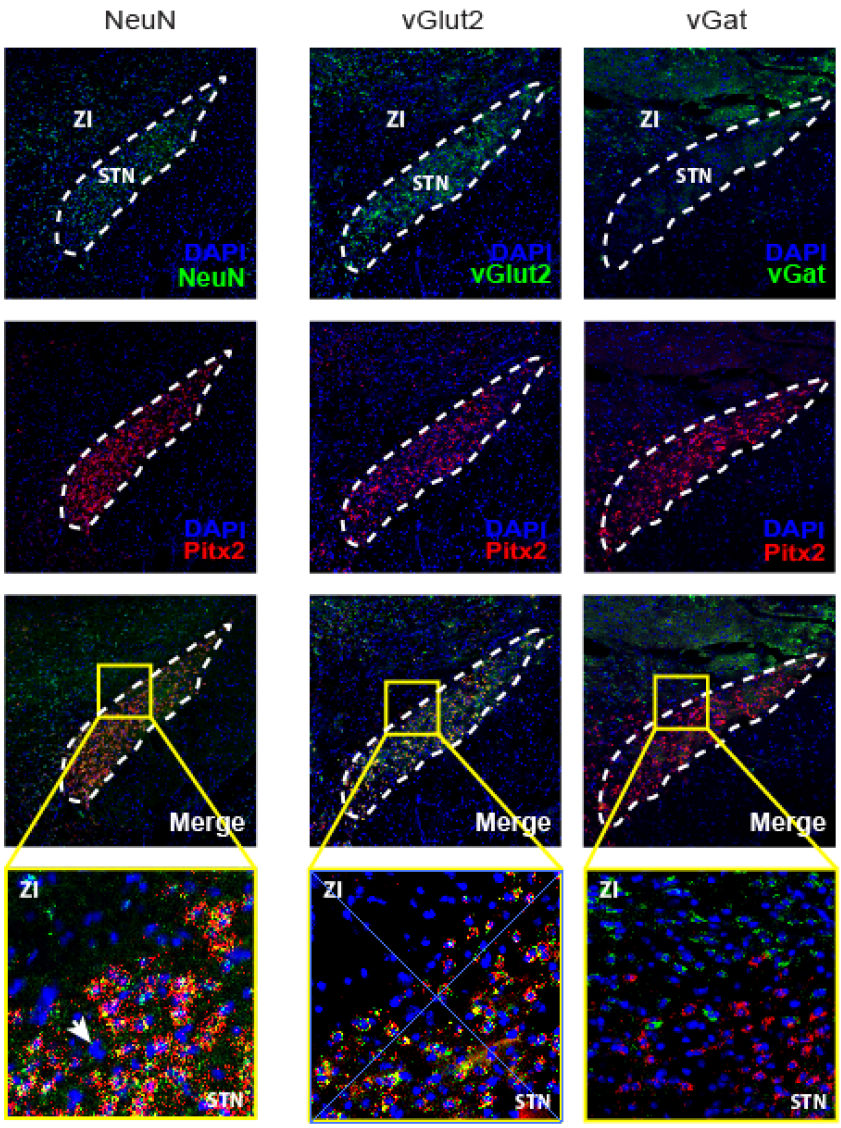

Figure 2B. Characterization of *Pitx2*-expressing Cells of the STN.
Characterization of Pitx2 neurons by colocalization with neuronal marker *NeuN* (left), glutamatergic *vGlut2* (center) and GABAergic *vGat* (right). White arrow in bottom left panel designates DAPI+, NeuN- Pitx2- non-neuronal cells.

Identification of Markers for STN Subpopulations of Neurons.

In contrast to *Pitx2*, *Nos1*, *Ndnf* and *Gabrr3* were expressed only in smaller clusters of STN cells. To further investigate how these markers are anatomically distributed, we next performed multiple fluorophore ISH experiments and quantified the extent of overlap between each combination of gene pairs (Figure 2C, left). We established that *Nos1*, *Ndnf* and *Gabrr3* cells represent 55%, 70% and 65% of STN^{Pitx2} neurons, respectively. Additionally, more than half of *Nos1 (54%)* and *Ndnf (66%)* positive cells exhibited extensive overlap between them. Finally, a higher percentage of *Gabrr3*-positive cells expressed *Ndnf*+ (86%) than *Nos1*+ *(59%)* (Figure 1c, right).

In sum, (i) *Pitx2* is a general marker for STN neurons, (ii) *Ndnf*- and *Nos1*-expressing neurons represent two partially overlapping clusters of STN neurons and (iii) *Gabrr3*-expressing neurons represent a smaller subpopulation accounting for ~60% of the total population, overlapping with both *Nos1* and *Ndnf* cells (Figure 2C, right).

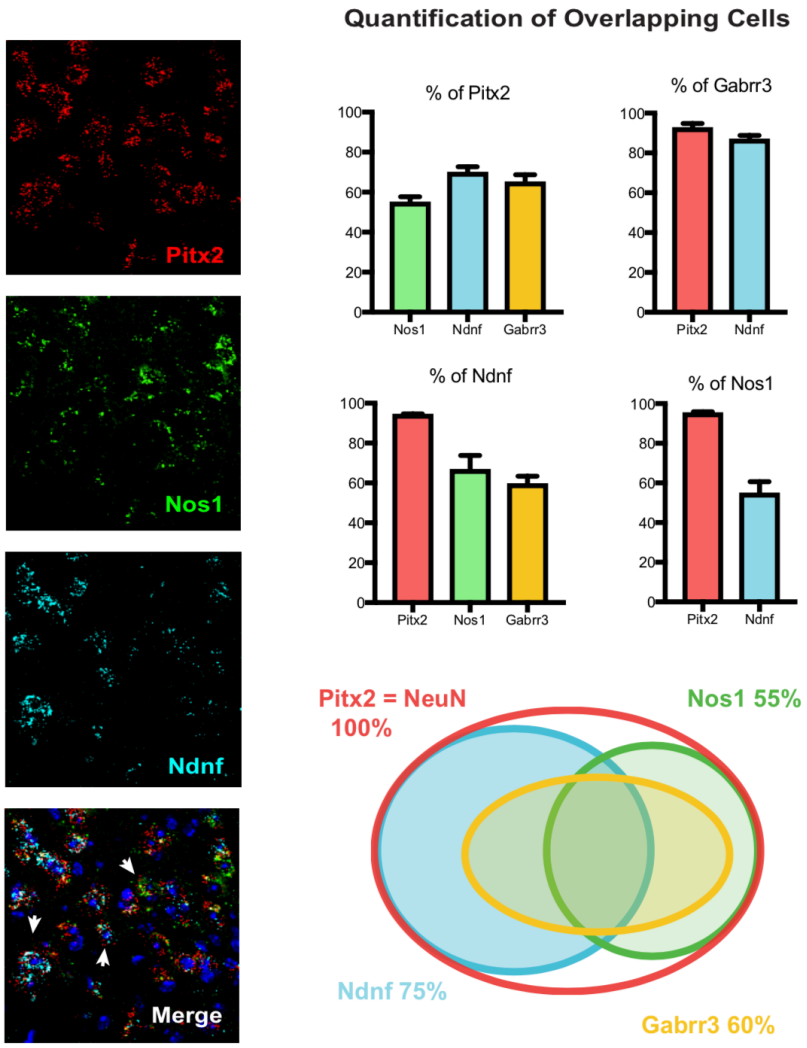

Figure 2C. Colocalization (and Quantification) between *Pitx2*, *Nos1*, *Ndnf* and *Gabrr3* expressing neurons.

Left: example of triple FISH experiment showing colocalization between Pitx2, Nos1 and Ndnf neurons; white arrows designate triple-labeled cells. Right, top: percentage of cells expressing gene on Y axis that co-express gene on X axis. Data are presented as mean ± SEM. Right, bottom: Venn diagram summarizing quantitative overlapping of the 4 neuronal populations.

DISCUSSION:

Although the STN has been widely studied in health and disease, its cell populations and their role on PD and OCD pathogenesis are poorly understood. Our data, in addition to published work (Schweizer *et al*, 2014; Schweizer *et al*, 2016), demonstrate that most STN neurons are glutamatergic and express the transcription factor *Pitx2*. Additionally, *Pitx2* is expressed at very low levels across the mouse brain, and most importantly it is not expressed in areas adjacent to the STN. In combination with molecular biology tools such as transgenic mice expressing Cre-recombinase under specific promoters, the gene *Pitx2* can thus be employed as a molecular handle, allowing cell-specific targeting of all STN neurons, while sparing cells and fibers of passage in adjacent areas.

Prior to this work, specific STN neuronal subpopulations had not been characterized. Here we first confirm that all STN neurons are excitatory and express *vGlut2*, while none of the cells is positive for the GABA market *vGat*. However, we identified three overlapping sets of STN neurons, expressing *Ndnf*, *Nos1* and *Gabrr3*. *Ndnf* is an evolutionarily well-conserved neurotrophic factor that has been suggested as a possible candidate for the treatment of neuronal degeneration diseases and nerve injuries (Kuang *et al*, 2010). In the adult mouse brain, it is expressed at low levels outside the STN and scattered cells of the brainstem (Table 1; Lein *et al*, 2007). *Nos1* is an enzyme necessary for the synthesis of Nitric Oxide (NO), a chemical messenger with tropism for several body tissues, including vessels and macrophages. In the brain, NO displays

many properties of a neurotransmitter and may be involved in processes including long term potentiation (Gruetter *et al,* 1979; Rajifer *et al,* 1992; Griscavage *et al,* 1996). Finally, the *Gabrr3* gene encodes for a subunit of the GABA-Aρ receptor, a rare type of GABA-A receptor, and could thus represent a potential target for new pharmacologic treatments (Bailet *et al*, 1999).

In aggregate, these data provide three important insights: 1) STN^{Pitx2} neurons can be used as a proxy for all STN neurons, 2) all STN^{Pitx2} neurons are excitatory glutamatergic, and 3) STN^{Pitx2} neurons include 3 partially overlapping subpopulations defined by the genes *Ndnf*, *Nos1* and *Gabrr3*. By defining neuronal subpopulations of STN neurons, these markers provide a target for further studies to assess their function.

CHAPTER 3

Functional Analysis of the STN in Locomotion and Repetitive Behaviors

INTRODUCTION:

After identifying in *Pitx2* the marker of choice to target all STN neurons, we proceeded to test the function of these cells. To do so we used optogenetics, a technique that allows to instantly activate or inhibit selected neurons (Boyden *et al.*, 2005; Kravitz *et al.*, 2010). This is achieved by engineering neurons of interest to express light-activated ion channels, and subsequently flooding them with laser lights of the specific wave lengths they are receptive to. Viruses are used as vectors to engineer neurons into expressing specific ion channels: the sodium-channel Channelrhodopsin 2 (ChR2) to activate neurons, and the proton-channel Archaerhodopsin3 (eArch3.0) to inhibit them. Viral vectors can be cloned to express a given channel only in the presence of the enzyme Cre-recombinase. For our experiment, we used transgenic mice that express Cre-recombinase under the *Pitx2* promoter (Pitx2-Cre) (Martin *et al.*, 2004). Therefore, after surgical injection of the viral vector in the STN, only Pitx2-expressing neurons express ChR2 or eArch3.0, allowing for cell-specific neuronal modulation.

In order to investigate if direct manipulation of STN neurons can regulate motor functions, we used optogenetics to activate STN^{Pitx2} neurons and evaluated the effects on movement. To this end, we adopted the rotation assay, a common test of locomotor function in mice (Gradinaru *et al*, 2009; Ungerstedt *et al*, 1970). Because modulating the activity of one side of the brain induces motor changes in the opposite (contralateral) side of the body, increasing the activity of the indirect pathway by photoactivating STN^{Pitx2} neurons in the left brains induces motor deficits in the contralateral (right) limbs. In mice, the

imbalance between left and right pull during locomotion results in a tendency of the animals towards turning leftward, which can be scored as an increase in the ratio between leftward and rightward rotations.

To test whether STN^{Pitx2} neurons play a role in controlling repetitive behaviors in mice, we focused on assessing grooming behavior. Self-grooming is an innate spontaneous behavior involved in hygiene maintenance and other physiologically important processes in mice, including thermoregulation, social communication (Kalueff *et al*, 2016). It is one of the most frequently observed behaviors in awake rodents and has a patterned, sequential organization with characteristic cephalocaudal progression. Excessive self-grooming in rodents is thought to recapitulate the pathological repetitive behaviors and perseverations observed in certain psychiatric disorders, including OCD and Autism Spectrum Disorder, and it is the most consistent feature in mouse models of these diseases (d'Angelo *et al*, 2014).

RESULTS:

Optogenetic Activation of STN Neurons Decreases Movement of the Contralateral Side.

The test the role of STN^{Pitx2} neurons in locomotion, we injected Cre-dependent AAV expressing activatory ChR2 (AAV5-EF1a-DIO-ChR2-EYFP) in the left STN of Pitx2-Cre mice (Figure 3A). As predicted, unilateral optogenetic

activation of left STN^{Pitx2} neurons induced motor deficits in the right limbs and induced leftward rotations (ie, toward the side of the stimulation). Rotations were measured as the ratio between anti-clockwise (leftward) to clockwise (rightward) turns (positive values) and clockwise to anti-clockwise (negative values) (repeated measures two-way ANOVA with Sidak's multiple comparison test; On epoch: ChR2 mean 29.17 Vs. Control mean -0.71, **** $p < 0.0001$, n = 6/group; Figure 3C). Interestingly, the observed effect was scalable, with a maximum effect reached at 40 Hz (t-test: increase of mean Control Vs. 10 Hz: 19-fold, * $p < 0.05$; Vs 40 Hz: mean increase 29-fold, *** $p < 0.001$; Vs. 120 Hz: 13-fold, ** $p < 0.01$; n = 6/group; Figure 3B).

On the other hand, photoinhibition of STN^{Pitx2} neurons with inhibitory eArch3.0 did not affect the rotation ratio (repeated measures two-way ANOVA with Sidak's multiple comparison test; Stimulation On epoch: eArch3.0 mean 0.80 Vs. Control mean -0.93, n.s. $p > 0.05$, n = 6/group; Figure 3D). Finally, we tested whether selective ablation of STN^{Pitx2} neurons with diphtheria toxin subunit A (AAV1-EF1a-DIO-dtA) affects rotation behavior. Consistent with photoinhibition, no difference was observed between STN^{Pitx2} ablated mice and control virus injected mice (t-test: dtA mean 1.11 Vs. Control mean -0.70, n.s. $p > 0.05$, n = 6-9/group; Figure 3E).

Overall, these data demonstrate that direct activation of the STN through STN^{Pitx2} neurons can regulate motor functions, while acute inhibition or ablation of these neurons is insufficient to induce unilateral rotations.

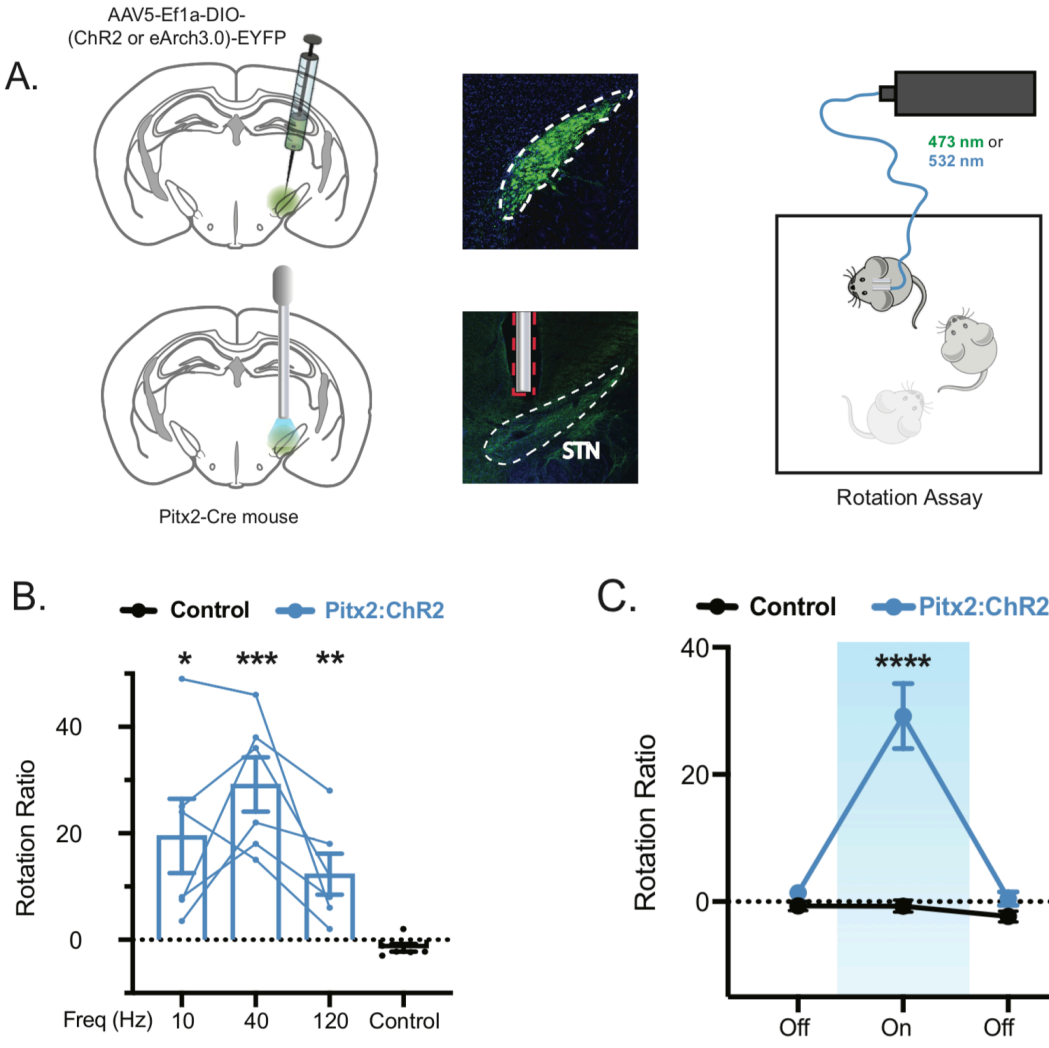

Figure 3A-C. Effects of Optogenetic Activation of STN Neurons (STN^{Pitx2}) on Locomotion.

(A) Schema for unilateral optogenetic modulation of STN^{Pitx2} neurons in the Rotation Assay, and representative IHC for validation of viral expression and optic fiber placement.

(B) Optogenetic photoactivation of STN^{Pitx2} neurons at different frequencies increases unilateral rotation ratio in mice in a scalable manner. T-student test comparing the effect of stimulation at 10, 40 and 120 Hz to control (* $p < 0.05$, ** $p < 0.01$, *** $p < 0.001$; n = 6 mice per group).

(C) Photoactivation (40 Hz) of Pitx2:ChR2 mice increases unilateral rotations compared to control mice. Repeated-measures two-way ANOVA, followed by ad hoc Sidak's multiple comparison test comparing treated and control groups (**** $p < 0.0001$, n = 6). Blue-shaded region highlights 532nm Laser On epoch.

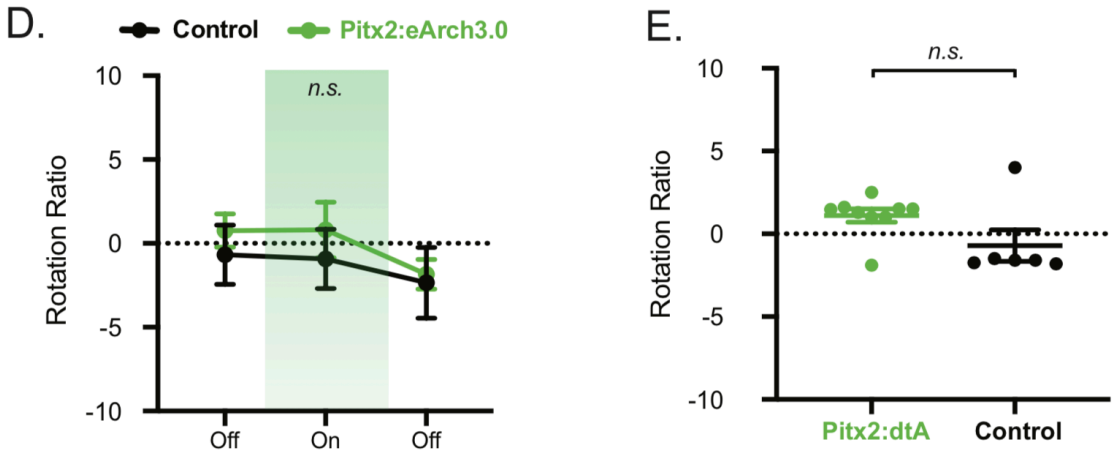

Figure 3D-E. Effects of STN Neurons (STN^{Pitx2}) Silencing on Locomotion.
(D) Photoinhibition of Pitx2:eArch3.0 does not alter the rotation ratio compared to control. Repeated-measures two-way ANOVA, followed by ad hoc Sidak's multiple comparison test comparing treated and control groups (n.s. $p > 0.05$; n = 6 mice per group). Green-shaded region highlights 473 nm Laser On epoch.
(E) Unilateral ablation of STN^{Pitx2} neurons with diphtheria toxin A (dtA) does not alter the rotation ratio of treated mice compared to controls. T-student test comparing Pitx2:dtA to control (n.s. $p > 0.05$; n = 6-9 mice per group).

Acute Activation of STN Neurons Elicits Grooming.

Extensive evidences have established the STN as a key node in regulating limbic-associative functions and OCD. Previous reports have shown that inhibition of the STN with high frequency stimulation suppresses excessive self-grooming in mouse models of autism (Chang *et al*, 2016). To evaluate this effect, we initially tested the effect of bilateral photoactivation of STN^{Pitx2} neurons at optimal 40 Hz frequency.

Freely moving mice were blindly scored for the time spent grooming during a 15-minute session (5-min pre-stimulation, 5-min stimulation "On", 5-min post-stimulation) (Figure 3F). Strikingly, a significant increase of highly repetitive self-grooming behavior was observed comparing the stimulation period to both the pre- and post-stimulation period. Littermate controls did not exhibit such effects in grooming (repeated measures two-way ANOVA with Sidak's multiple comparison test; Stimulation On epoch: ChR2 mean 103.4s Vs. Control mean 13.96s, **** $p < 0.0001$, n = 6/group; Figure 3G). Inhibition of STN^{Pitx2} neurons with eArch3.0 did not affect grooming behavior between treated and control groups (repeated measures two-way ANOVA with Sidak's multiple comparison test; Stimulation On epoch: eArch3.0 mean 19.37s Vs. Control mean 13.96s, n.s. $p > 0.05$, n = 6/group; Figure 3H).

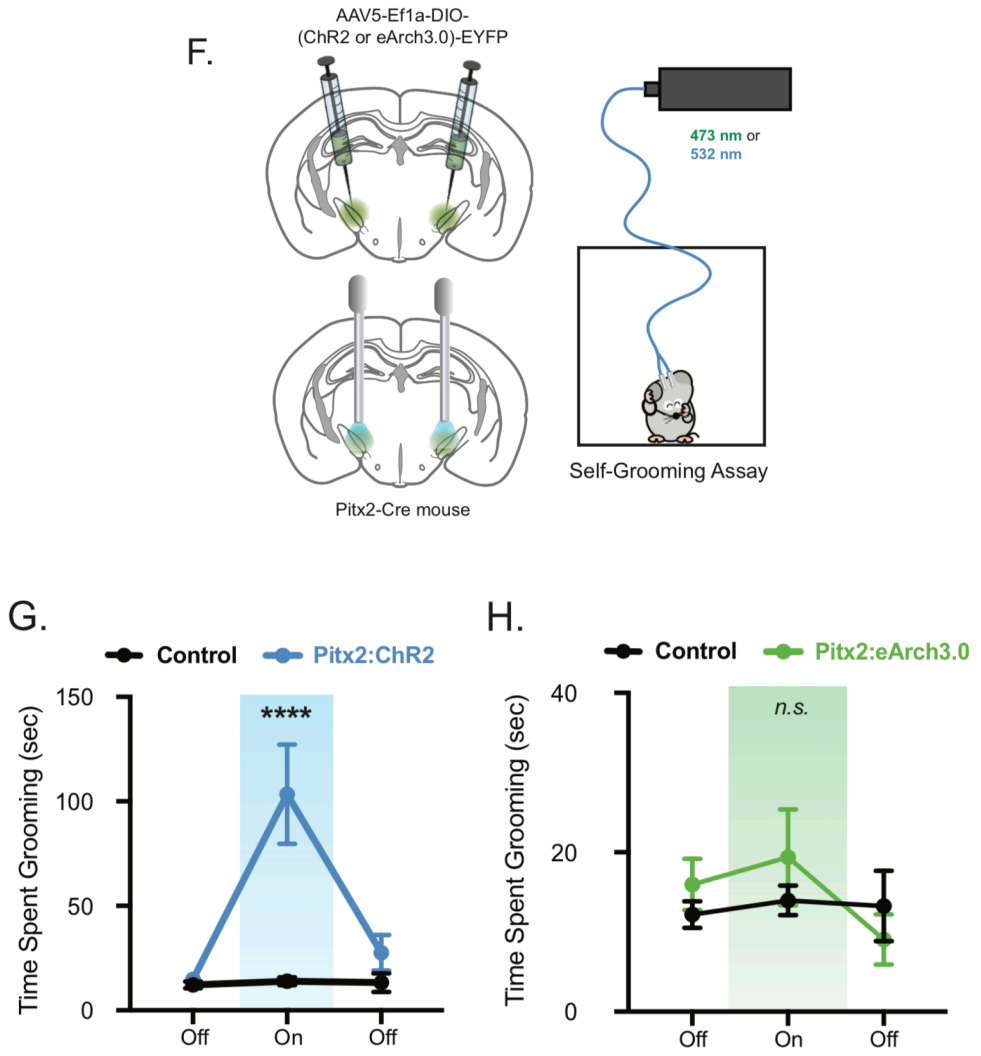

Figure 3F-H. Effects of Optogenetic Modulation of STN Neurons (STN^{Pitx2}) on Self-Grooming.

(F) Schema for bilateral optogenetic modulation of STN^{Pitx2} neurons in the Self-Grooming Assay.

(G and H) Photoactivation (40 Hz) of Pitx2:ChR2 mice bilaterally increases the time spent grooming acutely (during Laser "On" epoch) compared to control mice (G), whereas bilateral photoinhibition of Pitx2:eArch3.0 does not alter the grooming time compared to control (H). Repeated-measures two-way ANOVA, followed by *ad hoc* Sidak's multiple comparison test comparing treated and control groups (**** $p < 0.0001$, *n.s.* $p > 0.05$; n = 6 mice per group). Blue-shaded region highlights 532nm Laser On epoch. Green-shaded region highlights 473 nm Laser On epoch. All data are presented as mean ± SEM.

Repeated Activation of STN Neurons Elicits Persistent Grooming.

Importantly, this repetitive behavior was extinguished almost immediately after photostimulation ceased. This suggested that inducing a more sustained pattern of repetitive, stereotyped behavior, independent of acute photostimulation, would replicate OCD features more closely. Prior studies have shown that optogenetic activation of a cortico-striatal sub-circuit can increase baseline grooming in mice only after several daily repetitions (Ahmari *et al,* 2013). Furthermore, DBS and selective serotonin reuptake inhibitors (SSRI) drug treatments of OCD require days or weeks to become effective (Follet *et al,* 2010; Odekerken *et al,* 2013). This suggests that repeated activation could lead to sustained grooming behavior even after photostimulation has ceased.

We thus analyzed grooming after repeated photo-stimulations of STN^{Pitx2} neurons over 7 consecutive days and compared the amount of time spent grooming before and after the week-long paradigm (Figure 3I). We observed a significant increase in grooming during a 5-minute period 24 hours after the final bout of photostimulation (repeated measures two-way ANOVA with Sidak's multiple comparison test; Day 7 ChR2 Vs. Control: mean increase 2.34-fold, * $p < 0.05$, ** $p < 0.01$; ChR2 Day 0 Vs. Day 7: mean increase 2.1 -fold, * $p < 0.05$, n = 6/group; Figure 3J, left). Computerized grooming recording over 2 hours confirmed this data in a separate set of experiments (t-test Day 7: ChR2 mean 2350s Vs. Control mean 1679s, * $p < 0.05$, n = 6/group; Figure 3J, right). Next, to rule out locomotion as a cause for the observed increase in grooming, we quantified the distance traveled by mice and observed no change between

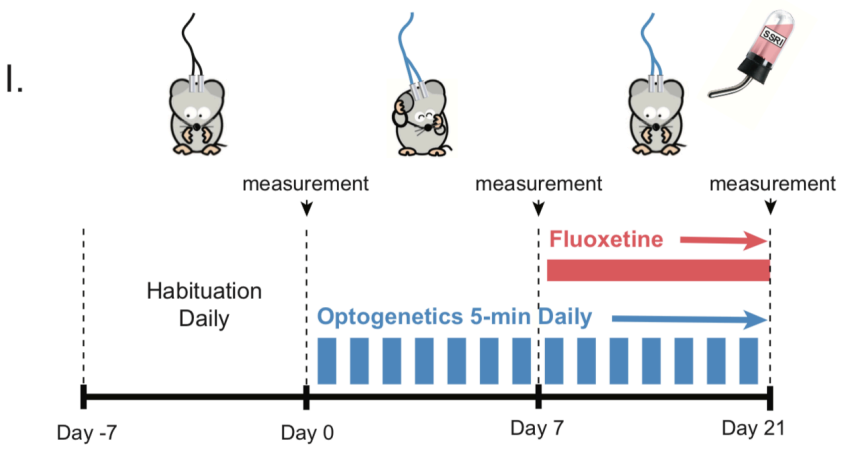
I.
measurement
measurement
measurement
Fluoxetine
Habituation
Daily
Optogenetics 5-min Daily
Day -7
Day 0
Day 7
Day 21

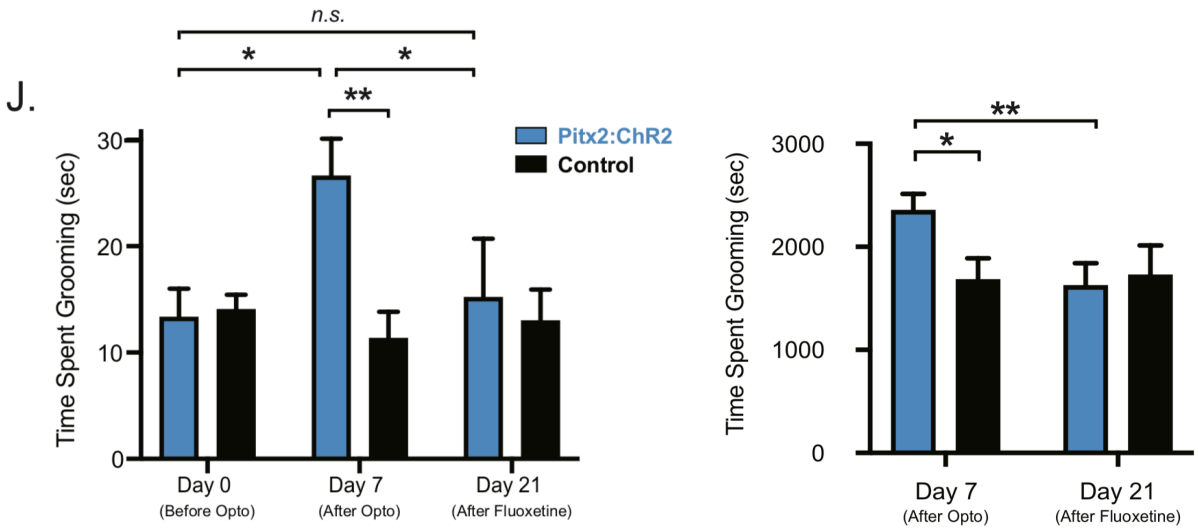
J.
n.s.
*
*
**
Pitx2:ChR2
Control
Time Spent Grooming (sec)
30
20
10
0
Day 0
(Before Opto)
Day 7
(After Opto)
Day 21
(After Fluoxetine)
**
*
3000
2000
1000
0
Day 7
(After Opto)
Day 21
(After Fluoxetine)

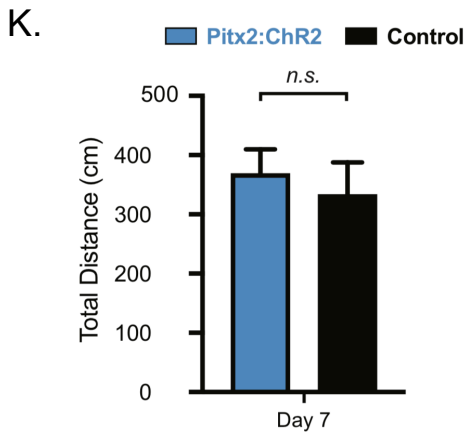
K.
Pitx2:ChR2
Control
n.s.
Total Distance (cm)
500
400
300
200
100
0
Day 7

L.

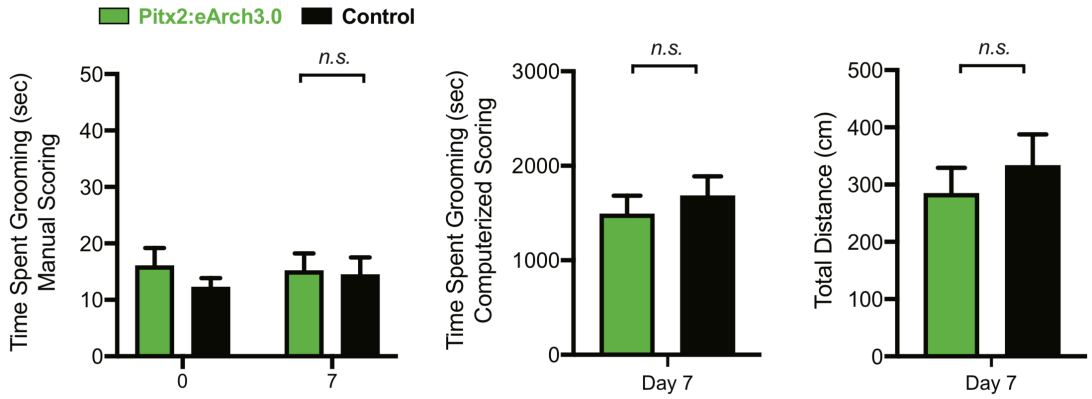

Figure 3I-L. Effects of Repeated Optogenetic Activation of STN Neurons (STN^{Pitx2}) on Self-Grooming.

(I) Schema for repeated bilateral optogenetic modulation of STN^{Pitx2} neurons in the Self-Grooming Assay. After 7 days of habituation to the optic fiber, Pitx2:ChR2 and control mice were photoactivated (40 Hz) for 5 minutes daily for 7 days. The photostimulation paradigm was then continued for an additional 14 days, while mice were treated with SSRI fluoxetine. Self-grooming time was measured before (Day 0) and after (Day 7) the optogenetic stimulation paradigm, and after the treatment with fluoxetine (Day 21).

(J) Photoactivation (40 Hz) of Pitx2:ChR2 mice bilaterally for 7 consecutive days increases the time spent grooming at baseline (24 hours after last Laser On epoch) compared to self at Day 0, and to control mice at Day 7, while the addition of treatment with SSRI fluoxetine reverts the grooming time back to initial levels; scored manually (left) and with computerized system (right). Repeated-measures two-way ANOVA, followed by *ad hoc* Sidak's multiple comparison test comparing treated and control groups, and treated group between Day 0, 7 and 21 (** $p < 0.01$, * $p < 0.05$, *n.s.* $p > 0.05$; $n = 6$).

(K) Photoactivation (40 Hz) of Pitx2:ChR2 for 7 consecutive days does not change the total locomotion of mice at day 7, measured as total distance walked in 5 minutes. T-student test comparing treated and control groups (n.s. non-significant; n = 6 mice per group).

(L) Photoinhibition of Pitx2:eArch3.0 mice bilaterally for 7 consecutive days does not change the time spent grooming at baseline compared to control as measured manually (left) and by automatized computer system (center), nor the total locomotion over 5 minutes (right). Repeated-measures two-way ANOVA, followed by *ad hoc* Sidak's multiple comparison test (left), and t-student test comparing treated and control groups (center and right) (n.s. non-significant; n = 6 mice per group).

treated and control groups (t-test Day 7: ChR2 mean 368 cm Vs. Control mean 333 cm, n.s. $p > 0.05$, n = 5/group; Figure 3K). Similar to the effects on rotations, 7 days of repeated photoinhibition of STN^{Pitx2} neurons using eArch3.0 did not alter baseline grooming or total locomotion (repeated measures two-way ANOVA with Sidak's multiple comparison test, left; t-test, center and right; eArch3.0 Vs. Control, n.s. $p > 0.05$, n = 6/group; Figure 3L).

To confirm that the increased grooming represented an OCD-like phenotype, we tested whether drugs used to treat OCD could reverse this photostimulation-induced repetitive behavior. SSRIs like fluoxetine are first-line treatment for OCD patients and have been shown to successfully reduce excessive grooming in mouse models of OCD after two weeks of daily treatment (Ahmari *et al,* 2013; Welch *et al,* 2007). Therefore, after inducing over-grooming with 7 successive daily photostimulations of STN^{Pitx2} neurons, we tested whether fluoxetine treatment (20mg/kg) could reverse the behavioral effects of daily stimulation (Figure 3I). Importantly, 14 days of fluoxetine treatment in conjunction with repeated stimulation significantly restored the grooming time to levels comparable to baseline, as analyzed both manually (repeated measures two-way

ANOVA with Sidak's multiple comparison test; Day 21: ChR2 mean 15.17s Vs. Control 12.98s, n.s. $p > 0.05$; ChR2 Day 0 Vs. Day 21, n.s. $p > 0.05$; ChR2 Day 7 Vs. Day 21, 1.8-fold mean decrease, * $p < 0.05$; n = 6/group; Figure 2J, left) and with an automated computer system (repeated measures two-way ANOVA with Sidak's multiple comparison test; ChR2 mean Day 7: 2350s Vs. Day 21: 1621s, ** $p < 0.01$; n = 6/group; Figure 2J, right).

.

Functional Studies of Subpopulations of STN Neurons.

Next, to determine whether subpopulations of STN^{Pitx2} neurons (see Figure 2) could recapitulate the observed behavioral responses, we injected a Cre-dependent AAV expressing ChR2 in into the STN of mice expressing Cre-recombinase under the promoters Nos1 (Nos1-Cre), Ndnd (Ndnf-Cre) and Gabrr3 (Gabrr3-Cre) (Figure 3M). Similar to the results using Pitx2-Cre mice, unilateral photostimulation at 40 Hz of each of these three subpopulations induced a significant change in rotation (t-test: increase of mean Control Vs. Ndnf: 8.6-fold, * $p < 0.05$; Vs Nos1: 6.9-fold, ** $p < 0.01$; Vs. Gabrr3: 7.4-fold, ** $p < 0.01$; n = 4-6/group; Figure 3N). Additionally, except in Nos1-Cre mice, we could also recapitulate the acute effects on grooming (t-test: increase of mean Control Vs. Ndnf: 6.7-fold, * $p < 0.05$; Vs Nos1: 4.9-fold, n.s. $p > 0.05$; Vs. Gabrr3: 7.6-fold, * $p < 0.05$; n = 4-6/group; Figure 3O).

Altogether, these data demonstrate that while activation of each of the three subpopulations exhibits qualitatively analogous behaviors, activation of Gabrr3 and Ndnf expressing neurons have stronger effects on rotation and grooming than activation of Nos1 neurons. Additionally, Gabrr3 is a smaller cell population and is more specific to the STN than Ndnf. Finally, and most importantly, Gabrr3 is a gene that encodes for a membrane GABA receptor and therefore could be an interesting druggable candidate for translational work.

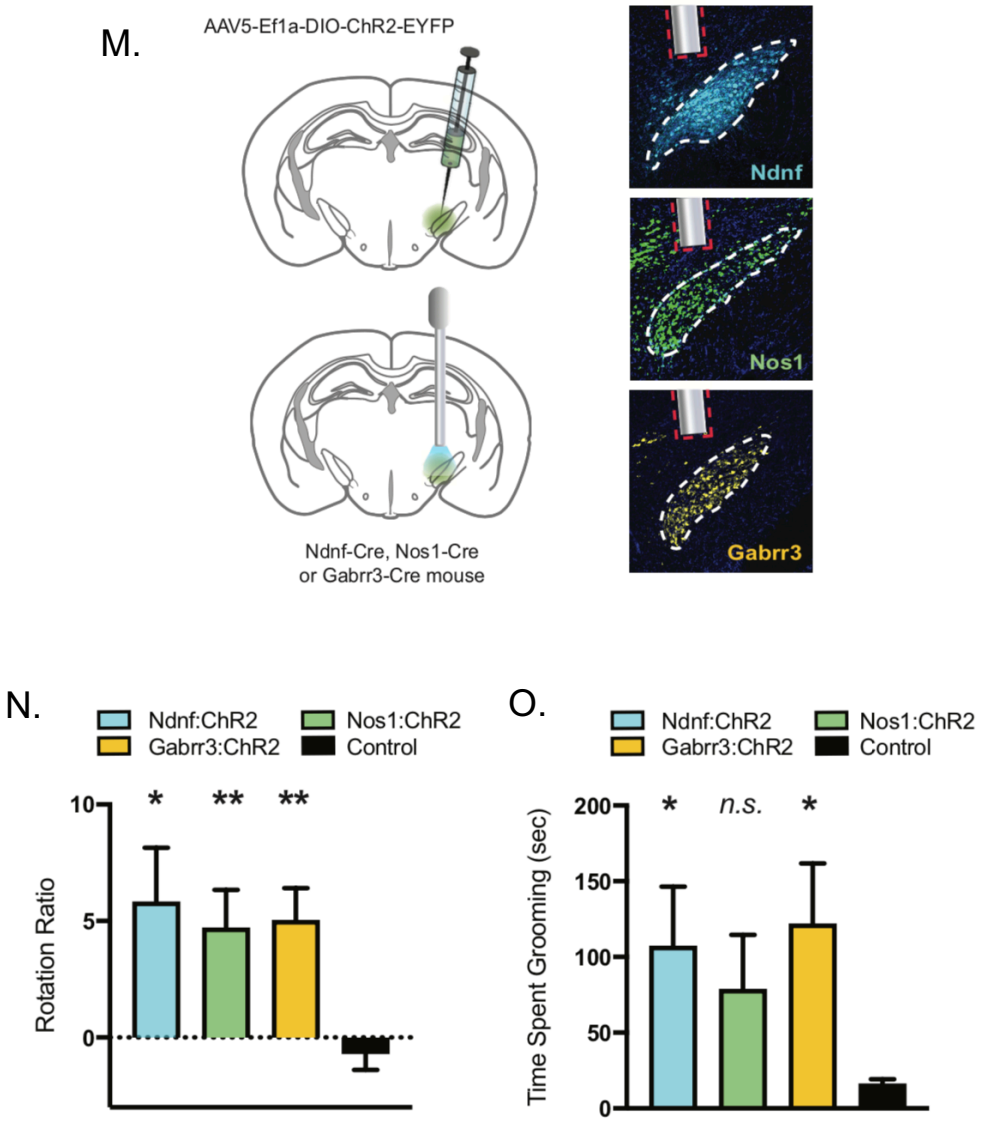

Figure 3M-O. Functional Analysis of STN Neuronal Subpopulations

(M) Schema for unilateral optogenetic modulation of STN neuronal subpopulations in the Rotation Assay, and representative IHC for validation of viral expression and optic fiber placement in Ndnf:ChR2, Nos1:ChR2 and Gabrr3:ChR2 mice.

(N, O) Optogenetic photoactivation (40 Hz) of Ndnf, Nos1 and Gabrr3 STN neuronal subpopulations increases unilateral rotations (N), while it significantly increases the time spent grooming only in Ndnf and Gabrr3 populations (O). T-student test comparing each treated group to control (* $p < 0.05$, ** $p < 0.01$, *n.s.* $p > 0.05$; n = 4-6 mice per group).

STN^{Gabrr3} Neuronal Subpopulation Regulate Locomotion and Repetitive Grooming.

We thus decided to evaluate the effect of modulating Gabrr3-expressing neurons (hereafter STN^{Gabrr3}) activity in finer detail. First, we confirmed that 40 Hz is the optimal frequency for STN^{Gabrr3} photostimulation (t-test: increase of mean Control Vs. 10 Hz: 27-fold, * $p < 0.05$; Vs 40 Hz: mean increase 68-fold, *** $p < 0.001$; Vs. 120 Hz: 17-fold, n.s. $p > 0.05$; n = 5-6/group; Figure 3P). Importantly, unilateral photostimulation of STN^{Gabrr3} neurons at this frequency acutely induced a significant increase in ipsilateral rotations. These rotations were quantitatively double to the response to STN^{Pitx2} photoactivation (repeated measures two-way ANOVA with Sidak's multiple comparison test; On epoch: ChR2 mean 58.33 Vs. Control mean -1.23, **** $p < 0.0001$, n = 5-6/group; Pitx2 29.17 Vs. Gabrr3 58.33; Figure 3Q). Similarly, bilateral photostimulation significantly induced an increase in grooming. This effect was also stronger than when evaluating Pitx2 activation (repeated measures two-way ANOVA with Sidak's multiple comparison test; On epoch: ChR2 mean 143.3 s Vs. Control mean 15.44, **** $p < 0.0001$, n = 5-6/group; Pitx2 103.4s Vs. Gabrr3 143.3s; Figure 3R).

These results further support Gabrr3 as a particularly valuable marker for STN neuronal modulation of both PD- and OCD-like behaviors.

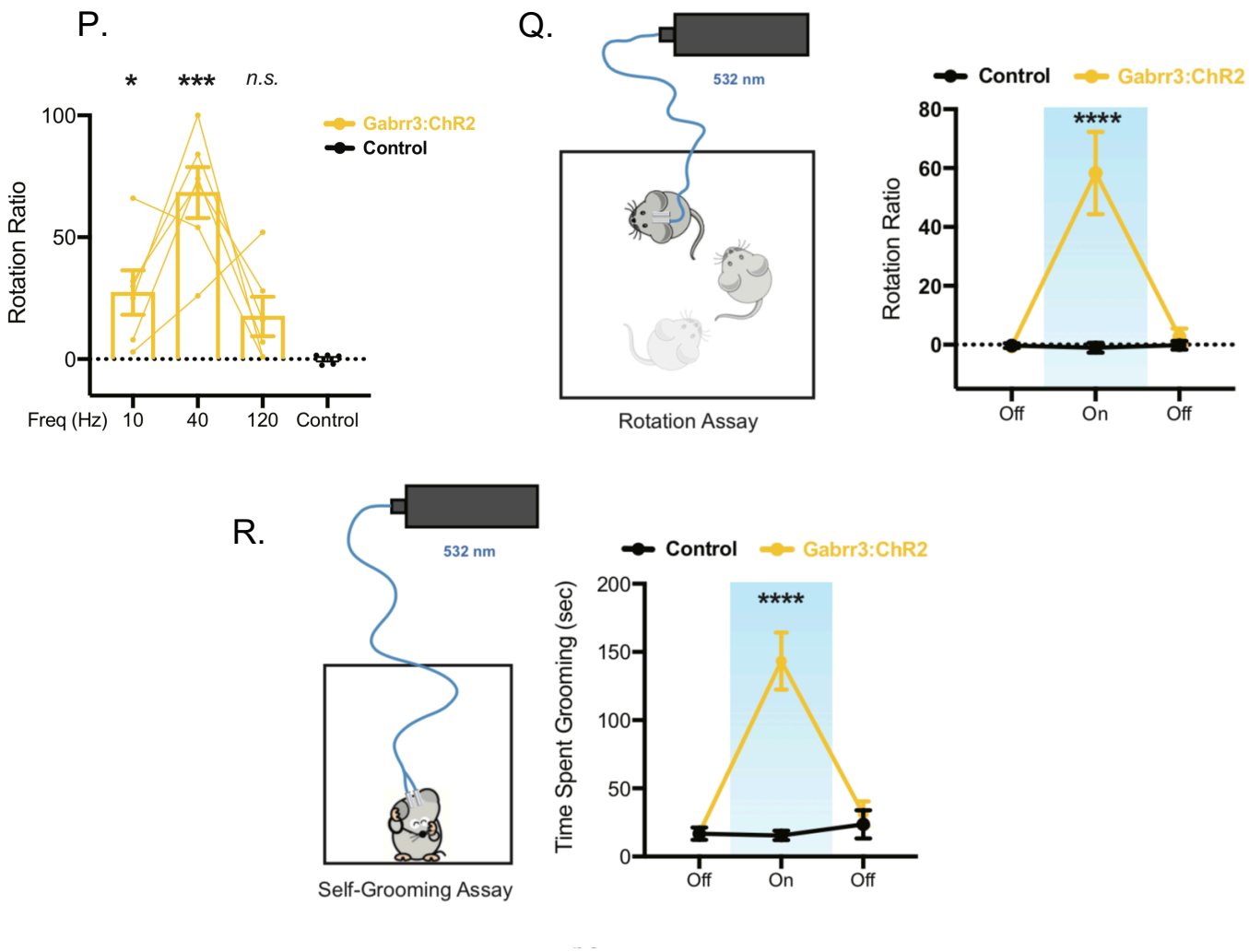

Figure 3P-R. Optogenetic Activation of STN^{Gabrr3} Neurons Inhibits Locomotion and Induces OCD-like Repetitive Behavior in Mice.

(P) Optogenetic photoactivation of STN^{Gabrr3} neurons increases unilateral rotation ratio in mice in a scalable manner. T-student test comparing the effect of stimulation at 10, 40 and 120 Hz to control (* $p < 0.05$, *** $p < 0.001$; n = 5-6) (Q and R) Schema and data from photoactivation (40 Hz) of STN^{Gabrr3} neurons in the Rotation and Self-Grooming Assays; unilateral photoactivation of Gabrr3:ChR2 mice increases unilateral rotations compared to control mice (Q), and bilateral photoactivation increases the time spent grooming compared to control mice (R). Repeated-measures two-way ANOVA, followed by *ad hoc* Sidak's multiple comparison test comparing treated and control groups (**** $p < 0.0001$; n = 5-6 mice per group). Blue-shaded region highlights 532nm Laser On.

To determine whether the chronic stimulation paradigm adopted in STN^{Pitx2} neurons (see Figure 3I) led to spontaneous and persistent grooming even after photo-stimulation had ceased also in the STN^{Gabrr3} subpopulation, we repeated photostimulation of these neurons for 7 days and evaluated grooming. Indeed, we observed a significant increase in grooming time in the treated group at day 7 (mixed-effect analysis with Sidak's multiple comparison test; Day 7 ChR2 Vs. Control: mean increase 2.1-fold, ** $p < 0.01$; ChR2 Day 0 Vs. Day 7: mean increase 1.8-fold, * $p < 0.05$, n = 5-6/group; Figure 3S, left). These data were confirmed using an automatized computer system (t-test Day 7: ChR2 mean 2216s Vs. Control mean 1539s, * $p < 0.05$, n = 5-6/group; Figure 3S, right). Similar to STN^{Pitx2} neurons repeated stimulation of STN^{Gabrr3} did not alter total locomotion (t-test Day 7: ChR2 mean 1685 cm Vs. Control mean 1535 cm, n.s. $p = 0.67$, n = 5-6/group; Figure 3T). As predicted, treatment with fluoxetine for two weeks suppressed the repetitive grooming behavior as measured both manually (mixed-effect analysis with Sidak's multiple comparison test; Day 21: ChR2 mean 11.33s Vs. Control 12.61s, n.s. $p = 0.98$; ChR2 Day 7 Vs. Day 21: mean decrease 2.3-fold, ** $p < 0.01$, n = 5-6/group; Figure 3S, left), and with the automated computerized system (t-test Day 21: ChR2 mean 1575s Vs. Control mean 1597s, n.s $p = 0.97$, n = 5-6/group; Figure 3S, right).

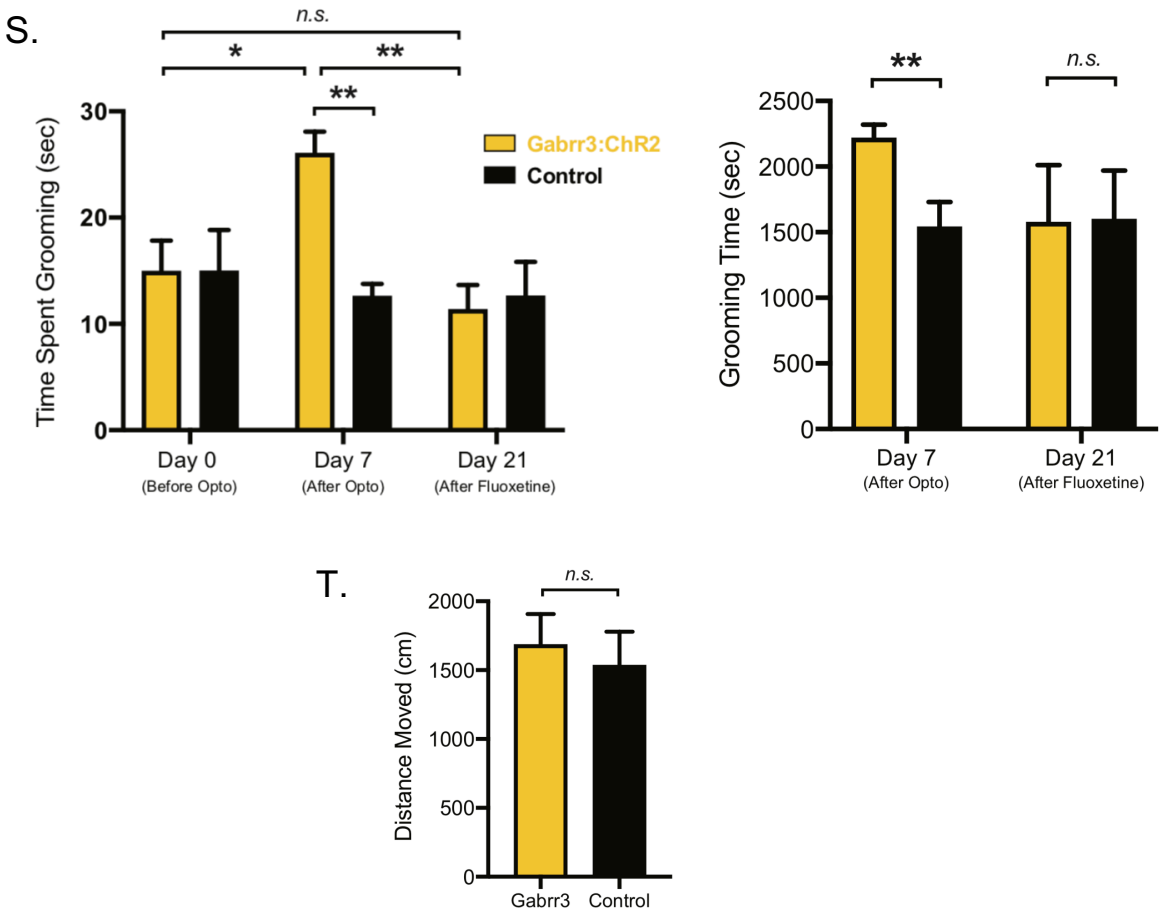

Figure 3S-T. Optogenetic Activation of STN^{Gabrr3} Neurons Inhibits Locomotion and Induces OCD-like Repetitive Behavior in Mice.

(S) Photoactivation (40 Hz) of Gabrr3:ChR2 mice bilaterally for 7 consecutive days increases the time spent grooming at baseline (24 hours after last Laser On epoch) compared to self at Day 0, and to control mice at Day 7, while the addition of treatment with SSRI fluoxetine reverts the grooming time back to initial levels. Scored manually (left). Mixed-model two-way ANOVA, followed by *ad hoc* Sidak's multiple comparison test comparing treated and control groups, and within groups between Day 0, 7 and 21 (* $p < 0.05$, ** $p < 0.01$, *n.s.* $p > 0.05$; n = 5-6 mice per group). Scored with computerized system (right). T-student test comparing treated and control groups (** $p < 0.01$, n.s. non-significant; n = 5-6). (T) Photoactivation (40 Hz) of Pitx2:ChR2 for 7 consecutive days does not change the total locomotion of mice, measured as total distance walked in 5 minutes. T-student test comparing treated and control groups (n.s. non-significant; n = 5-6 mice per group). All data are presented as mean ± SEM.

DISCUSSION:

Motor Effects. Several lines of evidence suggest that the STN inhibits movement initiation, and that when it is disinhibited in PD, the resulting hyperactivity is associated with hypokinesis of movements (Alexander *et* al, 1990; DeLong *et al*, 1984). It has been further suggested that the symptomatic improvement conferred by DBS in PD patients is the result of STN inhibition (Benabid, 2003). The experimental support for this possibility includes the following: i. anatomical lesions of the STN improve hypokinesia (Patel *et al*, 2003), ii. DBS-STN in mice decreases the firing rate of STN neurons (Tai *et al*, 2003) as well as its excitatory output to the SNr (Dvorzhak *et al*, 2013), iii. injection of muscimol - a GABA agonist and neuronal inhibitor - in the STN of monkeys increases contralateral limb movements (Karachi *et al*, 2009), and iv. decreased glutamatergic signaling in STN neurons increases locomotion in mice (Schweizer *et al*, 2016). However, cell-type specific modulation of STN neurons on locomotion or grooming has not been evaluated in mice. Importantly, assessment of unilateral optogenetic manipulation of the STN on rotation in rats did not show an effect either at “low-frequency” (20 Hz) or “high frequency” (120 Hz) photostimulation (Gradinaru *et al*, 2009). Because the effect of DBS is frequency-dependent, we asked whether rotation required frequencies different than those that were tested. STN neurons have been reported firing at spontaneous spike frequencies between 5-40 Hz *ex vivo* (Heida *et al*, 2008), with an average in rodents of around 10-12 Hz *in vivo* (Tai *et al*, 2003). We thus decided to empirically test 10 Hz, as an average low frequency; 40 Hz, the upper

limit of spontaneous STN frequency range (Fife *et al*, 2017), and 120 Hz, to mimic the frequency used in DBS (Gradinaru *et al*, 2009). Intriguingly, our data demonstrate a maximal effect at 40 Hz in both STN^{Pitx2} (Figure 3B) and STN^{Gabrr3} neurons (Figure 3P). This suggests that increasing the firing of STN neurons within the physiological range has stronger functional effects than stimulation at higher, non-physiologic frequencies such as those employed in DBS, which may induce detrimental effects including conduction block, synaptic fatigue and antidromic stimulation of afferents (Bourne *et al*, 2012).

Consistent with a previous report (Gradinaru *et al*, 2009) acute unilateral photoinhibition of STN^{Pitx2} neurons did not induce unilateral rotations in mice (Figure 3D). It is plausible that STN neurons, while not silent at baseline (Tai *et al*, 2003; Heida *et al*, 2008), may not exert behavioral effects significant enough to induce rotations. In line with this hypothesis, unilateral ablation of STN neurons in animals using diphtheria toxin also did not induce unilateral rotations (Figure 3E). A second possibility is that, at least acutely, ionotropic inhibition of STN neural activity using optogenetics may not be sufficient to tip the electrophysiological balance between direct and indirect pathways within the basal ganglia neural circuit. In the future, it will thus be interesting to evaluate the effect of other silencing approaches, such as metabotropic inhibition with chemogenetics. Finally, it is possible that loss of basal ganglia output does not cause severe behavioral disturbances in normal animals, but gain of abnormal basal ganglia output (as in the disease state) can. Distinguishing how the basal

ganglia circuit functions in normal versus pathological states remains thus an important question (Nelson *et al*, 2014).

Limbic-Associative Effects. Grooming in mice follows a patterned, sequential organization with a characteristic cephalocaudal progression (Kalueff *et al*, 2016). While in healthy mice about 10-15% of grooming bouts proceed to completion of all 4 phases, photostimulation of STN^{Pitx2} and STN^{Gabrr3} neurons induced repetitive movements consistent with only phase 1 of the syntactic chain (ie, elliptical strokes of the snout), which only rarely proceeded to completion of the entire sequence. We thus asked if these features where consistent with a repeated involuntary movement (eg, dyskinesia), or a complex stereotypy suggesting an involvement of limbic-associative functions. After accurate analysis, we are confident that the repetitive behavior observed is not purely motor, but instead reflects altered limbic-associative functions. In fact, the movements were stereotyped, directed and regular, which is not typical of a "pure" movement disorder, and were qualitatively similar to behaviors characteristic of several psychiatric conditions, such as hand-wringing in certain autistic patients. This is particularly relevant because increased self-grooming has been linked to behavioral perseverations and repetitions typical of both autistic and OCD patients (Welch *et al*, 2007; Wan *et al*, 2014). This conclusion is also supported by the fact that the behavior could be interrupted when the animal was distracted (such as the examiner entering the room) which is not generally observed in dyskinesia. We also found that the mice showed

decreased locomotion, spending most of their time grooming rather than exploring their surroundings (data not shown).

Taken together, these results indicate that STN^{Pitx2} and neurons can be photostimulated to induce an acute increase in repetitive grooming. Moreover, repeated photostimulation induces a persistent over-grooming phenotype, similar to OCD in mice, which can be reversed with fluoxetine treatment. Additionally, modulation of the activity of STN^{Gabrr3} neurons recapitulates the behavior observed when manipulating the entire STN (*Pitx2*), but has a quantitatively stronger effect.

CHAPTER 4

STN^{Gabrr3} Neurons as a Target to Treat PD and OCD

INTRODUCTION:

Our results showing that activation of STN^{Gabrr3} neurons could lead to rotations and induce repetitive grooming behavior suggested that modulating the activity of these neurons might be a viable approach to improve the phenotypes of common mouse models of PD and OCD.

To test this possibility, we adopted a mouse model in which PD is induced by the toxic dopamine analogue 6-hydroxydopamine (6-OHDA). When mice are unilaterally injected with 6-OHDA into the left medial forebrain bundle (MFB), an area dense of dopaminergic fibers of passage, most dopaminergic cells in the ipsilateral side of the brain will die (Ungerstedt *et al*, 1970). Successful ablation of dopaminergic neurons can be tested by assessing the drastic decrease of dopamine marker tryptophan hydroxylase (TH) in the striatum of the injected side (Figure 4A). As a consequence, mice display deficits in the contralateral (right) side of the body and rotate in a direction ipsilateral to the lesion (leftward). Moreover, administration of amphetamine, by increasing the synaptic release of dopamine, exacerbates the effects and facilitates functional evaluation.

To assess if modulation of STN^{Gabrr3} neurons can improve OCD-like symptoms in mice, we used Sapap3 KO mice, one of the most established models of the disease (Welch *et al*, 2007; d'Angelo *et al*, 2014). These transgenic animals lack functional copies of SAPAP3, a postsynaptic scaffolding protein highly expressed in glutamatergic synapses of the striatum, the basal ganglia nucleus most highly implicated in the pathophysiology of OCD. As a consequence, these mice display a reduction in cortico-striatal synaptic

transmission and defects in glutamatergic system. Behaviorally, these animals display excessive self-grooming and increased anxiety-like behaviors, which can be alleviated by repeated treatment with the selective serotonin reuptake inhibitor (SSRI) fluoxetine. To investigate if inhibition of STN^{Gabrr3} neurons repeated over time could partially restore the OCD-like phenotype, we thus set out to photoinhibit these neurons daily for 10 days and quantify the change in time spent grooming.

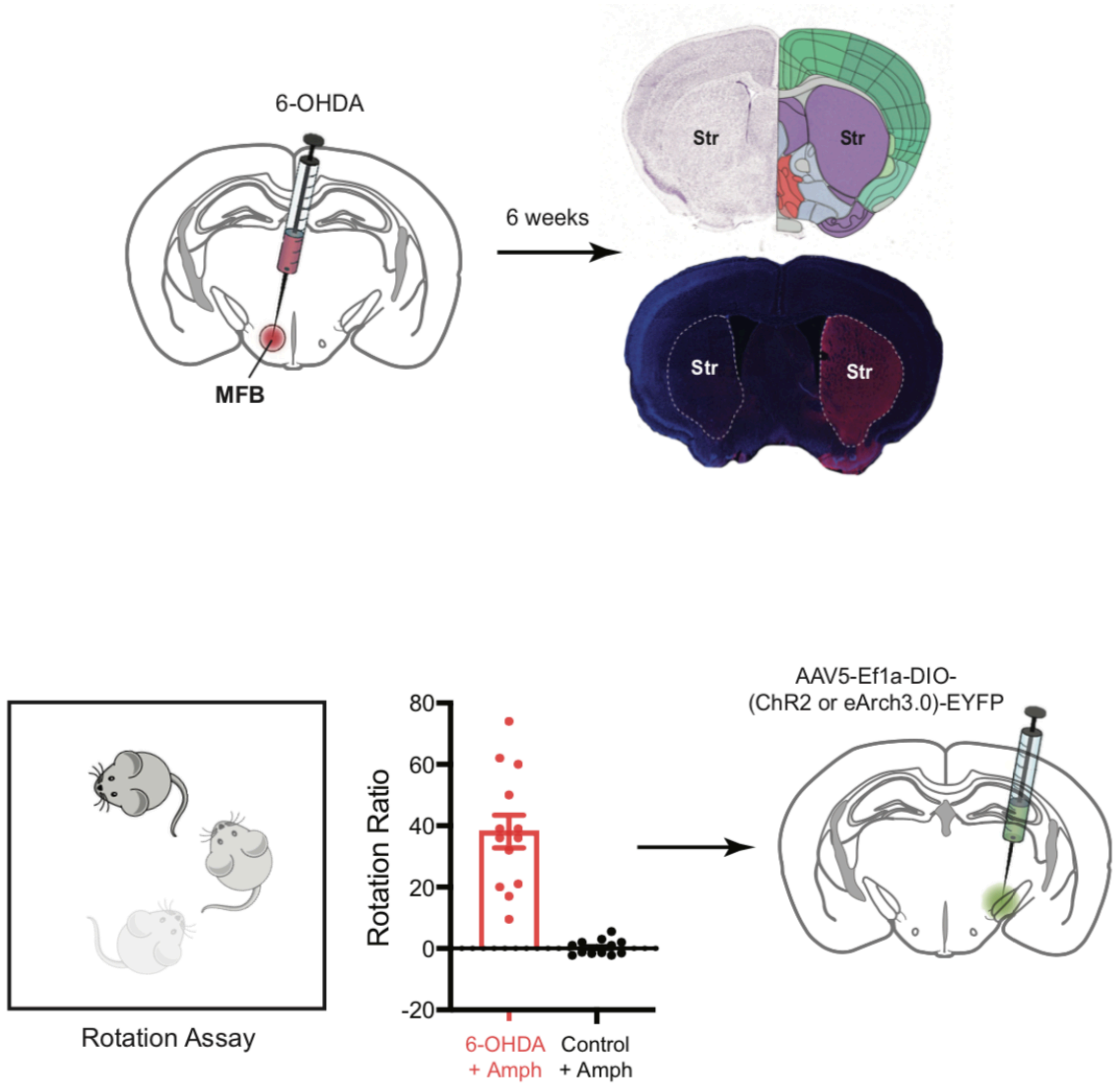

Figure 4A. Induction of Hemi-Parkinsonian Phenotype in Mice with 6-OHDA. Top: Injection of 6-OHDA in the left medial forebrain bundle (left) induces ipsilateral dopaminergic neuronal ablation, which results in a drastic decrease of dopamine marker TH in the striatum (right). Bottom: The lesion induces an increase in ipsilateral rotations in treated animals compared to controls, which is exacerbated by amphetamine (Amph). Individual animals displaying a Rotation Ratio > 5 were selected to undergo optogenetics surgery for further functional analysis.

RESULTS:

Modulation of STN^{Gabrr3} Neurons in Mouse Models of Parkinson's Disease.

Successful ablation of dopaminergic neurons in the left side of the brain was assessed by scoring the rotation ratio of animals at 6 weeks after surgery. Mice displaying a Rotation Ratio > 5 were selected to undergo optogenetics surgery for further functional analysis. Additional confirmation of dopaminergic ablation was performed *postmortem* by assessing with immunohistochemistry the decrease of TH in the striatum of the injected side (Figure 4A).

Our results show that in 6-OHDA-amphetamine-treated mice photostimulation of contralateral STN^{Gabrr3} neurons, opposite to the side of the lesion, restored the ipsilateral rotations to normal levels (repeated measures two-way ANOVA with Sidak's multiple comparison test; Stimulation On epoch: ChR2 mean -6.21 Vs. Control mean 19.50, **** $p < 0.0001$, n = 8/group Figure 4B). Similar to the lack of effect when inhibiting Pitx2 neurons, photoinhibition of STN^{Gabrr3} neurons ipsilateral to the lesion failed to diminish the leftward-to-rightward rotation ratio to baseline in amphetamine-treated animals (repeated measures two-way ANOVA with Sidak's multiple comparison test; Stimulation On epoch: eArch3.0 mean 32.16 Vs. Control mean 43.40, *n.s* $p > 0.05$, n = 5/group Figure 4C).

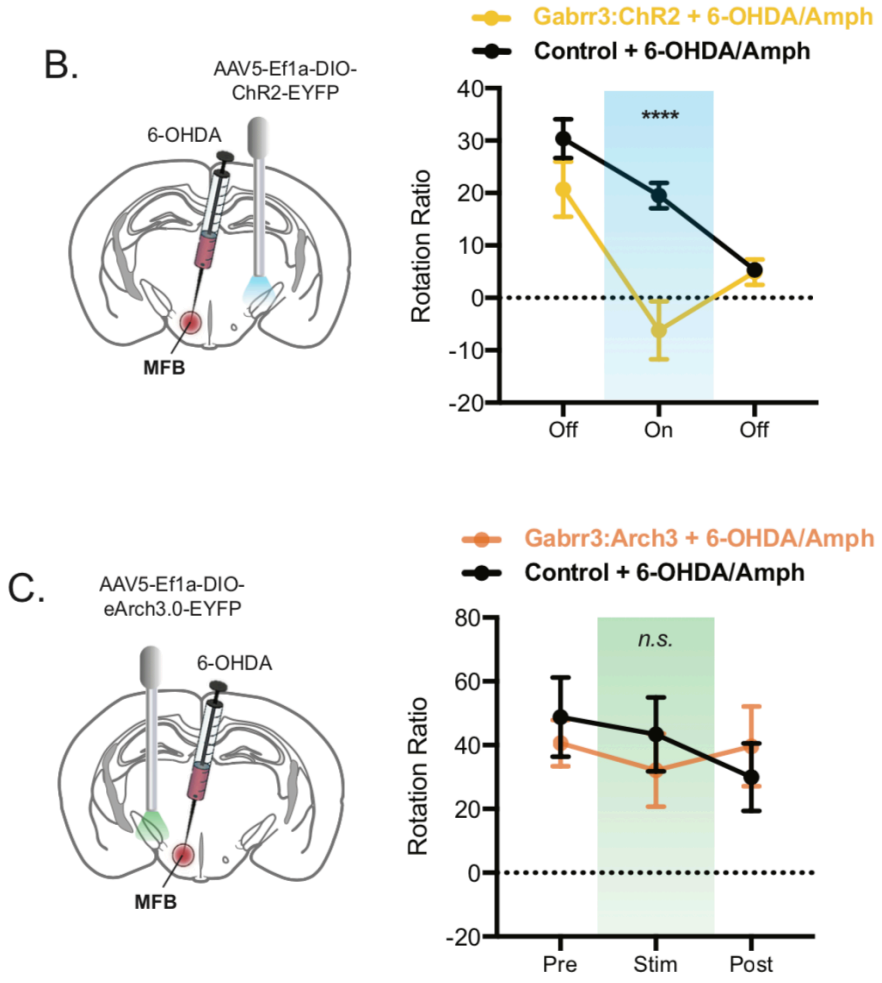

Figure 4B-C. Optogenetic Modulation of STN^{Gabrr3} Neurons Improves the Pathologic Phenotype of a Mouse Model of PD.

Schema and data showing that photoactivation of STN^{Gabrr3} neurons contralateral to the 6-OHDA lesion rescues the hemi-parkinsonian rotation behavior of the treated group to normal levels (B), whereas photoinhibition (40 Hz) of ipsilateral STN^{Gabrr3} neurons did not change the rotation behavior of hemi-parkinsonian mice compared to controls (C). Repeated-measures two-way ANOVA, followed by *ad hoc* Sidak's multiple comparison test comparing treated and control groups (**** $p < 0.0001$, *n.s.* $p > 0.05$; n = 5-8 mice per group). Green-shaded region highlights 473 nm Laser On epoch. Blue-shaded region highlights 532nm Laser On epoch.

Modulation of STN^{Gabrr3} Neurons in Mouse Models of OCD.

In order to evaluate a role for STN^{Gabrr3} neurons in OCD, we tested the effect of repeated photomodulation of STN^{Gabrr3} neurons on Sapap3 KO mice. Because repeated photoactivation of STN^{Gabrr3} neurons increases baseline grooming (Figure 3G), we hypothesized that repeated photoinhibition of the same neurons could decrease the pathological over-grooming in Sapap3 KO mice (Figure 4D, left). Indeed, bilateral photoinhibition of STN^{Gabrr3} for 10-min/day over 7 days significantly decreased the time Sapap3 KO mice spent grooming to the same level as their phenotypically normal, heterozygous littermates (repeated measures two-way ANOVA with Sidak's multiple comparison test; eArch3.0 mean Day 0: 4330s Vs. Day 7: 2449s, ** $p < 0.01$, n = 5-9/group; Figure 4D, right).

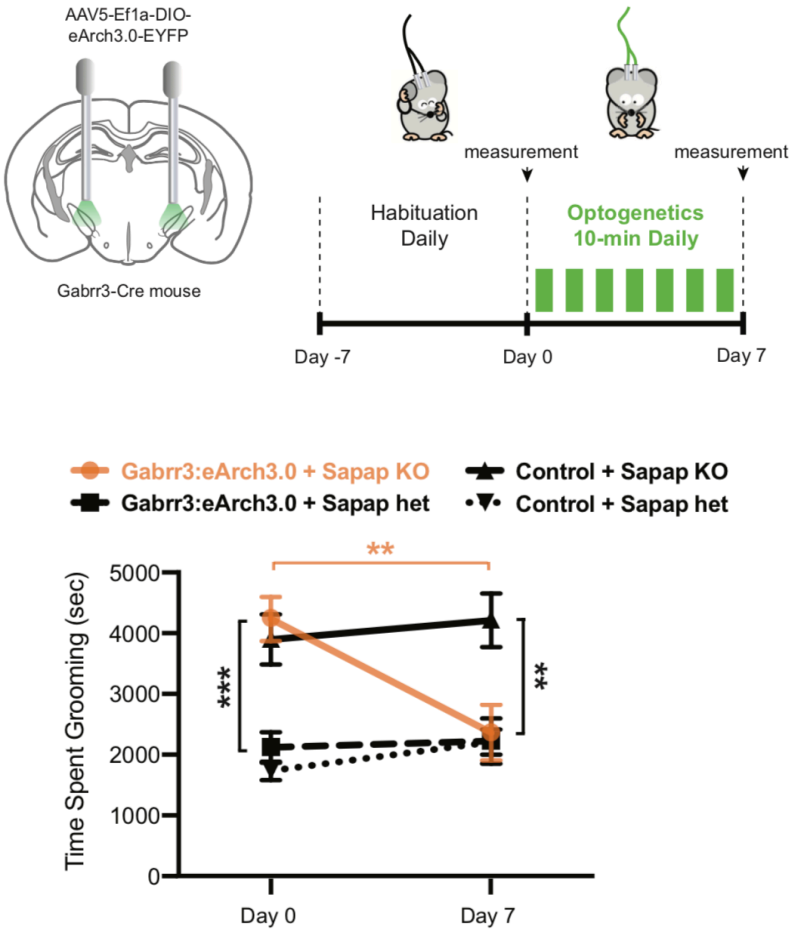

Figure 4D. Optogenetic Inhibition of STN^{Gabrr3} Neurons Improves the Pathologic Phenotypes of a Mouse Model of OCD.

Schema and data for repeated bilateral optogenetic inhibition of STN^{Gabrr3} neurons in Sapap3-KO mice in the Self-Grooming Assay. After 7 days of habituation to the optic fiber, Gabrr3:eArch3.0 and control mice of both Sapap3 KO and Sapap3 heterozygous genotype were photoinhibited for 10 minutes daily for 7 days. Self-grooming time was significantly decreased in the Sapap3 KO treated mice after photoinhibition, while it was not significantly altered in the three control groups (Sapap3 KO control, Sapap3 heterozygous treated, Sapap3 heterozygous control). Repeated-measures two-way ANOVA, followed by *ad hoc* Tukey's multiple comparison test comparing treated and control groups, and comparing before and after photostimulation within each group (** $p < 0.01$, *** $p < 0.001$, n.s. non-significant; n = 5-7). All data are presented as mean ± SEM.

DISCUSSION:

Consistent with previous reports (Gradinaru *et al*, 2009) and our observation that photoinhibition of STN^{Pitx2} does not induce unilateral rotations (Figure 3D), also acute unilateral photoinhibition of STN^{Gabrr3} neurons ipsilateral to the 6-OHDA lesion did not rescue the hemiparkinsonian rotation phenotype (Figure 4C). We discussed several possible interpretations of these results at the end of Chapter 3. Photoactivation of STN^{Gabrr3} neurons contralateral to the dopaminergic lesion, however, was sufficient to equilibrate the rotation ratio to levels close to baseline and improve the hemiparkinsonian pathologic phenotype (Figure 4B).

While it is well established that loss of dopaminergic innervation in PD leads to an increase in STN activity (Alexander *et al*, 1990; DeLong *et al*, 1984), the changes in dopaminergic innervation and circuit alterations in OCD are less clear. Several lines of evidence point towards an increase in the activity of the cortico-striato-thalamo-cortical circuit (Milad *et al*, 2012), and the STN. In fact, electrophysiological studies in OCD patients show a correlation between severity of symptoms, responsiveness to DBS, and overall activity of STN neurons (eg, increased burst frequency and theta oscillatory activity) (Welter *et al*, 2011; Rappel *et al*, 2018). In mice, the Sapap3-KO model of OCD shows defects in excitability more prominent in striato-nigral (direct pathway) than in striato-pallidal neurons (indirect pathway) (Wan *et al*, 2014). This suggests that a relative increase in the activity of the indirect pathway activity, and consequently of the STN, may contribute to the symptoms. Consistent with this, high-frequency

stimulation of the STN has proved effective in suppressing self-grooming in mouse models of autism (Chang *et al*, 2016) and in reducing compulsive lever pressing in rats (Klavir *et al*, 2009). In line with these extensive evidences, selective and direct optogenetic activation of all STN (Pitx2) neurons or the Gabrr3-expressing subpopulation can induce excessive grooming in mice (Figures 3G, 3J and Figures 3R, 3S), and repeated inhibition of STN^{Gabrr3} cells reduces the over-grooming of Sapap3-KO mice (Figure 4D). Taken together, these data show that direct neuronal modulation of the STN can regulate grooming behavior in mice, and that cell-specific inhibition can be a potential therapeutic approach to treat OCD.

A previous report showed that repeated optogenetic activation of a cortico-striatal sub-circuit increased repetitive grooming in mice even after the activation had stopped (Ahmari *et al*, 2013). In line with this, we observed that repeated photoactivation of STN^{Pitx2} and STN^{Gabrr3} neurons induced sustained grooming behavior even after photostimulation had ceased (Figure 3J, 3S). Similarly, in Sapap3-KO mice, repeated photoinhibition of STN^{Gabrr3} neurons decreased pathologic grooming (Figure 4D). These protracted effects are consistent with: (i) inhibition of the STN with DBS suppresses excessive self-grooming in autism-like mice progressively over the 3-5 days post stimulation (Chang *et al*, 2016); (ii) chronic but not acute DBS-STN restores cortico-striatal synaptic plasticity and normalizes glutamate and GABA levels in other basal ganglia nuclei, including striatum and SNr (Chassain *et al*, 2016). Similarly, in the clinic, repeated external modulation is required to achieve therapeutic efficacy in several pharmacologic

(eg, SSRI) and neuro-modulatory treatments of psychiatric patients (eg, DBS, electroconvulsive therapy, transcranial magnetic stimulation) (APA, 2016). Taken together, these and our results suggest that immediate modifications in electrical activity may not be sufficient to correct the aberrant neural activity observed in OCD patients, that instead depends on slower-acting mechanisms, such as changes in neural plasticity and gene expression in the STN and downstream basal ganglia nuclei.

Finally, a consideration on the value of *Gabrr3* as a potential druggable target. GABA-Aρ receptors (formerly known as GABA-C) are a subgroup of GABA-A receptors composed of homo or heteropentamers of the rho subunites 1 (encoded by the gene *Gabrr1*), 2 (*Gabrr2*) and/or 3 (*Gabrr3*) (Martínez-Delgado *et al*, 2010). They display different electrophysiological properties from other GABA-A receptors, including slower gating dynamics (longer latency to open and close), lower conductance and higher sensitivity to GABA (ie, activated by smaller concentrations). GABA-Aρ are most widely expressed and studied in the retina, where they are highly enriched in bipolar cells. While our data confirm the expression of *Gabrr3* in about 60% of all STN neurons (Figure 2C), ISH studies from the Allen Brain Atlas (Lein *et al*, 2007) database seem to suggest that *Gabrr1* and *Gabrr2* are not expressed this nucleus. Instead, STN cells express genes encoding for other GABA receptor subunits, including *Gabbr1* and *Gabbr2* (GABA-B receptors 1 and 2), *Gabra1* (GABA-A, subunit alpha 1), *Gabrb2* and *Gabrb3* (GABA-A, subunit beta 2 and 3), *Gabrg2* and *Gabrg3* (GABA-A, subunit gamma 2 and 3), *Gabrp* (GABA-A, subunit pi), and *Gabarapl1* (GABA receptor

associated-like protein1), thus indicating that STN neurons express GABA-A and GABA-B receptors. It is important to note that the expression of GABAρ3 doesn't imply the presence of GABAρ receptors. In fact, GABA-A subunits have been reported to occasionally co-assemble with GABAρ1 and 2 subunits in the retina, resulting in channels that lack the typical GABAρ properties (Bormann, 2000). However, to our knowledge, co-assembly of GABA-A subunits with GABAρ3 has not been described in literature. To exclude this possibility, electrophysiologic studies of STN^{Gabrr3} neurons are required to confirm the presence of GABAρ receptor-like currents. Their existence would suggest that STN^{Gabrr3} neurons express the highly uncommon homopentameric GABAρ3 receptor (Bormann, 2000; Martínez-Delgado *et al*, 2010), making it an ideal drug target. While there are known selective GABAρ agonists [*Cis-4-aminocrotonic acid (CACA) and cis-2-aminomethyl cyclopropanocarboxylic acid (CAMP)*] and antagonists [*1, 2, 5, 6-tetrahydropyridine-4 methylphosphinic acid (TPMPA) and 3-aminocyclopentyl methylphosphinic acid ((±)-cis-3-ACPMPA*], as well as selective GABAρ2 and GABAρ3 antagonists, there are no known selective agonists to GABAρ3 receptors (Martínez-Delgado *et al*, 2010). Development of such compounds could provide a pharmacologic approach to selectively inhibit STN^{Gabrr3} neurons, with high potential for clinical applications.

In summary, the data here presented demonstrate that modulation of STN^{Gabrr3} neuronal activity can ameliorate the symptoms associated with PD and OCD, and highlights *Gabrr3* in the STN as an interesting marker for neuronal modulation and drug development.

CHAPTER 5

Anatomic and Functional Mapping of STN^{Gabrr3} Projections.

INTRODUCTION:

As a crucial component of the indirect and hyperdirect pathways, the STN receives dense GABAergic innervation from the globus pallidus externa (GPe) (indirect pathway) and glutamatergic from the cortex (hyper-direct pathway), and sends glutamatergic projections to the globus pallidus interna (in rodent entopeduncular nucleus, EP) and to the substantia nigra reticulata (SNr) (Alexander *et* al, 1990; DeLong *et* al, 1984; Kitai *et* al, 1987). As previously mentioned, several studies in primates show that the STN is divided in three areas with different functions, and that each of them is connected uniquely with other areas of basal ganglia nuclei involved in the same function. In primates, the anterior-ventral-medial area of the STN has been involved in the regulation of limbic function, the central territory area associative functions, the posterior-dorsal-lateral are sensorimotor functions (Karachi *et al*, 2005; Karachi *et al*, 2009). Additionally, *in vivo* imaging studies with diffusion tensor imaging MRI in human showed that also projections from different cortical and GPe areas reach the respective anatomo-functional compartment of the STN (Lambert *et al*, 2012).

Some anatomic studies have suggested that the rodent STN might be similarly compartmentalized, with a dorsal part modulating motor functions via a GP/EP projection, and a ventral-medial area (corresponding to the paraSTN) regulating limbic-associative functions via projections to the SNr and ventral pallidum (de Koning *et* al, 2011; Benarroch *et* al, 2008; Aljemade *et* al, 2014). However, other studies reported that neurons of the paraSTN are involved in

limbic functions through projections to the GP (Stephenson-Jones *et al*, 2016), not the SNr. Finally, it is unclear whether the STN^{Gabrr3} neuronal population shows the same connectivity of the STN nucleus as a whole.

We therefore set out to map the projections of this population of neurons in the mouse brain, and assess the role of each individual projection in mediating locomotion and grooming behavior.

RESULTS:

Anatomical Mapping of STN^{Gabrr3} Projections.

First, we focused on identifying the targets of STN^{Gabrr3} to evaluate whether this population of neurons is projecting to the known targets of the STN. To do so, we injected a Cre-dependent AAV expressing the red fluorescent protein mCherry fused to a transmembrane receptor (AAV-hSyn1-DIO-hM3(Gq)-mCherry) into the STN of Gabrr3-Cre mice (Figure 5A, top). Six weeks after the injection, which enabled expression and transport of mCherry through neuronal axons, we used the whole-brain immunolabeling approach iDISCO+ paired to tissue clearing (Renier *et al*, 2014), enabling us to visualize both STN^{Gabrr3} soma and axon terminals in optical sections of intact brains. Importantly, we found that dense projections of STN^{Gabrr3} neurons where found both in the entopeduncular nucleus (EP) and globus pallidus (GP) anteriorly, and in the substantia nigra (SNr) posteriorly (Figure 5A, bottom). This projection pattern is similar to that of

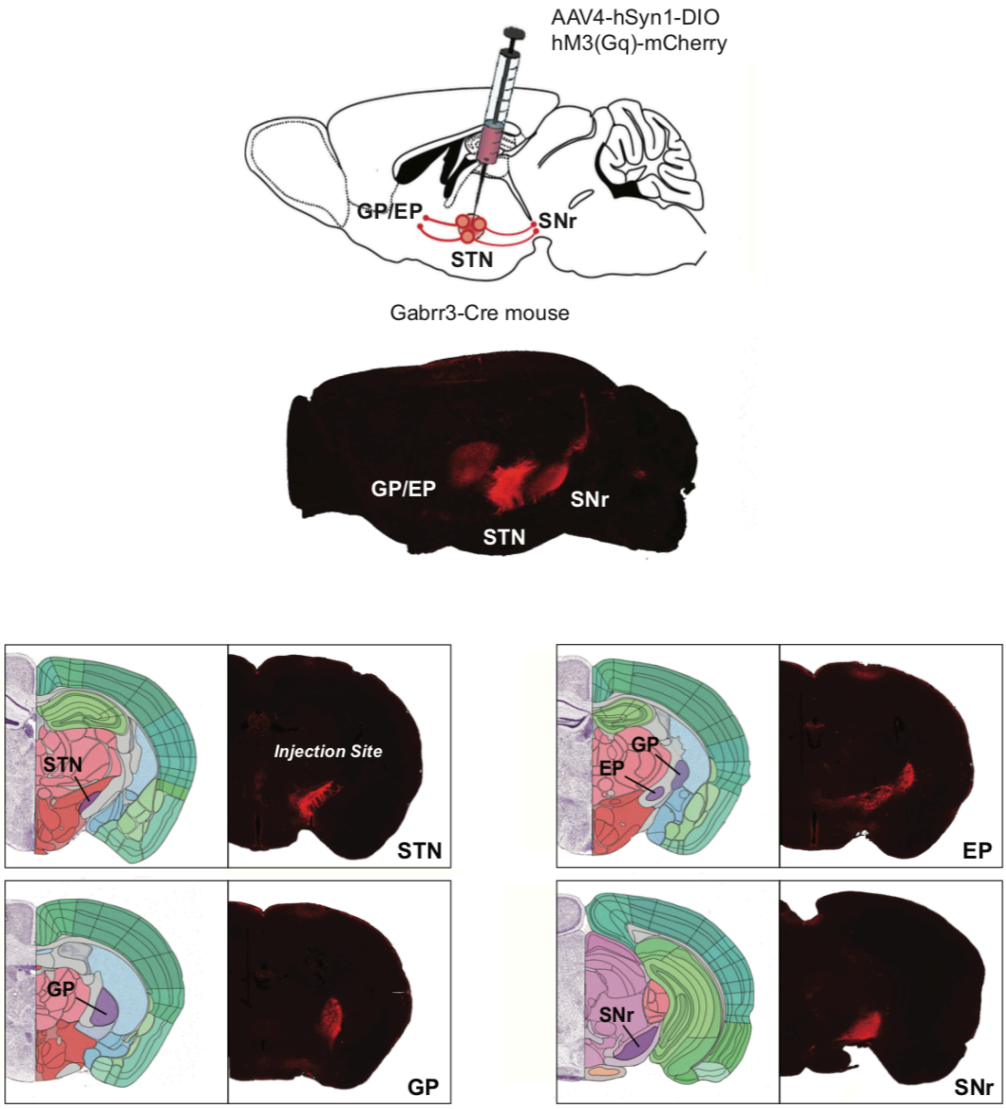

Figure 5A. STN^{Gabrr3} Neurons Projections Mapping.

Schema and representative images of whole-brain projection mapping of STN^{Gabrr3} neurons. Top: schema of projections traced via injection of a Cre-dependent AAV expressing a red fluorescent protein in the STN of Gabrr3-Cre mice. Below, optical sagittal section of whole-brain cleared with iDISCO+ showing injection site (STN) and projections (GP/EP, SNr.). Bottom: left panels represent Allan Brain Atlas annotations for STN, EP, GP and SNr; right panel represent coronal sections from iDISCO+ experiment of the corresponding brain areas.

the STN as a whole (Kitai *et al*, 1987).

We next asked whether the STN^{Gabrr3} neurons that project to the SNr and GP/EP represent distinct, partially overlapping, or the same cell populations. To address this, we performed a dual color tracing approach using retrogradely transported AAVs expressing different Cre-dependent fluorescent proteins. We used Gabrr3-Cre mice and injected an AAV expressing a Cre-dependent green fluorescent protein (GFP) into the GP/EP, and a second AAV expressing a Cre-dependent red fluorescent protein (RFP) into the SNr. As a result, STN^{Gabrr3} neurons projecting to the GP/EP express GFP, STN^{Gabrr3} neurons projecting to the SNr express RFP, and neurons projecting to both sites are yellow (Figure 5B). Quantitative analysis of the images revealed that 27% of STN^{Gabrr3} neurons project exclusively to the GP/EP (green), 37% of STN^{Gabrr3} project to the SNr (red) and 36% project to both sites (yellow) (Figure 5C). These data suggest that STN^{Gabrr3} neurons project equally to the two known targets of the STN, and that more than one third of the population sends collateral projections to both.

Functional Analysis of STN^{Gabrr3} Projections.

Finally, we tested whether STN^{Gabrr3} projections are functionally distinct. To do so, we injected a Cre-dependent AAV expressing ChR2 in the STN of Gabrr3-Cre mice, and placed an optic fiber at each of the projection sites (GP/EP or SNr). We analyzed the number of rotations in response to unilateral photostimulation, and the grooming behavioral assay during bilateral photostimulation at each of these sites. We found that photoactivation of projections to both the GP/EP and the SNr significantly increased the number of

Figure 5B-C. Mapping and Quantification of STN^{Gabrr3} Neurons Collateral Projections

(B) Schema and representative images of dual color retrograde tracing from STN^{Gabrr3} neuronal terminals. Previous page. Left: neuronal terminals were infected with Cre-dependent AAVs expressing RFP in the SNr, and GFP in the GP/EP of Gabrr3-Cre mice. Right: representative IHC and respective Allan Brain Atlas annotations confirming accurate surgical targeting of terminals. Current page: representative IHC images of the STN showing STN^{Gabrr3} neurons labeled in green, red or both (yellow, white arrows) in the anterior and posterior STN. (C) Quantification of percentage of STN^{Gabrr3} neurons projecting to the GP/EP (green), SNr (red) and both (yellow), and Venn diagram summarizing quantitative overlapping of the neuronal sub-populations based on projections.

B.

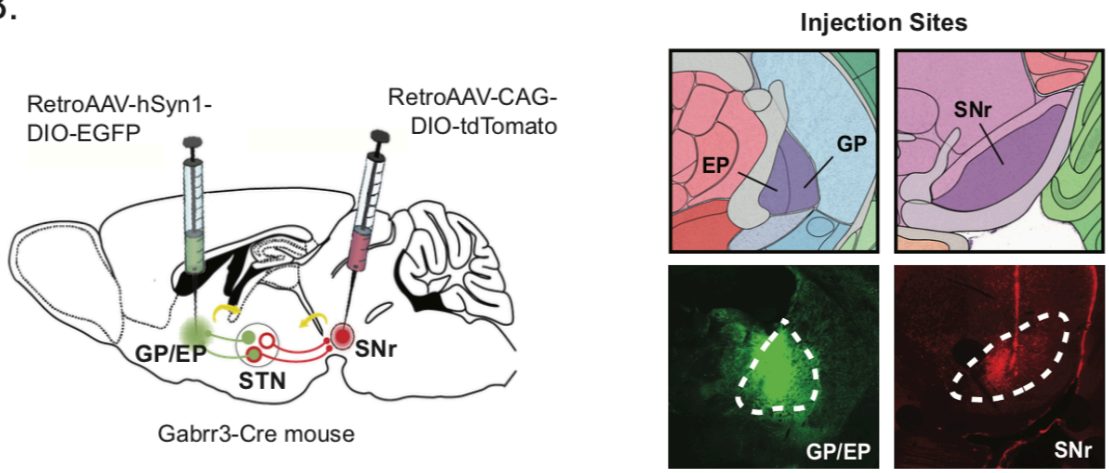
RetroAAV-hSyn1-
DIO-EGFP
RetroAAV-CAG-
DIO-tdTomato
GP/EP
STN
SNr
Gabrr3-Cre mouse
Injection Sites
EP
GP
SNr
GP/EP
SNr

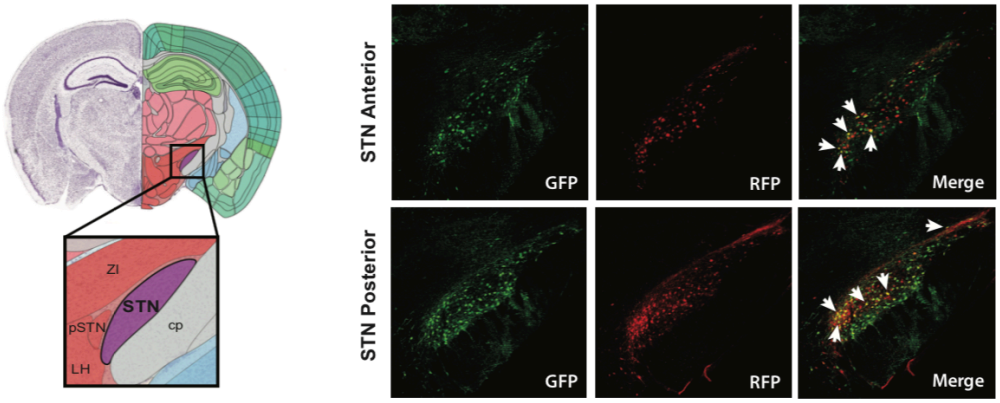
ZI
STN
pSTN
cp
LH
STN Anterior
GFP
RFP
Merge
STN Posterior
GFP
RFP
Merge

C.

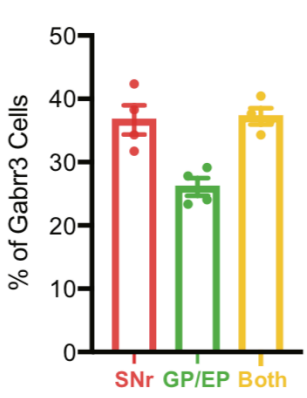
% of Gabrr3 Cells
50
40
30
20
10
0
SNr
GP/EP
Both

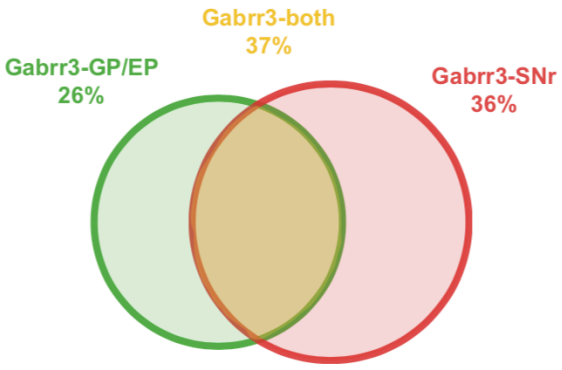
Gabrr3-both
37%
Gabrr3-GP/EP
26%
Gabrr3-SNr
36%

unilateral rotations (repeated measures two-way ANOVA with Sidak's multiple comparison test; On epoch mean: Gabrr3-SNr 23.33 Vs. Control 1.533 *** $p < 0.001$, n = 5-6/group; Gabrr3-GP/EP 20.40 Vs. Control 1.533 ** $p < 0.01$, n = 5/group; Figure 5D). However, the magnitude of the effect was significantly smaller than the photoactivation of the entire STN^{Gabrr3} population (one-way ANOVA with multiple comparisons: On epoch mean: Gabrr3 58.33 Vs. Gabrr3-SNr 23.33, * $p < 0.05$; Gabrr3 58.33 Vs. Gabrr3-GP/EP 20.40, * $p < 0.05$; n = 5-6/group; Figure 5D, right). Similarly, photostimulation at each of these sites increased grooming (repeated measures two-way ANOVA with Sidak's multiple comparison test; On epoch mean: Gabrr3-SNr 112.3s Vs. Control 15.15s **** $p < 0.0001$, n = 5-6/group; Gabrr3-GP/EP 120.80s Vs. Control 15.15s **** $p < 0.0001$, n = 5/group; Figure 5E). This increase was less than that induced by photoactivation of the entire STN^{Gabrr3} population, but not significantly smaller (one-way ANOVA with multiple comparisons: mean On epoch: Gabrr3 143.3s Vs. Gabrr3-SNr 112.3s, *n.s.* $p = 0.71$; Gabrr3 143.3s Vs. Gabrr3-GP/EP 120.80s, *n.s.* $p = 0.51$; n = 5-6/group). Importantly, the magnitude of effect was similar after activation of STN^{Gabrr3} terminals in the GP/EP and SNr projections, further suggesting that both projections can similarly regulate locomotor and limbic-associative functions (t-test Gabrr3-SNr Vs. Gabrr3-GP/EP: rotations, *n.s.* $p > 0.05$; grooming, *n.s.* $p > 0.05$; Figure 5D and E, right).

In aggregate, these results suggest that STN^{Gabrr3} neurons mediate their limbic-associative and motor functions through projections to both the GP/EP and SNr, and they do not present a projection-dependent functional segregation.

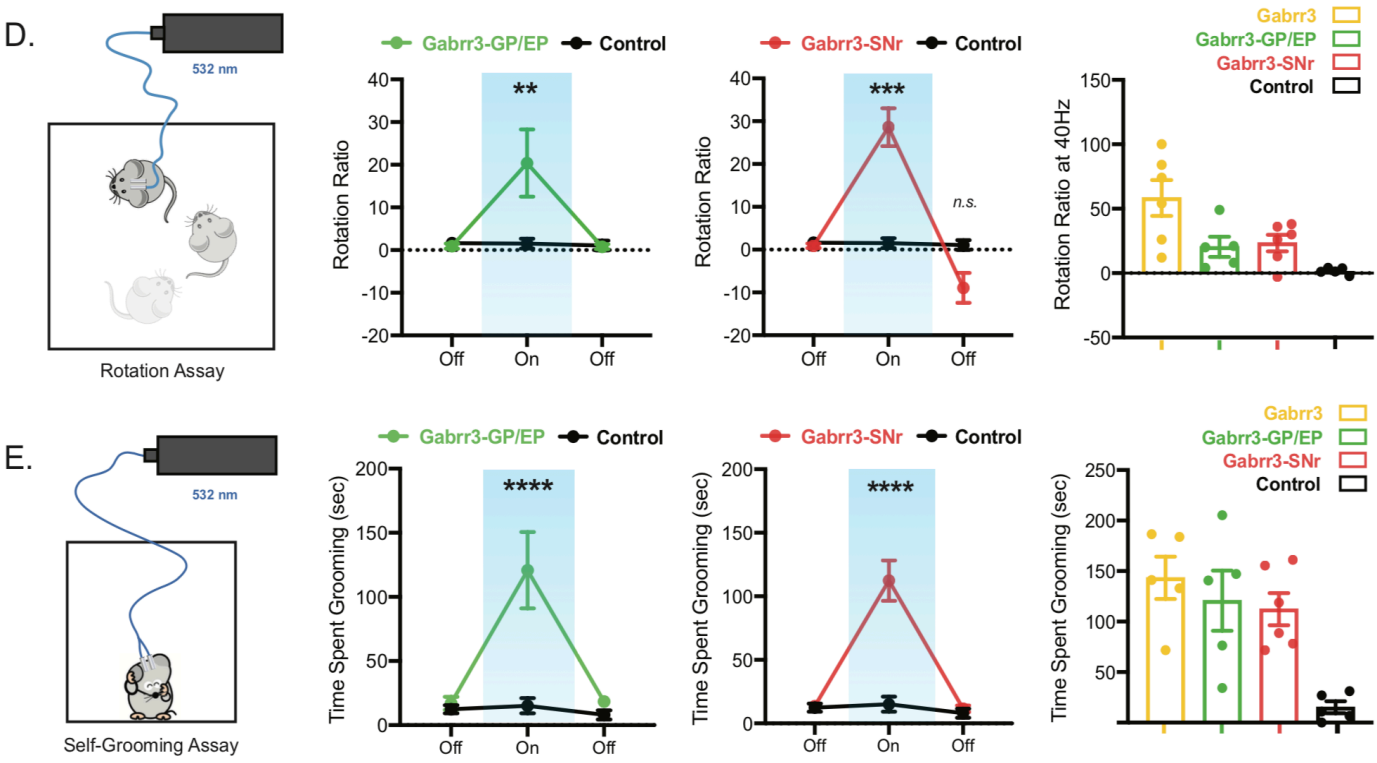

Figure 5D-E. Functional Analysis of STN^{Gabrr3} Neurons Projections

Schema and data from photoactivation (40 Hz) of STN^{Gabrr3} projections in the Rotation and Self-Grooming Assays. (D) Unilateral photoactivation of Gabrr3:ChR2 projections to GP/EP (center-left panel) and SNr (center-right panel) increases rotations compared to control. Right panel: compared effect between groups during Laser On epoch. (E) Bilateral photoactivation of STN^{Gabrr3} neurons projecting to GP/EP (center-left panel) or SNr (center-right panel) increase the time spent grooming compared to control. Right panel: compared effect between groups during Laser On epoch. Repeated-measures two-way ANOVA, followed by *ad hoc* Sidak's multiple comparison test comparing treated and control groups (** $p < 0.01$, *** $p < 0.001$, **** $p < 0.0001$, n.s. non-significant; n = 5-6 mice per group). Blue-shaded region highlights 532nm Laser On epoch. All data are presented as mean ± SEM.

DISCUSSION:

The results discussed in Chapter 4 and 5 seem to suggest that immediate modulation of electrical activity in the STN may not be sufficient to correct the aberrant neural activity observed in OCD patients. On the contrary, repeated photoinhibition of STN^{Gabrr3} over time is effective in reversing OCD-like grooming, while repeated photoactivation can induce it. These observations seem to suggest that the functional effects may depend on slower-acting mechanisms, such as changes in neural plasticity and gene expression in the STN and downstream basal ganglia nuclei. To address this possibility, we analyzed the role of these other basal ganglia circuit elements by mapping the projections of STN^{Gabrr3} populations and by testing their functions.

As previously mentioned, functional and anatomical studies in humans and non-human primates suggest that the STN is divided into three anatomically segregated areas with different functions: limbic, associative and motor (Mallet *et al*, 2007; Karachi *et al*, 2005; Karachi *et al*, 2009;). To investigate possible anatomic and functional segregation in mice, we first tested whether STN^{Gabrr3} neurons projecting to the GP/EP Vs. SNr are located in anatomically segregated areas of the STN, and if selective photostimulation of different projections induces distinct behaviors. Dual color retrograde tracing from STN^{Gabrr3} terminals in GP/EP and SNr failed to show anatomic segregation, in that neurons of the ventral-medial or dorsal STN did not project preferentially to one target or the other (Figure 5B). Consistent with this, photoactivation of STN^{Gabrr3} projections to the GP/EP or SNr had quantitatively similar effects in inducing rotation and

grooming behavior in mice, although the overall effect was lower than activating STN^{Gabrr3} neurons as a whole (Figure 5D and 5E, right).

In summary, these observations suggest that STN^{Gabrr3} neurons mediate both their motor and limbic-associative functions via projections to the GP/EP and SNr, but also that both projections are needed to convey the full behavioral effect.

CHAPTER 6

Summary and Conclusions.

Movement Disorders and Psychiatric Diseases including PD and OCD are associated with alterations of the activity in the basal ganglia circuit. Treatments employing electrical modulation such as DBS, transcranial magnetic stimulation and electroconvulsive therapy have proved effective in improving the symptoms of several of these conditions. However, it is still unclear how these effects are achieved, and DBS is an invasive procedure with high variability in efficacy and is associated with not uncommon, serious complications. Identifying the specific cell populations that mediate these effects, and elucidating the mechanisms in normal and disease states would contribute to a deeper understanding of the pathophysiology of these conditions. In addition, this could potentially enable new therapeutic approaches using chemo-genetics and cell-specific promoters to regulate the activity of these neurons.

With the present work, we report new data identifying and testing the function of specific cell types in the subthalamic nucleus (STN) and establishing their role to control movement and regulate limbic-associative functions. Specifically, we characterized three partially overlapping subsets of STN neurons expressing *Ndnf*, *Nos1* and *Gabrr3*. We found that despite marking the smallest subset of neurons in the STN, the subpopulation expressing the GABA-Aρ receptor subunit *Gabrr3* can still regulate locomotion and grooming, behaviors often associated with PD and OCD in mice. Modulation of the same cells successfully improved the phenotype of common mouse models of PD and OCD, consistent with the possibility that DBS acts to improve symptoms in these disorders by directly modulating STN neurons, as opposed to fibers of passage or neighboring areas. Anatomical and functional dissection of the STN circuit

showed that these effects are mediated by projections to either of two known basal ganglia nuclei.

Together, this work identifies a novel molecular target for cell-specific modulation of the STN and its circuit in the treatment of PD and OCD, and helps improving our understanding of the mechanisms through which DBS asserts its effects. Additionally, the *Gabrr3* gene encodes a subunit of a rare GABA-A membrane receptor, identifying a potential druggable target to selectively control these cells using a standard pharmacologic approach. The data we present thus have important implications for the physiology and pathophysiology of movement and psychiatric disorders with the potential for enabling translational studies.

EXPERIMENTAL PROCEDURES

Multiplex Fluorescence In Situ Hybridization (FISH).

Mice were anesthetized and perfused transcardially with RNase-free PBS, followed by 4% PFA. Brains were harvested and post-fixed overnight in 4% PFA, incubated for 24h sequentially in 10%, 20% and 30% glucose solution, sliced with temperature-controlled cryostat (17um thickness), and mounted on Superfrost Plus Adhesion slides (Fisher). Multiplex FISH was then performed using the RNAscope system (ACDBio) as per the manufacturer's protocol. The slides were mounted using Prolong Gold Antifade Mountant (Thermo Fisher). The target probe sets used included vGlut2 (Slc17a6), vGat (Slc32a1), NeuN, Pitx2, Nos1, Ndnf and Gabrr3. Images were captured using confocal microscopy (Zeiss or Leica), and subsequently manually counted for the number of cells single-, double- or triple-labelled fluorescent cells using Fiji ImageJ.

Animals.

All experiments were conducted in accordance with the guidelines of the National Institutes and the protocols approved by the The Rockefeller University Institutional Animal Care and Use Committees. Mice were housed in a 12 hr light-dark cycle (lights on at 7:00) with ad libitum access to food and water. Male mice were used for all the behavioral and histological studies; both male and female mice were used for tracing studies. Mice were at least 8 weeks old at the time of surgery. All mouse lines were in a wild-type (C57BL/6J; Jackson Laboratory; stock 000664) background. The following mouse lines were used: Pitx2-Cre (Dr Tim Cox, The University of Washington (Martin *et al*, 2004)), Gabrr3-Cre (KC112 line; GENSAT; Dr Nat Heintz, The Rockefeller University), Sapap3-KO (Jackson Laboratory; stock 008733). For all experiments,

hemizygous Cre-positive animals were compared with wild-type littermates as controls. For Sapap3-KO experiments, knockout animals were compared with heterozygous littermates. A het × KO breeding scheme was used to yield a sufficient number of knockouts with heterozygous littermates as controls.

Viral Vectors.

All viruses used in these experiments were purchased from Addgene and UNC Vector Core. The following viruses were used for optogenetic studies: AAV5-EF1a-DIO-hChR2(H134R)-EYFP (activation; Addgene 20298), AAV5-EF1a-DIO-eArch3.0-eYFP (inhibition; UNC Vector Core). For tracing studies: AAV5-hSyn-DIO-hM3D(Gq)-mCherry (anterograde; Addgene 44361), rgAAV-hSyn-DIO-EGFP (retrograde green; Addgene 50457), rgAAV-CAG-FLEX-tdTomato (retrograde red; Addgene 28306). For ablation study: AAV8-EF1a-lox-Cherry-lox-(dtA)r-lox2.ape (lot # AV6241B).

Stereotaxic surgeries.

Mice were anesthetized using isoflurane. Coordinates were identified using the Paxinos mouse brain atlas and adjusted over several rounds of practice using fluorescent beads. For viral injections (1.0uL Syringe, Hamilton 65458-01), the coordinates used were: STN (ML: ±1.68mm, AP: -2.00mm, DV: -4.68mm), GP/EP (ML: ±1.85mm, AP: -1.15mm, DV: -4.10mm), SNr (ML: ±1.50mm, AP: -3.80mm, DV: -4.20mm). Viral injection volumes were STN (0.04uL), GP/EP (0.10uL), SNr (0.30uL). Fiber optic ferrule (Thor Labs) implants were positioned at the same ML and AP coordinates, and 0.40mm more dorsal

than the injection site (ie, STN (DV: -4.28mm), GP/EP (DV: -3.70mm), SNr (DV: -3.80mm) to avoid structural damage to the targeted area. All listed DV coordinates are relative to pia. Optic fibers were secured in place with dental cement. Viral injections and optic fiber implants were performed unilaterally or bilaterally as specified in the Results section. Skin was closed using 5-0 silk sutures.

Considering the small size of the targets in mice, in particular the STN, each animal's skull was carefully adjusted to lay flat, allowing for a skew of 0.01mm or less both along the AP axis (ie, delta DV between bregma and lambda at skull surface) and ML axis (delta DV between ML: +1.68mm and ML: -1.68mm, at AP: -2.00mm at skull surface). Of note, AP coordinates for the STN were adjusted (AP -2.00mm ± 0.15mm) depending on the size of each animal skull, measured as distance between bregma and lambda.

To produce hemiparkinsonian mice, animals were injected with 20mg/kg i.p. desipramine hydrochloride (Sigma, D3900) 30-60 minutes prior to surgery to prevent 6OHDA-mediated noradrenergic lesion; 30-60 minutes later, animals were injected in the medial forebrain bundle (ML: ±1.20mm, AP: -1.10mm, DV: -5.20mm) with 0.2 mg/kg 6OHDA hydrobromide (Sigma, H116) dissolved in 0.1% ascorbic acid. To assist during post-op recovery, animals were i.p. injected daily with dextrose-saline solution and provided condensed milk *at libitum* for 5 days, as well as checked for their health condition daily until day 10 post-op.

Behavioral Assays:

Optogenetic Induction of Rotation Behavior in Healthy and Hemi-Parkinsonian Mice.

Pitx2-Cre, Gabrr3-Cre and control littermate mice were injected with channelrhodopsin or archaerhodopsin in the STN, followed by 3 weeks to allow for opsin expression and animal recovery; in the case of optogenetic stimulation of STN projections, at least 6 weeks were left to allow robust expression of Channelrhodopsin in the terminals.

On the day of the experiment, animals were placed in a clean and empty cage during the light phase, and connected to the laser via rotary joint (ThorLabs). Mice received 3-minutes laser stimulation with continuous green (532nm) or intermittent blue light (473nm, OEM Lasers/OptoEngine) at frequencies of 10, 40 or 120 Hz, 10ms pulse width, 5-10mW. Stimulation paradigms were programmed into an arbitrary waveform generator (Agilent). In all experiments, mice were given *ad libitum* access to food prior to and after the assay. Video was recorded with Logitech Webcam for offline analysis for a total of 9 minutes (3 minutes before, during and after stimulation). Rotations were recorded using a hand tally counter (Fisher Scientific) as full-body turns of at least 180° in either direction. The rotation ratio was calculated as counterclockwise divided by clockwise rotations if the ratio was ≥ 1; if this was < 1, then the ratio was reported as the opposite of its reciprocal. When the number of rotations performed in one direction was 0, the count was rounded to 1.

Hemiparkinsonian mice were left to recover from surgery for at least 6 weeks before the experiments; 30 minutes before the behavioral measurements, mice were i.p. injected with 2.6mg/kg of amphetamine hemisulfate (Sigma, A5880) to induce rotations ipsilateral to the 6-OHDA lesion. The subsequent behavioral paradigm was then carried

out as detailed above.

Optogenetic Induction of Acute and Chronic Grooming and Reversal with Fluoxetine.

Pitx2-Cre, Gabrr3-Cre and control littermate mice were injected with channelrhodopsin in the STN, followed by 3-6 weeks windows to allow for recovery and opsin expression in the cell soma and terminals, respectively. For habituation to the assay, mice were placed in an empty shoebox cage, connected to the laser cable via their optic fiber implants, and left to get accustomed to the setting for 1 minute/day for 7 consecutive days. On the 8th day, during the light phase, each animal was placed in a clean and empty cage and connected to the laser cable bilaterally. After 3 minutes of habituation to the novel environment, mice were video recorded while freely moving in the cage for 5 minutes, followed by 5 minutes of optogenetic stimulation (40Hz, 10ms pulse, 5-10mW), and 5 minutes after the laser was turned off. The acute grooming was manually scored with JWatcher to quantify the time spent grooming and the number of grooming bouts during each interval.

To induce the persistent grooming phenotype, optimal 40Hz optogenetic stimulation was repeated for 5 minutes/day for 7 consecutive days, at a consistent hour of the day. On the 8th day, mice were placed in a clean and empty cage and left to habituate for 3 minutes, plugged to the cable, recorded for 5 and the time spend grooming was quantified.

Mice then underwent an additional 14 consecutive days of daily 5-minutes optogenetic stimulations while treated with fluoxetine hydrochloride (Sigma, 1279804) 18mg/kg/day in drinking water, which was changed every 3 days to prevent inactivation of the drug.

After 2 weeks of treatment, on day 21st, mice were videorecorded one last time for 5 minutes while connected to the cable. Mice were given *ad libitum* access to food and water prior, during and after the 21-day assay. Total locomotion was measured on the videos recorded using Noldus Ethovision XT 9.0 Software.

Optogenetic Reversal of Increased Grooming in Sapap3 KO mice.

Gabrr3-Cre and control littermate mice, each divided in two groups of heterozygous and homozygous Sapap3 knockouts, were bilaterally injected with archaerhodopsin and implanted with optic fibers, followed by a 3-week recovery window. After 7 days of habituation to handling and to the cable, mice were optogenetically inhibited with continuous green light for 10 minutes/day for 7 days. The total time spent grooming was measured with Home Cage Environment computerized scoring system before the 1st day, and 24h after the 7th day of daily optogenetic inhibition.

Computerized Scoring of Grooming with Home Cage Environment (Clever Sys Inc.).

Mice were transported in their housing cages to the procedure room 1h before testing for acclimation. 15 minutes before the experiment, animals were single-caged in clean new shoe-size cages, and the Home Cage Environment (Clever Sys Inc.) was calibrated for cage position and background. Recording was conducted for 2.5 hours, during which time the animals were left free to explore the cage, during light cycle, with ad libitum access to food and water. In the case of repeated measurements over different days (ie, before/after optogenetics or fluoxetine treatment) the same animals were recorded at consistent times during their light cycle.

Immunohistochemistry.

Mice were transcardially perfused with PBS, followed by 10% formalin. Brains were then post-fixed for 24-36h in formalin 10%, and sectioned by vibratome (50um thickness). Primary antibodies used for immunohistochemistry were chicken anti-GFP (Abcam, 13970), chicken anti-RFP (Abcam 62341), rabbit anti-RFP (Rockland, 600-401-379) and rat anti-TH (Immunogen, AB152); secondary antibodies were Alexa Fluor conjugated (Life Technologies). Slides were mounted using Prolong Gold Antifade Mountant (Thermo Fisher). All images were captured using confocal microscopy (Zeiss or Leica).

Brain Clearing and iDISCO.

Mice were perfused transcardially with PBS followed by 4% PFA. After a 24 hr post-fixing period, immunolabeling and whole-brain clearing and immunolabeling was performed (Renier *et al*, 2014). A LaVision Ultramiscrope was used for light sheet imaging of cleared brains. Antibody used was rat monoclonal anti-mCherry (16D7; ThermoFisher M11217). For acquisition, cleared samples were imaged in a sagittal orientation (left lateral side up) on a light-sheet microscope (LaVision Biotec) equipped with a sCMOS camera and LVMI-Fluor 4x objective lens equipped with a 6-mm working distance dipping cap. Version v144 and v210 of Inspector Microscope controller software was used. Samples were scanned in the 640 nm channel. Images were taken every 6 mm and reconstructed with Imaris 9.1 software for visualization. For autofluorescence, the 480 nm channel was used with a 1.3x objective lens.

Quantification and Statistical Analysis.

Statistical parameters reported are: sample size (n = number of animals or samples per group), mean, statistical test used, and statistical significance. All data are displayed as mean ± SEM. Significance was defined as $p < 0.05$. Significance annotations are: * $p < 0.05$, ** $p < 0.01$, *** $p < 0.001$, **** $p < 0.0001$. Mice were randomized into control or treatment groups. Control mice were age-matched littermate controls where possible. All statistics and data analysis were performed using GraphPad Prism 9.

APPENDIX

Regulation of Energy Expenditure by Brainstem GABA Neurons

INDEX TO THE APPENDIX

*** Experimental Procedures and Supplementary Data can be found online at DOI:https://doi.org/10.1016/j.cell.2019.05.048

SUMMARY

Core body temperature is tightly regulated by the central nervous system to ensure survival. This is accomplished in part by both behavioral (i.e. locomotion) and physiologic (i.e. thermogenesis, vasodilatation) mechanisms. Here, we report that a population of GABAergic (Vgat-expressing) neurons in the dorsolateral portion of the dorsal raphe nucleus (DRN), hereafter DRN^{Vgat} neurons, are activated by ambient heat and bidirectionally regulate energy expenditure through changes in both thermogenesis and locomotor activity. We find that DRN^{Vgat} neurons polysynaptically innervate brown fat through a descending projection to the raphe pallidus. These neurons also exhibit significant ascending projections, which densely innervate numerous loci implicated in the central regulation of energy expenditure, such as the hypothalamus and extended amygdala. Optogenetic stimulation of these projection targets demonstrates that DRN^{Vgat} neurons are capable of regulating thermogenesis through a number of downstream effectors. This work establishes a key regulatory role for DRN^{Vgat} neurons in controlling energy expenditure.

INTRODUCTION

Core body temperature is maintained with great precision in mammals. This is accomplished through coordinated thermoregulatory processes that include both behavioral and autonomic components, such as shivering, adaptive thermogenesis, and skin vasodilatation. In addition to regulating core temperature, these processes are also fundamental to maintaining proper energy balance, and concomitantly, body weight (Munzberg et al., 2016; Saltzman and Roberts, 1995). While several recent reports have identified neuronal populations that regulate energy expenditure and thermogenesis, the neural mechanisms by which these pathways modulate the autonomic nervous system to control these processes is incompletely understood.

The anterior hypothalamus, particularly the preoptic area (POA), is a key node controlling thermoregulation (Hemingway et al., 1954; Magoun et al., 1938). Recent studies on the POA have identified specific cell types in this nucleus that are warm-sensitive, GABAergic neurons, which project broadly throughout the brain to regulate core body temperature. This is brought about through changes in interscapular brown adipose tissue (iBAT) thermogenesis and skin vasodilatation, as well as heat/cold seeking and avoidance behaviors (Tan et al., 2016; Zhao et al., 2017). While these data have established that the POA can sense and respond to changes in temperature, many other downstream nuclei are likely to be directly capable of regulating thermogenesis to augment or reduce energy expenditure.

Converging lines of functional and anatomic evidence implicate several brainstem nuclei in the central regulation of thermogenesis; however, the

functional significance of these populations in controlling thermogenesis has not been evaluated. One brainstem region that could potentially play a role in regulating thermogenesis is the dorsal raphe nucleus (DRN). Pharmacological and electrophysiological manipulations within the DRN can lead to changes in core and iBAT temperature (Dib et al., 1994; Hillegaart, 1991), and neurons within the DRN have been suggested to be sensitive to local and ambient increases in temperature (Hori and Harada, 1976; Weiss and Aghajanian, 1971). The DRN and bordering ventrolateral periaqueductal gray also receive input from warm-sensitive neurons within the medial preoptic area (Tan et al., 2016). Furthermore, the DRN potently regulates feeding, suggesting that this nucleus could play a more general role in controlling overall energy homeostasis (Nectow et al., 2017b).

In the current work, we use an unbiased whole-brain screen to identify brain regions that are activated in response to a thermal challenge. We find that GABAergic (Vgat-expressing) neurons within the DRN are activated by an increase in ambient temperature, and that chemogenetic modulation of these neurons potently regulates energy expenditure through changes in both thermogenesis and locomotor activity. We also find that these neurons polysynaptically innervate interscapular brown adipose tissue (iBAT) through a descending projection to the raphe pallidus to regulate iBAT thermogenesis. Furthermore, these neurons exhibit ascending projections to numerous loci directly implicated in the regulation of energy balance, such as the bed nucleus of the stria terminalis (BNST), dorsomedial hypothalamus (DMH), and medial preoptic area (MPOA), through which they are also capable of suppressing iBAT thermogenesis. Together, these studies identify the DRN as an important node embedded within

a distributed thermoregulatory circuit, and reveal a novel mechanism by which this brainstem nucleus regulates energy expenditure.

RESULTS

1) Whole-Brain Activity Mapping to Identify Neurons Within a Heat-Sensing Circuit

We set out to identify cell types within the brain that sense and respond to increases in ambient temperature in an unbiased manner using whole-brain activity mapping (Nectow et al., 2017b; Renier et al., 2016). Wild-type mice were either housed at room temperature (RT) conditions or exposed to a heat challenge of 38°C for 4 hr. After brain isolation, we used whole-brain clearing technology in tandem with whole-mount immunostaining (iDISCO+) (Renier et al., 2016) to identify sites of immediate-early gene Fos expression (Figure 1A). ClearMap software was then used for unbiased cell detection and registration to the Allen Brain Atlas. In this manner, we identified a number of brain regions with significantly increased levels of Fos expression after exposure to 38°C vs. RT conditions.

These analyses identified several brain regions that have previously been implicated in thermoregulation, including the ventromedial preoptic area (VMPO), the dorsomedial hypothalamus (DMH), and the paraventricular hypothalamus (PVH) (Figure 1B) (Morrison and Nakamura, 2011; Tan et al., 2016; Zhao et al., 2017). Indeed, the most significant activation was observed in the VMPO and the PVH, which are well-established sites of thermoregulation (Figure 1B). Having validated that this unbiased approach was capable of detecting heat-sensitive neurons distributed throughout the brain, we next searched for brain regions that have not directly been implicated in the central regulation of thermogenesis.

One of the brain regions that was significantly enriched in the warm (38°C) condition over RT was the brainstem's dorsal raphe nucleus (DRN). The DRN exhibited a 3.8-fold increase in Fos+ neurons in mice treated at 38°C, as compared to RT, an effect which was also dependent on the time mice were exposed to ambient warmth (Figure 1B). Previous studies from our group and others have implicated the DRN in the control of food intake and locomotor activity, but it is unknown whether neurons within this nucleus are directly capable of regulating thermogenesis (Dib et al., 1994; Nectow et al., 2017b; Veasey et al., 1997; Warden et al., 2012; Waterhouse et al., 2004). The pattern of neuronal activation we observed was predominantly in the dorsolateral aspects of the DRN, bordering along the ventrolateral periaqueductal gray (vlPAG). This sub-region of the DRN predominantly contains GABAergic neurons, which led us to hypothesize that the heat-sensitive neurons in the DRN could be GABAergic.

To test this hypothesis, we performed immunohistochemistry studies to co-localize Vgat, a marker of GABAergic neurons, and Fos in the DRN. Toward this end, we crossed Vgat-IRES-Cre knock-in mice to Cre-dependent GFPL10 reporter mice (Rosa26-LSL-GFPL10) followed by exposure of animals to RT or 38°C. We found a significant increase in Fos and Vgat co-localization after a thermal challenge of 38°C vs. RT controls (45% of Fos+ neurons were Vgat+ at 38°C, as compared to 20% at RT) (Figure 1C). These results demonstrate that GABAergic neurons within the DRN (hereafter, DRN^{Vgat} neurons) are activated by ambient warmth.

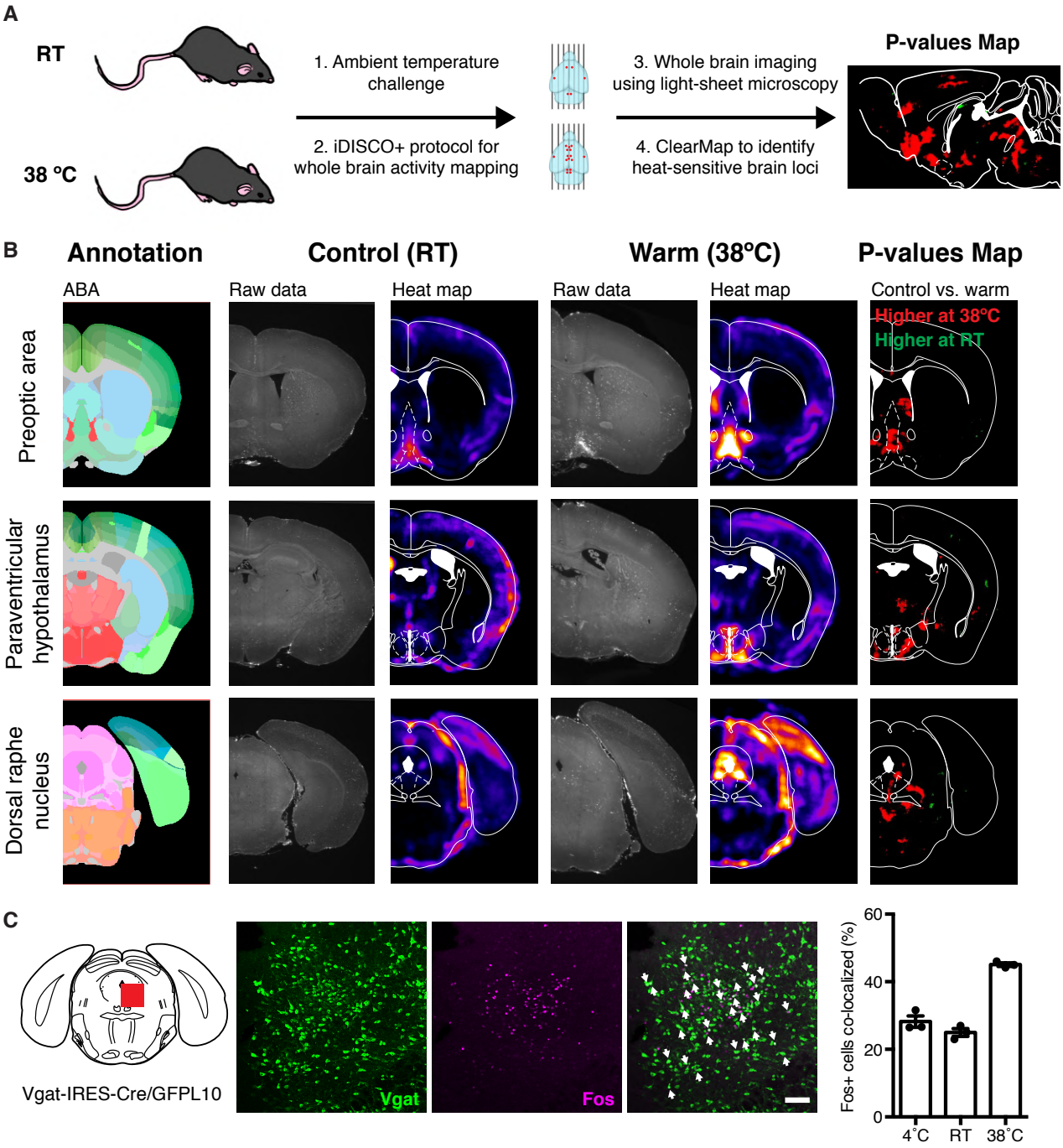
A
RT
38 °C
1. Ambient temperature challenge
2. iDISCO+ protocol for whole brain activity mapping
3. Whole brain imaging using light-sheet microscopy
4. ClearMap to identify heat-sensitive brain loci
P-values Map
B
Annotation
Control (RT)
Warm (38°C)
P-values Map
ABA
Raw data
Heat map
Raw data
Heat map
Control vs. warm
Higher at 38°C
Higher at RT
Preoptic area
Paraventricular hypothalamus
Dorsal raphe nucleus
C
Vgat-IRES-Cre/GFPL10
Vgat
Fos
Fos+ cells co-localized (%)
60
40
20
0
4˚C
RT
38˚C

Figure 1. Whole-Brain Fos Mapping Identifies Heat-Sensitive Neurons

(A) Schema for whole-brain activity mapping in response to ambient temperature challenge (RT vs. 38°C). Mice are sacrificed after a 4 hr challenge, followed by whole-brain clearing/immunostaining and registration with ClearMap, which generates a brain-wide p-values map.

(B) Whole-brain imaging and ClearMap results for the POA (top), hypothalamus (middle), and DRN (bottom). The ABA annotation is provided alongside raw Fos data, heat maps generated from these data, and p-values maps, which display differentially activated brain regions in warm versus RT conditions (n = 5 mice per group).

(C) Colocalization between Vgat and Fos after 38°C ambient temperature challenge. Significantly increased Fos and Vgat colocalization was observed at 38°C, as compared to room temperature ($p < 0.0001$). Unpaired t-test comparing treatments (n = 3 mice per group). White arrows designate double-labeled cells. Scale bar, 100 μm. ****$p < 0.0001$. Data are presented as mean ± SEM. See also Figures S1 and S2, and Table S1.

2) DRN^{Vgat} Neuron Activation Suppresses Energy Expenditure through Multiple Mechanisms, Including iBAT Thermogenesis

To assess whether DRN^{Vgat} neurons are capable of directly regulating thermogenesis, we used chemogenetics to activate these neurons and monitored changes in iBAT activity, as well as core and tail temperature. The activating designer receptor exclusively activated by designer drug (DREADD) hM3D(Gq) was targeted to DRN^{Vgat} neurons by injecting a Cre-dependent AAV5-hSyn-DIO-hM3D(Gq)-mCherry virus into the DRN of Vgat-IRES-Cre mice (Figure 2A, top). After at least three weeks, the mice received a set of sham injections to acclimate them to the procedure, after which they were given intraperitoneal (i.p.) injections of either vehicle (saline) or the DREADD ligand clozapine N-oxide (CNO) (Figure 2A, bottom). Changes in iBAT, core, and tail temperature were measured between 20 min pre-injection, through 3 hr post-injection. iBAT temperature was measured using either an infrared thermography camera, for thermal imaging of the shaved interscapular region in a first experiment (Figure 2B), and later using wireless, implantable temperature probes implanted in iBAT. Core body temperature was measured using an anal probe, while tail temperature was assessed using thermal imaging.

In our initial tests using infrared thermography of iBAT, we found that chemogenetically activating DRN^{Vgat} neurons significantly suppressed iBAT thermogenesis (Figure 2B). Building on this work, we again tested the effect of DRN^{Vgat} neuronal activation on modulating iBAT temperature (using thermal implants), but this time testing for changes in core body and tail temperatures, as well. Chemogenetic activation of DRN^{Vgat} neurons using CNO resulted in a

significant decrease in both iBAT and core body temperature, an effect which lasted as long as 3 hr post-injection of CNO (Figure 2C-2D). No changes were observed in tail temperature throughout the duration of these manipulations (supplementary data online).

Critically, these studies were performed in a 2x2 design, where DREADD-expressing (Vgat:hM3D(Gq)) mice were compared to non-DREADD expressing (control) mice, under both CNO- and saline- (vehicle) injected conditions. Thus, when these same groups of mice were injected with vehicle (saline) instead of CNO, we observed no changes in iBAT, core, or tail temperature within or between groups (supplementary data online). Together, this design enabled us to demonstrate that the observed effects were due specifically to DRN^{Vgat} neuron activation, namely that activation these neurons robustly suppresses iBAT, and concomitantly, core body temperature, with no changes in tail temperature.

We next tested whether activation of DRN^{Vgat} neurons could suppress energy expenditure through mechanisms other than iBAT thermogenesis. Towards this end, a new cohort of Vgat-IRES-Cre mice were injected with AAV5-hSyn-DIO-hM3D(Gq)-mCherry and were then placed in metabolic cages, enabling automated phenotyping of whole animal metabolic activity. After activation of DRN^{Vgat} neurons by injection of CNO, we observed a significant decrease in locomotor activity, oxygen consumption, carbon dioxide production, and concomitantly, overall energy expenditure, with no effect on control animals injected with CNO, which did not express the DREADD receptor (Figure 2E). Here, we also used a 2x2 study design, confirming that none of these effects occurred with injections of saline (vehicle) (supplementary data online).

Given that activating DRN^{Vgat} neurons suppresses locomotor activity (Figure 2E, right), we next asked whether the effects on thermogenesis were independent of locomotor activity suppression. To address this question, we repeated the above thermogenesis studies using an anesthetized preparation, placing mice in a lightly sedated plane of anesthesia, where they were thus experimentally immobilized. This experimental design would thus enable us to directly test the effect of activating DRN^{Vgat} neurons on iBAT temperature suppression, without the potentially confounding locomotor activity.

Critically, we found that chemogenetic activation of DRN^{Vgat} neurons under anesthesia was still able to significantly suppress both iBAT and core temperatures, with no effect on tail temperature (supplementary data online). Importantly, when these studies were repeated with saline (vehicle) injection instead of CNO (2x2 study design), no effects were observed (supplementary data online). These data together demonstrate 1) that activation of DRN^{Vgat} neurons reduces whole body energy expenditure by suppressing both thermogenesis and locomotor activity, and 2) that the effect on thermogenesis is independent of the suppression of locomotor activity.

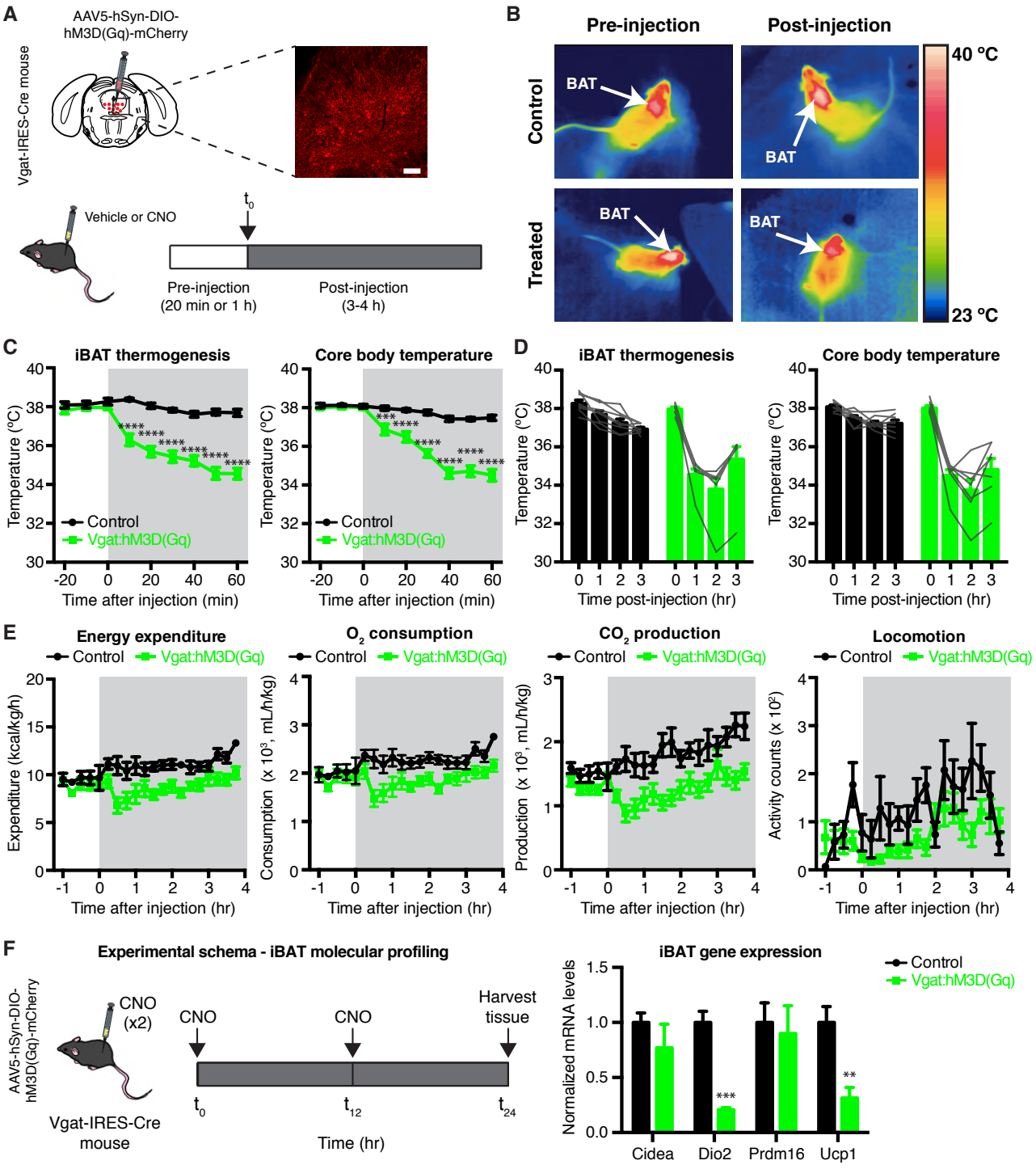
A
AAV5-hSyn-DIO-hM3D(Gq)-mCherry
Vgat-IRES-Cre mouse
Vehicle or CNO
t0
Pre-injection (20 min or 1 h)
Post-injection (3-4 h)
B
Pre-injection
Post-injection
Control
Treated
BAT
40 °C
23 °C
C
iBAT thermogenesis
Core body temperature
Temperature (ºC)
Control
Vgat:hM3D(Gq)
Time after injection (min)
D
iBAT thermogenesis
Core body temperature
Temperature (ºC)
Time post-injection (hr)
E
Energy expenditure
O2 consumption
CO2 production
Locomotion
Control
Vgat:hM3D(Gq)
Expenditure (kcal/kg/h)
Consumption (x 10³, mL/h/kg)
Production (x 10³, mL/h/kg)
Activity counts (x 10²)
Time after injection (hr)
F
Experimental schema - iBAT molecular profiling
AAV5-hSyn-DIO-hM3D(Gq)-mCherry
Vgat-IRES-Cre mouse
CNO (x2)
CNO
CNO
Harvest tissue
t0
t12
t24
Time (hr)
iBAT gene expression
Normalized mRNA levels
Control
Vgat:hM3D(Gq)
Cidea
Dio2
Prdm16
Ucp1

Figure 2. Chemogenetic Activation of DRN^{Vgat} Neurons Suppresses Energy Expenditure through Decreased iBAT Thermogenesis and Locomotor Activity

(A) Experimental schema for monitoring changes in thermogenesis and energy expenditure, and representative IHC for DRN^{Vgat} neurons infected with excitatory DREADD construct AAV5-hSyn-DIO-hM3D(Gq)-mCherry.

(B) Representative thermal images of iBAT (control or Vgat:hM3D(Gq)) before and after injection of CNO. Chemogenetic activation of DRN^{Vgat} neurons suppresses iBAT thermogenesis.

(C-D) Short- and long-term changes in iBAT temperature and core (anal) temperature after chemogenetic activation of DRN^{Vgat} neurons. (C) Activation of DRN^{Vgat} neurons significantly suppresses iBAT (Treatment: $p < 0.0001$) and core temperature (Treatment: $p < 0.0001$). Two-way RM-ANOVA comparing control and treated groups (n = 7-8 mice per group). (D) Average iBAT and core temperature at 0 to 3 hours post-CNO injection. iBAT ($p < 0.0001$) and core ($p < 0.0001$) temperatures remain significantly suppressed 3 hr post-CNO injection. Two-way RM ANOVA comparing t=0 and t=3 hr post-CNO injection (n = 7-8 mice per group).

(E) Chemogenetic activation of DRN^{Vgat} neurons suppresses locomotor activity (Treatment: $p < 0.05$), oxygen consumption (Treatment: $p < 0.05$), carbon dioxide production (Treatment: $p < 0.01$), and concomitantly energy expenditure (Treatment: $p < 0.01$). Two-way RM ANOVA comparing control and treated groups after CNO injection (n = 4-6 mice per group).

(F) Molecular profiling of iBAT after chemogenetic activation of DRN^{Vgat} neurons. Genes tested: *Cidea* ($p > 0.05$), *Dio2* ($p < 0.001$), *Prdm16* ($p > 0.05$), *Ucp1* ($p < 0.01$). Unpaired t-tests comparing treatments (n =4-5 samples per group).

Scale bar, 100 μm. *$p < 0.05$, **$p < 0.01$, ***$p < 0.001$, ****$p < 0.0001$. Data are presented as mean ± SEM. See also Figure S2.

3) Inhibition of DRN^{Vgat} Neurons Augments Energy Expenditure Independent of Changes in iBAT Thermogenesis

We next investigated whether inhibition of DRN^{Vgat} neurons could augment energy expenditure. We transduced DRN^{Vgat} neurons with the inhibitory DREADD hM4D(Gi) by injecting the DRN of Vgat-IRES-Cre mice with Cre-dependent AAV5-hSyn-DIO-hM4D(Gi)-mCherry (Figure 3A, top). Following viral incubation and a series of sham injections, control and treated mice were then injected i.p. with either vehicle or CNO (vehicle and CNO studies were performed on separate days, in a 2x2 experimental design, as described above) (Figure 3A, bottom). In contrast to activation of DRN^{Vgat} neurons, chemogenetic inhibition of these neurons had no effect on iBAT temperature, as assessed by infrared thermography (Figure 3B). To ensure that this effect (or lack thereof) was not an artifact of the limited sensitivity of the combined shaved interscapular region/infrared thermography approach, we repeated these studies using implantable, wireless thermal probes, while also monitoring for core and tail temperature, as in the chemogenetic activation studies (**Figure 2**).

Consistent with the above results, we found that chemogenetic inhibition of DRN^{Vgat} neurons had no effect on iBAT temperature (**Figures 3C-3D**); however, inhibiting these neurons resulted in a small but significant increase of core body temperature (**Figures 3C-3D**). No effect was observed on tail temperature, suggesting that this increase in core body temperature was not due to a change in peripheral vasodilatation (supplementary data online). As expected, we did not observe any effect on iBAT, core, or tail temperature in control animals receiving CNO (Figures 3C-3D), or after injection of vehicle into

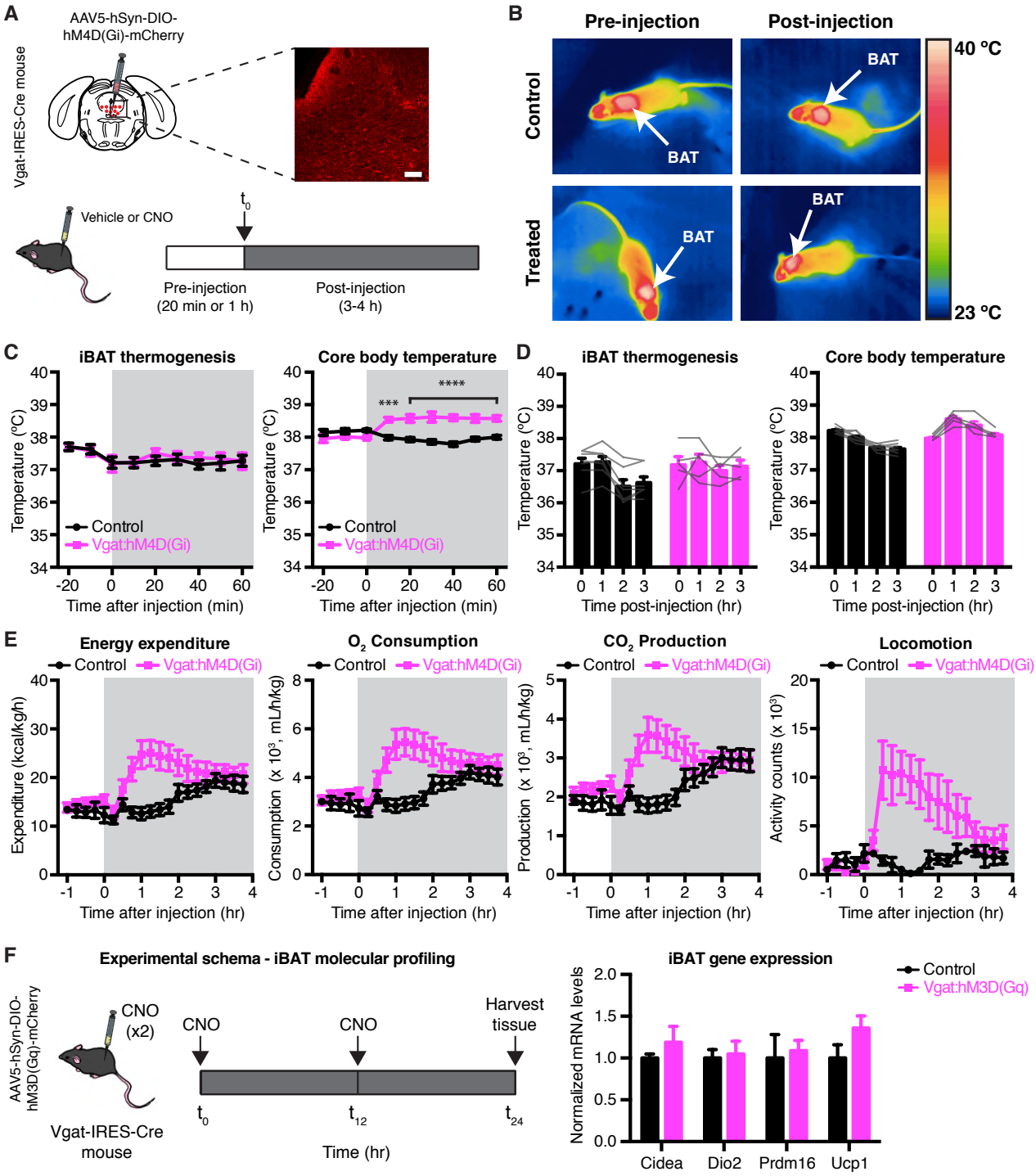
A
AAV5-hSyn-DIO-hM4D(Gi)-mCherry
Vgat-IRES-Cre mouse
Vehicle or CNO
t0
Pre-injection (20 min or 1 h)
Post-injection (3-4 h)
B
Pre-injection
Post-injection
Control
Treated
BAT
40 °C
23 °C
C
iBAT thermogenesis
Core body temperature
Temperature (°C)
Control
Vgat:hM4D(Gi)
***
****
Time after injection (min)
D
iBAT thermogenesis
Core body temperature
Temperature (°C)
Time post-injection (hr)
E
Energy expenditure
O2 Consumption
CO2 Production
Locomotion
Control
Vgat:hM4D(Gi)
Expenditure (kcal/kg/h)
Consumption (x 10³, mL/h/kg)
Production (x 10³, mL/h/kg)
Activity counts (x 10³)
Time after injection (hr)
F
Experimental schema - iBAT molecular profiling
AAV5-hSyn-DIO-hM3D(Gq)-mCherry
Vgat-IRES-Cre mouse
CNO (x2)
CNO
CNO
Harvest tissue
t0
t12
t24
Time (hr)
iBAT gene expression
Control
Vgat:hM3D(Gq)
Normalized mRNA levels
Cidea
Dio2
Prdm16
Ucp1

Figure 3. Chemogenetic Inhibition of DRN^{Vgat} Neurons Augments Energy Expenditure through Increased Locomotor Activity but not iBAT Thermogenesis

(A) Experimental schema for monitoring thermogenesis and energy expenditure, and representative IHC for DRN^{Vgat} neurons infected with inhibitory DREADD construct AAV5-hSyn-DIO-hM4D(Gi)-mCherry.

(B) Representative thermal images of iBAT (control or Vgat:hM3D(Gq)) before and after injection of CNO. Chemogenetic inhibition of DRN^{Vgat} neurons has no effect on iBAT thermogenesis.

(C-D) Quantification of iBAT temperature from thermal imaging and core (anal) temperature after chemogenetic inhibition of DRN^{Vgat} neurons. (C) Inhibition of DRN^{Vgat} neurons has no effect on iBAT temperature (Treatment: $p > 0.05$), but augments core temperature (Treatment: $p < 0.0001$). Two-way RM-ANOVA comparing control and treated groups (n = 5-7 mice per group). (D) Average iBAT ($p > 0.05$) and core temperature ($p > 0.05$) at 0 and 3 hours post-CNO injection. Two-way RM ANOVA comparing t=0 and t=3 hr post-CNO injection (n = 5-7 mice per group).

(E) Chemogenetic inhibition of DRN^{Vgat} neurons increases locomotor activity (Treatment: $p < 0.05$), oxygen consumption (Treatment: $p < 0.05$), carbon dioxide production (Treatment: $p = 0.087$), and concomitantly energy expenditure (Treatment: $p < 0.05$). Two-way RM ANOVA comparing control and treated groups after CNO injection (n = 7 mice per group).

(F) Molecular profiling of iBAT after chemogenetic inhibition of DRN^{Vgat} neurons. Genes tested: *Cidea* (n.s.), *Dio2* (n.s.), *Prdm16* (n.s.), *Ucp1* (n.s.). Unpaired t-tests comparing treatments (n =6 samples per group).

Scale bar, 100 μm. *$p < 0.05$, **$p < 0.01$, ***$p < 0.001$, ****$p < 0.0001$, n.s. not significant. Data are presented as mean ± SEM. See also Figure S3.

treated or control animals (supplementary data online), demonstrating that the observed effects are specific to inhibition of DRN^{Vgat} neurons.

The observation that DRN^{Vgat} inhibition increases core temperature in the absence of an increased iBAT temperature (and within the setting of no changes in peripheral vasodilatation) raised the possibility that this effect was mediated by an increase in locomotor activity. To address this, a separate cohort of Vgat-IRES-Cre mice was injected with AAV5-hSyn-DIO-hM4D(Gi)-mCherry, before being placed in metabolic cages. Inhibition of DRN^{Vgat} neurons resulted in a striking and significant increase in locomotor activity, as well as oxygen consumption and carbon dioxide production, with a concomitant increase in total energy expenditure, with no effects observed in CNO-injected control mice (Figure 3E). In contrast, neither control nor treated mice injected with vehicle exhibited any changes in these parameters (supplementary data online). These results – namely, the augmented locomotor activity and lack of effect on skin vasodilatation (tail temperature) – suggested that chemogenetic inhibition of DRN^{Vgat} neurons augments core body temperature secondary to an increase in locomotor activity.

We thus asked whether the observed increase in core body temperature after inhibiting DRN^{Vgat} neurons was dependent on augmented locomotor activity. To address this question, we performed chemogenetic inhibition studies of DRN^{Vgat} neurons under a sedating plane of anesthesia (as described earlier), which would enable the decoupling of DRN^{Vgat} neuron inhibition from increased locomotion. We predicted that by eliminating the locomotor activity increase during chemogenetic inhibition of DRN^{Vgat} neurons, we could occlude its effect on core body temperature. Consistent with this hypothesis, we found that lightly anesthetizing

mice while chemogenetically inhibiting DRN^{Vgat} neurons led to a complete occlusion of the DRN^{Vgat} inhibition-induced increase in core body temperature (supplementary data online). Of note, inhibition of DRN^{Vgat} neurons under anesthesia also had no effect on iBAT thermogenesis or tail temperature, and no effects were observed on any of these parameters in saline treated mice (supplementary data online).

The above studies demonstrate that inhibition of DRN^{Vgat} neurons has no effect on iBAT thermogenesis. In line with these findings, we expectedly found that inhibiting these neurons does not lead to any changes in biochemical markers on thermogenesis in brown fat (Figure 4F). Inhibition of DRN^{Vgat} neurons thus elevates core body temperature secondarily to augmentation of locomotor activity, and not through direct effects on brown fat thermogenesis or skin vasodilatation.

Together with the chemogenetic activation studies, these results demonstrate that DRN^{Vgat} neurons can robustly and bidirectionally modulate overall energy expenditure, albeit through asymmetrical effects on behavior and physiology. Namely, activation of DRN^{Vgat} neurons suppresses energy expenditure through a reduction of both iBAT thermogenesis and locomotor activity, whereas inhibition of these neurons augments energy expenditure through an increase in locomotor activity, independent of iBAT thermogenesis.

4) Retrograde Circuit Mapping Reveals a GABAergic Brainstem Projection Polysynaptically Innervating iBAT

We next asked whether DRN^{Vgat} neurons innervate brown fat, an organ critical for regulating thermogenesis, by performing polysynaptic tracing studies from interscapular brown adipose tissue (iBAT). In these studies, we combined retrograde tracing using a replication-competent pseudorabies virus (PRV) with whole-mount immunolabeling and clearing technology iDISCO+ (Figure 4A). To perform polysynaptic retrograde tracing from iBAT, we used a PRV engineered to constitutively express mCherry (PRV-lp298, hereafter PRV-mCherry) (Pomeranz et al., 2017). When injected into a neuron's terminal field, PRV is taken up by local axon terminals and retrogradely transported to the cell's soma, where it replicates and then 'hops' to neurons directly upstream; replicating PRV variants, such as PRV-mCherry, continue to 'hop' synapses retrogradely until the animal succumbs to the infection (after ~7 days) (Figure 4A). We thus set out to conduct a time course study to monitor the spread of PRV into the brain, which would indicate a polysynaptic circuit from the brain to iBAT. In these studies, the most proximate nodes in the circuit (with respect to iBAT) are labeled at the earliest time points, whereas more distal nodes are labeled at later time points.

PRV-mCherry was injected into iBAT of wild-type mice, followed by an incubation period of either 4 or 5 days, which were the earliest time points at which PRV was detected in the brain. At each time point, mice were sacrificed, and their brains were immunostained for mCherry and clarified using iDISCO+, followed by light-sheet imaging and analysis using ClearMap. At 4 days post-infection, we found sparse viral expression within the brain, with robust labeling in the raphe

pallidus (RPa), a site of sympathetic outflow, and the PVH, which is also known to project indirectly to iBAT (Figure 4B) (An et al., 2015; Cannon and Nedergaard, 2004; Ryu et al., 2015). These data suggest that these sites are early (i.e. first- or second-order) nodes in the brain circuit polysynaptically innervating iBAT. At day 5 post-infection, mCherry expression was relatively unchanged in these two regions (Figure 4C). In contrast, there was no PRV expression observed in the DRN at day 4 post-injection. However, at day 5, we observed strong labeling of the DRN, suggesting that neurons within this region also project polysynaptically to iBAT, presumably by sending outputs to the PVH and/or RPa (Figures 4B and 4C).

The PRV labeling at day 5 post-injection was located predominantly in the dorsolateral portion of the DRN (bordering along the ventrolateral portion of the periacqueductal gray, vlPAG), an area containing a significant number of Vgat-positive neurons. To confirm that DRN^{Vgat} neurons polysynaptically innervate iBAT, we repeated our PRV tracing studies in transgenic mice where DRN^{Vgat} neurons are fluorescently labeled. We accomplished this aim by crossing Vgat-IRES-Cre mice to Cre-dependent GFPL10 reporter mice, followed by injection of PRV-mCherry into the iBAT of these mice. After a 5 day viral incubation period (allowing for robust labeling of the dorsolateral DRN), we found significant colocalization between neurons labeled for Vgat and PRV, with ~56% of DRN^{Vgat} neurons showing expression of mCherry, indicative of PRV infection. Similarly, ~55% of PRV+ neurons expressed Vgat (Figure 4D).

Notably, the dorsolateral compartment of the DRN (bordering along the vlPAG), is the same region where we identified warm-sensitive DRN^{Vgat} neurons

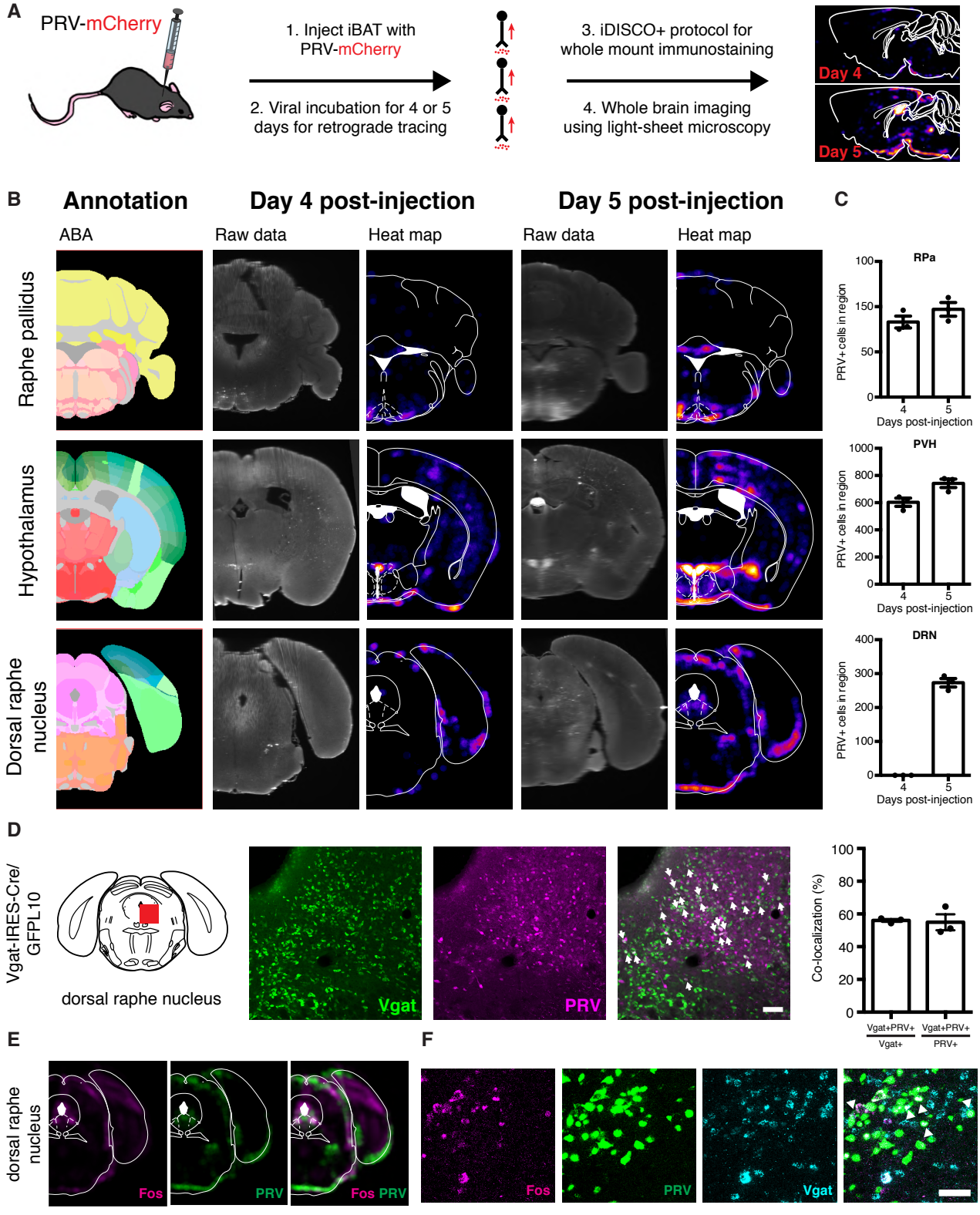
A
PRV-mCherry
1. Inject iBAT with PRV-mCherry
2. Viral incubation for 4 or 5 days for retrograde tracing
3. iDISCO+ protocol for whole mount immunostaining
4. Whole brain imaging using light-sheet microscopy
Day 4
Day 5
B
Annotation
Day 4 post-injection
Day 5 post-injection
ABA
Raw data
Heat map
Raw data
Heat map
Raphe pallidus
Hypothalamus
Dorsal raphe nucleus
C
RPa
PVH
DRN
PRV+ cells in region
Days post-injection
D
Vgat-IRES-Cre/ GFPL10
dorsal raphe nucleus
Vgat
PRV
Co-localization (%)
Vgat+PRV+ / Vgat+
Vgat+PRV+ / PRV+
E
dorsal raphe nucleus
Fos
PRV
Fos PRV
F
Fos
PRV
Vgat

Figure 4. DRN^{Vgat} Neurons Polysynaptically Project to Interscapular Brown Adipose Tissue (iBAT)

(A) Schema for whole-brain mapping of neurons projecting polysynaptically to iBAT. Mice are sacrificed after 4 d or 5 d post-iBAT injection of PRV, followed by whole-brain clearing and immunostaining for mCherry. After light-sheet imaging of the brains, ClearMap is applied, which generates brain-wide heat maps of PRV-infected neurons.

(B) iDISCO whole-brain imaging results (raw data and heat maps) alongside the ABA annotation for the RPa (top), hypothalamus (middle), and DRN (bottom).

(C) Cell counts (manual) from brain slices for PRV-infected cells at 4- and 5-days post-infection of PRV in iBAT. No changes were observed from day 4 to day 5 for RPa (n.s.), while significant increases in cell counts were observed for PVH ($p < 0.05$) and DRN ($p < 0.0001$). Unpaired t-test comparing treatments (n = 3 mice per group).

(D) Colocalization (and quantification) between Vgat and PRV retrogradely labeled from iBAT 5 d post-injection (n = 3 mice per group). White arrows designate double-labeled cells.

(E) Regional colocalization between warm-sensitive (Fos-positive) and iBAT-projecting (PRV-positive) neurons within the dorsolateral DRN (left).

(F) Cellular colocalization between DRN^{Vgat} neurons, tdTomato (warm-sensitive neurons), and EGFP (neurons polysynaptically innervating iBAT).

Scale bar, 100 μm. Data are presented as mean ± SEM.

by activity mapping (Figure 1). We confirmed this regional colocalization using ClearMap software to co-register the results from the DRN Fos activity mapping study (38°C treatment group) with the heat map of PRV brains at day 5 post-injection (enabling direct anatomic comparison of these two separate studies). Image co-registration demonstrated marked regional overlap between the heat-activated and polysynaptically iBAT-projecting DRN neurons (Figure 4E).

Building on this finding, we wanted to directly confirm that there is cellular overlap between heat-activated DRN^{Vgat} neurons and those DRN^{Vgat} neurons that project to iBAT. We thus performed dual activity-dependent genetic labeling of warm-activated DRN neurons in tandem with polsynaptic PRV mapping, followed by multiplex fluorescence *in situ* hybridization (FISH) to label Vgat-positive neurons. To label warm-activated DRN neurons, we crossed TRAP2 mice (which express an activity-dependent, inducible Cre, which is activated by injection of 4-hydroxytamoxifen, 4-OHT), to tdTomato reporter (Ai14) mice (Allen et al., 2017; Madisen et al., 2010). To fluorescently label warm-sensitive DRN neurons, we exposed these mice to 38°C ambient temperature for 4 hr, immediately after injecting them with 4-OHT (to activate expressed Cre recombinase). This procedure enabled us to label significant numbers of neurons within the dorsolateral DRN. We then injected these mice with a retrograde-tracing, replication-competent EGFP-expressing PRV (PRV-152, hereafter PRV-EGFP), allowing 5 days to elapse post-injection to label the DRN (Smith et al., 2000). These mice were then sacrificed, and multiplex FISH was performed to co-localize warm-sensitive (tdTomato-positive), iBAT-projecting (EGFP-positive), GABAergic (Vgat-positive) neurons within the DRN. Using this approach, we were able to

identify significant numbers of neurons within the dorsolateral aspect of the DRN, which are Vgat-positive, warm-sensitive, and polysynaptically innervate iBAT (Figure 4F).

Taken together, these studies demonstrate that subsets of DRN^{Vgat} neurons are both warm-sensitive and polysynaptically project to iBAT, and further suggest that these neurons may directly contribute to the sense-and-respond system that is responsible for regulating thermogenesis.

5) DRN^{Vgat} Neurons Project Broadly to Brain Loci Known to Regulate Energy Expenditure

The DRN projects broadly throughout the brain; however, the precise downstream projection targets of DRN^{Vgat} neurons have not been established. Thus, while previous studies have mapped the ascending (Vertes, 1991) and brainstem (Vertes and Kocsis, 1994) projections of the DRN overall, cell type-specific outputs have remained largely undefined (Ren et al., 2018). To systematically map these projections, we again used iDISCO+ whole-brian mapping (Renier et al., 2016; Renier et al., 2014) combined with adeno-associated virus (AAV)-mediated tracing. To selectively label the projections of DRN^{Vgat} neurons, we injected AAV9-FLEX-GFP into the DRN of Vgat-IRES-Cre mice (Figure 5A). After six weeks, mice were sacrificed and their brains were immunostained for GFP and cleared using the iDISCO+ protocol. We then used light sheet imaging of the cleared whole brain to visualize the projection sites of DRN^{Vgat} neurons ((supplementary movie online).

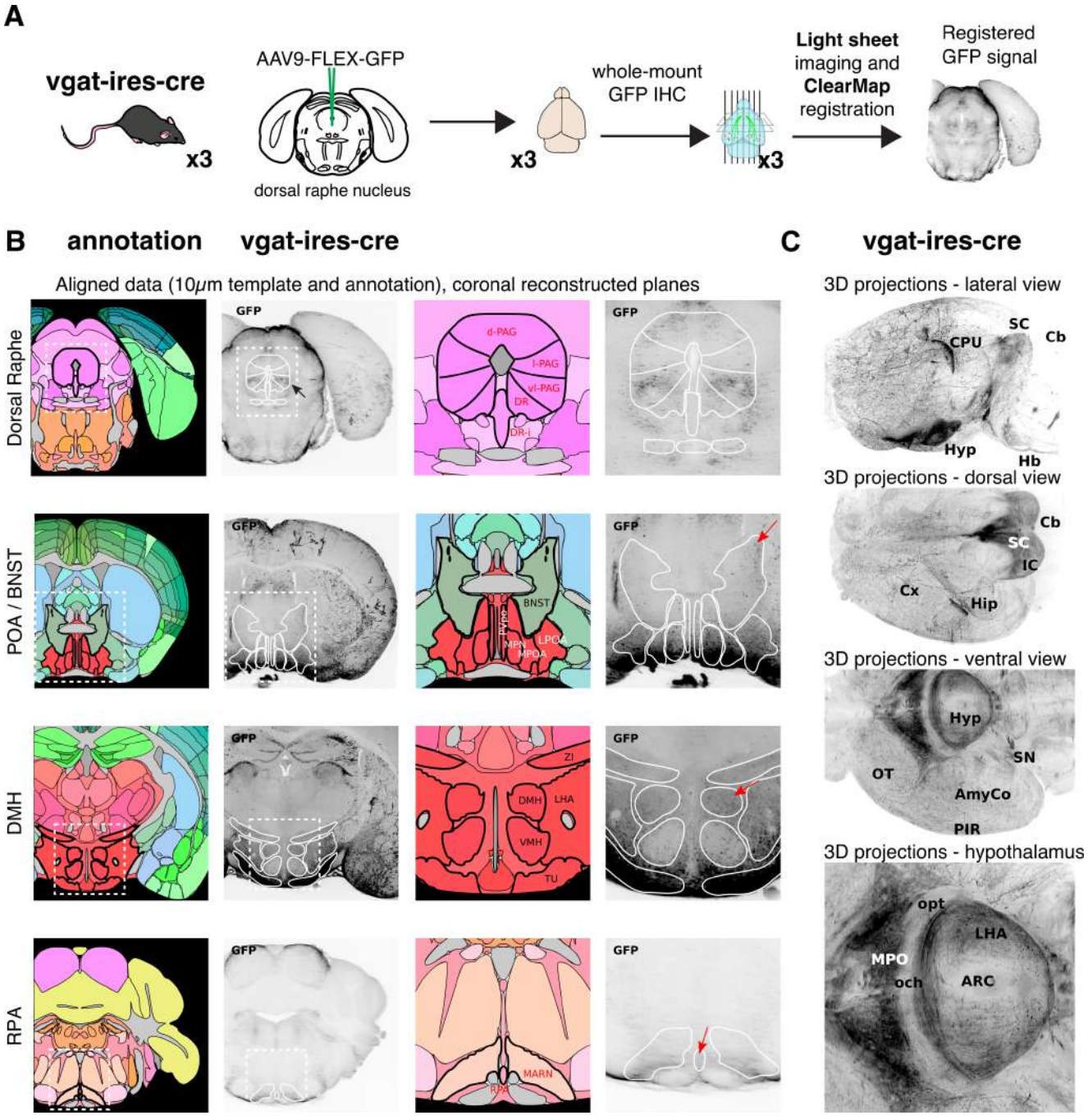
A
vgat-ires-cre
x3
AAV9-FLEX-GFP
dorsal raphe nucleus
x3
whole-mount
GFP IHC
x3
Light sheet
imaging and
ClearMap
registration
Registered
GFP signal
B
annotation
vgat-ires-cre
Aligned data (10μm template and annotation), coronal reconstructed planes
Dorsal Raphe
POA / BNST
DMH
RPA
GFP
d-PAG
l-PAG
vl-PAG
DR
DR-l
BNST
MPN
LPOA
MPOA
ZI
DMH
LHA
VMH
TU
MARN
RPA
C
vgat-ires-cre
3D projections - lateral view
SC
CPU
Cb
Hyp
Hb
3D projections - dorsal view
Cb
SC
IC
Cx
Hip
3D projections - ventral view
Hyp
SN
OT
AmyCo
PIR
3D projections - hypothalamus
opt
LHA
MPO
och
ARC

Figure 5. DRN^{Vgat} Neurons Project to Multiple Brain Regions Implicated in Regulating Thermogenesis

(A) Schema for whole-brain mapping of DRN^{Vgat} neurons. Terminal projection mapping is performed using AAV-mediated projection mapping in tandem with whole-brain imaging.

(B) Ascending projections from DRN^{Vgat} neurons are observed in numerous loci implicated in the central regulation of energy balance, such as the extended amygdala, and hypothalamic structures such as the dorsomedial hypothalamus and preoptic area. Descending projections to the brainstem are also validated for the RPa. Red arrows highlight (top to bottom) BNST, DMH, and RPa.

(C) Whole-brain, 3D images of DRN^{Vgat} projections throughout the brain, from multiple viewpoints.

Three-dimensional mapping of DRN^{Vgat} projections revealed broad projections throughout the (supplementary data online).only a few sparse projections from DRN^{Vgat} neurons were seen in cortex, principally in motor cortex, dense innervation was observed in a number of structures known to regulate energy balance (supplementary data online). For example, we observed dense innervation of the hypothalamus, notably within the POA, DMH, and lateral hypothalamus (LH), but not in the ventromedial hypothalamus (VMH) or paraventricular hypothalamus (PVH), as well as projections to the brainstem's raphe pallidus (RPa) (Figure 5B). We also noted significant projections to the amygdalar complex/extended amygdala (e.g. the bed nucleus of the stria terminalis, BNST), as well as the parabrachial nucleus (PBN), which have also been implicated in the central regulation of energy homeostasis (Tan and Knight, 2018; Waterson and Horvath, 2015; Yahiro et al., 2017). These results demonstrate that DRN^{Vgat} neurons send long-range ascending and descending projections to many regions known to regulate thermogenesis and other processes critical for the proper maintenance of energy balance.

6) DRN^{Vgat} Neurons Polysynaptically Innervate iBAT through a Projection to the Raphe Pallidus to Regulate Thermogenesis

We next set out to better understand the connectivity through which DRN^{Vgat} neurons polysynaptically innervate iBAT. From our polysynaptic retrograde circuit mapping studies using PRV, we had demonstrated that the two principal brain regions that could be downstream of DRN^{Vgat} neurons are the PVH or the RPa (Figure 4). However, from our projection mapping studies, we found that DRN^{Vgat} neurons appear to innervate the RPa, but not the PVH (Figure 5). We thus set out to validate the projection from DRN^{Vgat} neurons to the RPa.

To establish an anatomic connection between DRN^{Vgat} neurons and the RPa, we took two parallel approaches: retrograde tracing from the RPa (to DRN^{Vgat} neurons) and anterograde tracing from DRN^{Vgat} neurons (to the RPa). For our retrograde tracing studies, we injected the retrograde-tracing, Cre-dependent AAVrg-EF1a-DIO-ChR2-mCherry into the RPa of Vgat-IRES-Cre mice, a strategy which will label Vgat-positive neurons projecting to the RPa. After allowing for sufficient time for retrograde transport and gene expression, we performed immunohistochemical staining for mCherry within the DRN, observing significant labeling of neurons within the dorsolateral DRN (Figure 6A). In a separate cohort of mice, we injected the DRN of Vgat-IRES-Cre mice with the anterograde tracing AAV9-FLEX-GFP. After allowing for sufficient time for expression of GFP, we performed immunolabeling in the RPa against GFP, finding significant projections to this region (Figure 6B). Together, these two anatomic studies demonstrate that DRN^{Vgat} neurons innervate the RPa, suggesting that this is a functional component of the polysynaptic circuit from DRN^{Vgat} neurons to iBAT.

Having established that DRN^{Vgat} neurons project to the RPa, we next asked whether this circuit (which ultimately polysynaptically innervates iBAT) could suppress iBAT thermogenesis. To accomplish this aim, we injected the retrograde-tracing AAVrg-EF1a-DIO-ChR2-mCherry into the RPa of Vgat-IRES-Cre mice. Following placement of an optical fiber over the DRN, this would enable us to photoactivate DRN^{Vgat} neurons projecting to the RPa (Figure 6C). We tested the effect of stimulating this projection target on iBAT thermogenesis using wireless implants in iBAT. The assay was performed over the course of one hour, and was comprised of three, 20 min epochs: pre-stimulation, stimulation, and post-stimulation. We found that photoactivation of DRN^{Vgat} neurons projecting to the RPa at 20 Hz resulted in a significant suppression in iBAT temperature, an effect which rapidly diminished after cessation of photostimulation (Figure 6D). Notably, this effect was also frequency-dependent, as lower stimulation intensities of 5 and 10 Hz led to no effect on iBAT thermogenesis (Figure 6D).

Collectively, these results identify a polysynaptic circuit from DRN^{Vgat} neurons to iBAT (Figure 6F), routed as a descending projection through the RPa, which is directly capable of suppressing thermogenesis.

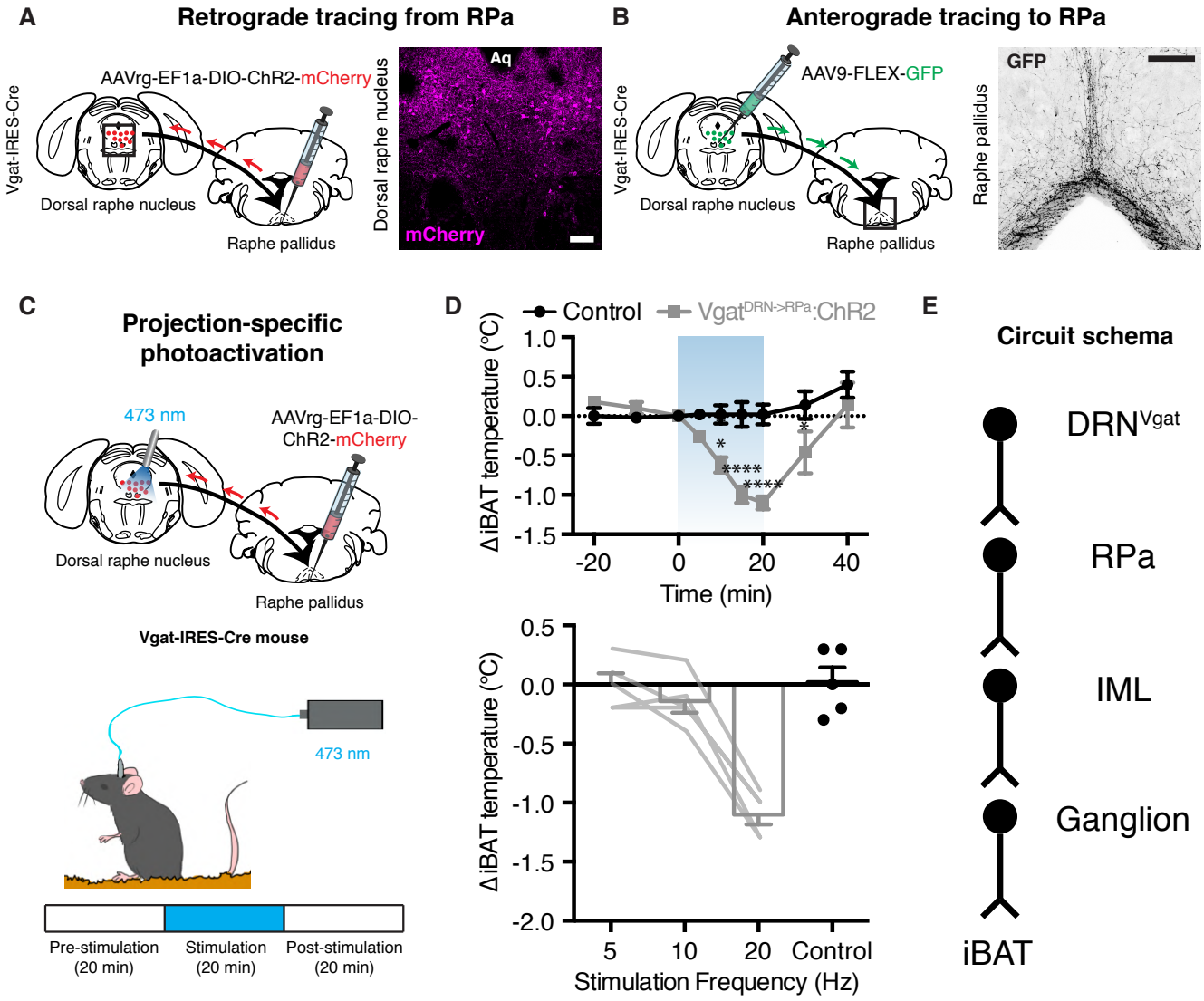

Scale bars, 100 um

Figure 6. DRN^{Vgat} Neurons Communicate with iBAT through the RPa to Regulate Thermogenesis.

(A) Retrograde labeling of DRN^{Vgat} neurons from injection of retrograde-tracing AAVrg-EF1a-DIO-ChR2-mCherry into the RPa of Vgat-IRES-Cre mice.

(B) Anterograde labeling of RPa after injection of anterograde-targeting AAV-EF1a-DIO-GFP into the DRN of Vgat-IRES-Cre mice.

(C) Schematic for projection-specific photoactivation of DRN^{Vgat} neurons innervating the RPa.

(D) (Top) Activation of DRN^{Vgat} neurons projecting to the RPa significantly suppresses iBAT temperature (Treatment: $p < 0.001$). Two-way RM ANOVA comparing control and treated groups (n = 5 mice per group). Blue-shaded region highlights Laser On epoch. (Bottom) This effect is frequency-dependent, with only 20 Hz – but not lower stimulation intensities – inducing changes in iBAT temperature.

(E) Circuit schema of DRN^{Vgat} neurons polysynaptically innervating iBAT through the RPa.

Scale bars, 100 μm. *$p < 0.05$, ****$p < 0.0001$. Data are presented as mean ± SEM.

7) Ascending DRN GABAergic Projections to BNST, DMH, and MPOA Regulate iBAT Thermogenesis

In our projection mapping studies, we found that DRN^{Vgat} neurons exhibit not only descending projections to the brainstem, but numerous ascending projections, as well. We thus set out to test whether any ascending projection sites of DRN^{Vgat} neurons could regulate thermogenesis, focusing on three nodes directly implicated in the central regulation of energy homeostasis: the BNST, DMH, and MPOA. The MPOA is contains 'warm-sensitive' neurons, which provide significant input to both the BNST and DMH; together with our projection mapping data, this suggests the intriguing possibility that DRN^{Vgat} neurons could be an important new node within this established thermoregulatory network (Tan et al., 2016; Zhao et al., 2017).

Before testing the functional effect of activating DRN^{Vgat} terminals, we reconfirmed that the DRN^{Vgat} neurons project to these regions using projection-specific terminal mapping. We accomplished this aim using synaptophysin-XFP fusion constructs, which direct fluorophore expression selectively to nerve terminals. These viruses were thus injected into the DRN of Vgat-IRES-Cre mice, followed by an incubation period of at least 4 weeks to allow for sufficient gene expression and anterograde transport of the synaptophysin-XFP fusion construct to nerve terminals. Mapping of fluorophore expression in nerve terminals indeed confirmed that DRN^{Vgat} neurons send projections to the BNST, DMH, and MPOA (Figure 7A).

We next asked whether activation of projections to these regions was sufficient to elicit a decrease in iBAT thermogenesis. Towards this end, we injected

AAV5-EF1a-DIO-ChR2-EYFP into the DRN of Vgat-IRES-Cre mice, followed by placement of an optical fiber above the BNST, DMH, or MPOA (Figure 7B, left). We then tested the effect of activating these projections by monitoring iBAT temperature using a wireless temperature transponder (as above) in three 20 min epochs (pre-stimulation, stimulation, and post-stimulation) using 20 Hz laser stimulation (Figure 7B, right). Photoactivation of projections to the BNST, DMH, and MPOA all led to a significant suppression of iBAT temperature, with temperature recovering to baseline levels 20 min after photostimulation ceased (Figure 7C). We also sought to better understand the dose response of stimulating DRN^{Vgat} neuron projections to suppress thermogenesis. We found that photostimulating DRN^{Vgat} terminals in each of the three loci dose-dependently suppressed iBAT thermogenesis, with maximal effect observed at 20 Hz (Figure 7D). In comparing the effect of iBAT suppression across projection targets, we found no differences in the magnitude of the observed reduction in brown fat temperature (supplementary data online). In previous work, we demonstrated that DRN^{Vgat} neurons also regulate food intake (Nectow et al., 2017b). We thus asked whether any of these projection sites could regulate food intake, as well. Of note, the BNST and DMH are important sites known to be integrated within core homeostatic circuits regulating both food intake and thermogenesis (Garfield et al., 2016; Tan et al., 2016). Our data thus suggest that these nuclei could serve as important convergence points through which DRN^{Vgat} neurons regulate energy homeostasis. Through projection-specific photostimulation studies, we found that DRN^{Vgat} projections to the BNST and DMH, but importantly not the MPOA or RPa, augment food intake in a scalable fashion,

consistent with our previous studies (supplementary data online). These data also demonstrate that different projection sets of DRN^{Vgat} neurons differentially regulate energy homeostasis through behavioral and physiologic means.

Together with our projection mapping studies, these data demonstrate that DRN^{Vgat} neurons can regulate energy balance via vast projections to the forebrain and hindbrain in a scalable fashion.

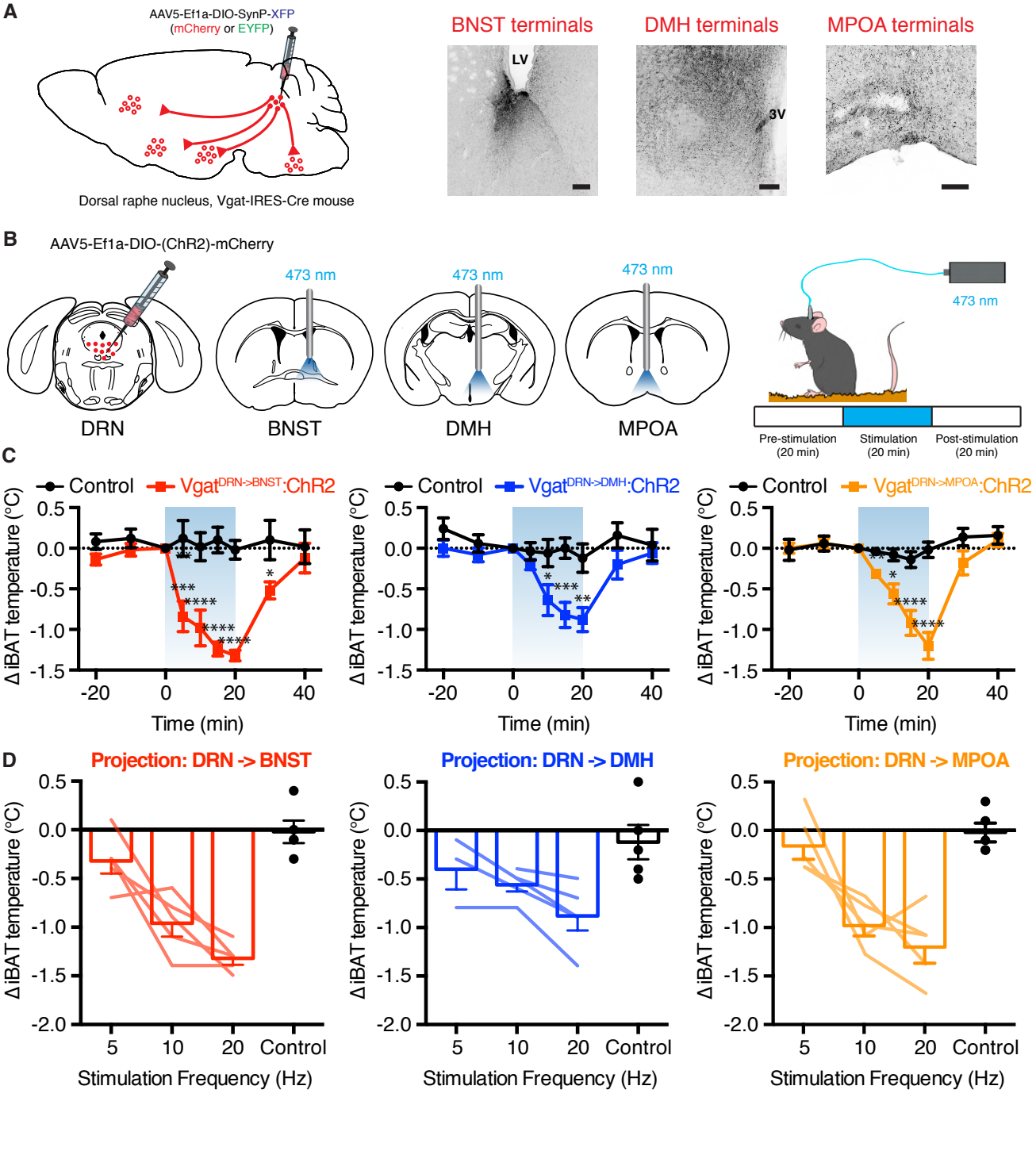

SCALE BARS???
MPOA = 100um

Figure 7. DRN^{Vgat} Neurons Regulate iBAT Thermogenesis through Multiple Ascending Projections

(A) Experimental schema and representative IHC for validation of DRN^{Vgat} projections to BNST, DMH, and MPOA. For terminal mapping, viral construct AAV9-DIO-SynP-mCherry is injected into the DRN of Vgat-IRES-Cre mice (left). Representative IHC of terminal staining in both the BNST (middle) and DMH (right).

(B) Experimental schema for DRN^{Vgat} neuron terminal stimulation. DRN^{Vgat} neurons are transduced with AAV5-EF1a-DIO-hChR2(H134R)-EYFP, followed by placement of an optical fiber above either the BNST, DMH, or MPOA. Mice are photostimulated from time 0 to 20 minutes (-20 to 0 and 20 to 40 min are pre- and post-stimulation epochs, respectively).

(C) Activation of DRN^{Vgat} terminals in either the BNST (Treatment: $p < 0.001$), DMH (Treatment: $p < 0.0001$), or MPOA (Treatment: $p < 0.01$) significantly suppresses iBAT temperature. Two-way RM ANOVA comparing control and treated groups (n = 5 mice per group). Blue-shaded region highlights Laser On epoch.

(D) Comparison of iBAT temperature suppression at t=20 min for projection-specific photoactivation (20 Hz) of DRN^{Vgat} neurons targeting BNST, DMH, and MPOA. Projection-specific photoactivation significantly suppresses iBAT temperature relative to controls (Treatment: $p < 0.0001$), with no differences observed between treatment groups ($p > 0.05$). One-way ANOVA comparing all groups (n = 5-15 mice per group).

Scale bars, 100 μm. *$p < 0.05$, **$p < 0.01$, ***$p < 0.001$, ****$p < 0.0001$. Data are presented as mean ± SEM. See also Figure S5.

DISCUSSION

In mammals, the central regulation of thermogenesis is essential for survival. Maladaptive changes in energy balance can ultimately lead to the development of debilitating disorders, such as obesity, cardiovascular disease, and type 2 diabetes, making this a critical clinical issue. However, while progress has been made in delineating the CNS pathways that control energy expenditure, our knowledge of the cellular and circuit mechanisms regulating thermogenesis is incomplete. In the current work, we took an unbiased approach to identify populations of neurons that can regulate adaptive thermogenesis, one critical aspect of energy expenditure.

To identify new nodes in the CNS that regulate thermogenesis, we performed unbiased whole-brain activity mapping. We found that DRN^{Vgat} neurons within the dorsolateral aspect of the DRN were activated by increased ambient temperature (Figure 1). Consistent with the observation that DRN^{Vgat} neurons are activated by ambient warmth, we found that activation of DRN^{Vgat} neurons potently suppresses energy expenditure through changes in iBAT thermogenesis and locomotor activity, but notably not peripheral vasodilatation (Figure 2). Notably, inhibition of these neurons augments energy expenditure through increased locomotor activity, but not through changes in iBAT thermogenesis (Figure 3). Together, these data suggest that inhibitory tone originating from DRN^{Vgat} neurons is sufficient to suppress iBAT temperature, but is likely not required for its maintenance.

Building on this work, we sought to better understand the circuit mechanisms through which DRN^{Vgat} neurons regulate thermogenesis. Performing polysynaptic retrograde tracing studies using PRV, we found that these neurons polysynaptically communicate with brown fat (Figure 4). Furthermore, these neurons exhibit unexpectedly vast projection sets, which can both ascend into the forebrain, as well as descend into the hindbrain (Figure 5).

The projection mapping results suggested to us that DRN^{Vgat} neurons might regulate thermogenesis through multiple circuit mechanisms. We first investigated descending projections from DRN^{Vgat} neurons to the brainstem's RPa, a major source of sympathetic outflow to brown fat. Our tracing studies had suggested that DRN^{Vgat} neurons are monosynaptically connected with the RPa, and could thus be one of its targets to regulate iBAT thermogenesis. Through a combination of anatomic and functional approaches, we validated this projection from DRN^{Vgat} neurons to the RPa and found that it is indeed capable of directly suppressing thermogenesis (Figure 6). Notably, DRN^{Vgat} neurons are a lower-order node within the brain as compared to 'warm-sensitive' neurons of the POA, (data not shown), which govern the behavioral and autonomic responses to innocuous increases in ambient temperature (Tan et al., 2016; Tan and Knight, 2018).

Through our anterograde projection mapping studies, we had also demonstrated that DRN^{Vgat} neurons ascend into the forebrain, innervating multiple sites, such as the BNST, DMH, and MPOA. Of note, these projection targets are key nodes embedded within the hunger and/or thermoregulatory circuits. Consistent with these findings, we found that optical activation of these projection targets significantly suppressed thermogenesis, demonstrating that DRN^{Vgat}

neurons likely have multiple redundant circuit mechanisms through which they can regulate energy balance (Figure 7).

While DRN^{Vgat} neurons potently and bidirectionally regulate thermogenesis, and more broadly energy homeostasis, the nature of the internal and external signals that regulate the activity of these neurons is unknown. Retrograde tracing studies from GABAergic neurons within the DRN have identified inputs from numerous nuclei implicated in the central regulation of energy balance, such as the hypothalamus, brainstem, and extended amygdala (Weissbourd et al., 2014); these are nuclei which often appear to have reciprocal interactions with the DRN, suggesting that it is an important node in the extended circuitry regulating energy balance. In further support of this notion, the DRN and bordering vlPAG receive inputs from arcuate nucleus 'hunger neurons' expressing AgRP (Steculorum et al., 2016), as well as from VMPO 'warm-sensitive' neuron expressing BDNF/PACAP (Tan et al., 2016). These anatomic data suggest that the DRN integrates multiple signals related to energy balance to effect changes in the animal's behavior and physiology.

In prior work, we found that DRN^{Vgat} neurons are sensitive to changes in metabolic state and related hormonal signals; these neurons in turn drive potent short- and long-term changes in food intake, resulting in significant shifts in overall energy balance (Nectow et al., 2017b). Consistent with these findings, the current work demonstrates that DRN^{Vgat} neurons can promote feeding specifically through projections to the BNST and DMH, but importantly not the MPOA or RPa. In addition to regulating appetite, these neurons (and their projections to the

aforementioned nuclei) also play a significant role in modulating energy balance through changes in both locomotor activity and thermogenesis.

The observations made in the current work are also consistent with previous results suggesting a role for the DRN in regulating thermogenesis. Earlier electrophysiological studies had demonstrated that subpopulations of DRN neurons are sensitive to both increases in external temperature, as well as to direct (local) heating (Hori and Harada, 1976; Weiss and Aghajanian, 1971). Later studies using pharmacological modulation and electrical stimulation within the DRN were also found to regulate some of the behavioral and physiologic components of energy expenditure, including locomotor activity and thermogenesis (Dib et al., 1994; Hillegaart, 1991; Przewlocka et al., 1979).

While DRN^{Vgat} neurons mediate a number of diverse functions, the extent of this population's heterogeneity is as yet unclear. While we have demonstrated that different subsets of DRN^{Vgat} neurons mediate different effects on energy balance (i.e. food intake, locomotor activity, and thermogenesis) based on their sites of projection, it is unclear whether further heterogeneity exists in terms of their molecular composition (i.e. neurotransmitter and neuromodulator profile). Indeed, molecular profiling of these neurons using viral TRAP revealed that they exhibit marked molecular heterogeneity (Nectow et al., 2017a; Nectow et al., 2017b), and it is still unknown whether the DRN^{Vgat} neurons sensing and responding to changes in ambient warmth are the same as those regulating hunger. Our projection-specific photostimulation studies demonstrating simultaneous effects on food intake and thermogenesis (via projections to BNST and DMH) suggest that there may, indeed, be significant overlap between these subpopulations. Similarly, while

we have shown that these neurons regulate energy balance through both behavioral and autonomic mechanisms, it is as yet unclear which DRN GABAergic cell subtypes are responsible for each of these effects. It will thus be essential in future studies to define the role of specific subpopulations that regulate the different functions known to be controlled by DRN^{Vgat} neurons, including the possible use of projection-specific and activity-dependent profiling approaches (Allen et al., 2017; Ekstrand et al., 2014; Knight et al., 2012; Nectow et al., 2015).

Together, this work demonstrates that DRN^{Vgat} neurons potently regulate energy expenditure, and together with our previous work, suggest that the DRN is a key node in the extended circuit regulating energy homeostasis.

REFERENCES

Ahmari SE, Spellman T, Douglass NL, Kheirbek MA, Simpson HB, Deisseroth K, Gordon JA, Hen R. Repeated cortico-striatal stimulation generates persistent OCD-like behavior. Science. 2013;7;340(6137):1234-9.

Alexander GE, Crutcher MD, DeLong MR. Basal ganglia-thalamocortical circuits: parallel substrates for motor, oculomotor, "prefrontal" and "limbic" functions. *Prog Brain Res.* 1990;85:119-46.

Alkemade A, Forstmann BU. Do we need to revise the tripartite subdivision hypothesis of the human subthalamic nucleus (STN)? Neuroimage. 2014 Jul 15;95:326-9.

Allen, W.E., DeNardo, L.A., Chen, M.Z., Liu, C.D., Loh, K.M., Fenno, L.E., Ramakrishnan, C., Deisseroth, K., and Luo, L. (2017). Thirst-associated preoptic neurons encode an aversive motivational drive. Science 357, 1149-1155.

American Psychiatric Association: Practice Guideline for the Treatment of Patients with Major Depressive Disorder, Third Edition, 2010. http://psychiatryonline.org/guidelines.aspx

An, J.J., Liao, G.Y., Kinney, C.E., Sahibzada, N., and Xu, B. (2015). Discrete BDNF Neurons in the Paraventricular Hypothalamus Control Feeding and Energy Expenditure. Cell metabolism 22, 175-188.

Bailey ME, Albrecht BE, Johnson KJ, Darlison MG (1999). "Genetic linkage and radiation hybrid mapping of the three human GABA(C) receptor rho subunit genes: GABRR1, GABRR2 and GABRR3". *Biochim. Biophys. Acta*. **1447** (2–3): 307–312.

Baunez C, Dias C, Cador M, Amalric M. The subthalamic nucleus exerts opposite control on cocaine and 'natural' rewards. Nat Neurosci. 2005 Apr;8(4):484-9.

Bejjani BP, Damier P, Arnulf I, Thivard L, Bonnet AM, Dormont D *et al.* Transient acute depression induced by high-frequency deep-brain stimulation. N Engl J Med. 1999 May 13;340(19):1476-80.

Benabid AL. Deep brain stimulation for Parkinson's disease. Curr Opin Neurobiol. 2003 Dec;13(6):696-706.

Benarroch EE. Subthalamic nucleus and its connections: Anatomic substrate for the network effects of deep brain stimulation. Neurology. 2008 May 20;70(21):1991-5.

Benazzouz A, Gross C, Féger J, Boraud T, Bioulac B. Reversal of rigidity and improvement in motor performance by subthalamic high-frequency stimulation in MPTP-treated monkeys. Eur J Neurosci. 1993 Apr 1;5(4):382-9.

Blomstedt P, Sjöberg RL, Hansson M, Bodlund O, Hariz MI. Deep brain stimulation in the treatment of obsessive-compulsive disorder. World Neurosurg. 2013 Dec;80(6):e245-53.

Bormann J. The 'ABC' of GABA Receptors. Trends Pharmacol Sci. 2000 Jan;21(1):16-9.

Bourne SK, Eckhardt CA, Sheth SA, Eskandar EN. Mechanisms of deep brain stimulation for obsessive compulsive disorder: effects upon cells and circuits. Front Integr Neurosci. 2012 Jun 14;6:29.

Boyden ES, Zhang F, Bamberg E, Nagel G, Deisseroth K. Millisecond-timescale, genetically targeted optical control of neural activity. Nat Neurosci. 2005 Sep;8(9):1263-8.

Breysse E, Pelloux Y, Baunez C. The Good and Bad Differentially Encoded within the Subthalamic Nucleus in Rats. eNeuro. 2015 Oct 15;2(5).

Camilla d'Angelo LS, Eagle DM, Grant JE, Fineberg NA, Robbins TW, Chamberlain SR. Animal models of obsessive-compulsive spectrum disorders. CNS Spectr. 2014 Feb;19(1):28-49.

Cannon, B., and Nedergaard, J. (2004). Brown adipose tissue: function and physiological significance. Physiological reviews 84, 277-359.

Castrioto A, Lhommée E, Moro E, Krack P (2014) Mood and behavioural effects of subthalamic stimulation in Parkinson’s disease. Lancet Neurol 13:287–305.

Cavanagh, J. F. *et al.* Subthalamic nucleus stimulation reverses mediofrontal influence over decision threshold. *Nat. Neurosci.* **14,** 1462–7 (2011).

Chang AD, Berges VA, Chung SJ, Fridman GY, Baraban JM, Reti IM. High-Frequency Stimulation at the Subthalamic Nucleus Suppresses Excessive Self-Grooming in Autism-Like Mouse Models. Neuropsychopharmacology. 2016 Jun;41(7):1813-21.

Chassain C, Melon C, Salin P, Vitale F, Couraud S, Durif F *et al*. Metabolic, synaptic and behavioral impact of 5-week chronic deep brain stimulation in hemiparkinsonian rats. J Neurochem. 2016 Mar;136(5):1004-16.

de Koning PP, Figee M, van den Munckhof P, Schuurman PR, Denys D. Current status of deep brain stimulation for obsessive-compulsive disorder: a clinical review of different targets. Curr Psychiatry Rep. 2011 Aug;13(4):274-82.

DeLong MR, Alexander GE, Georgopoulos AP, Crutcher MD, Mitchell SJ, Richardson RT. Role of basal ganglia in limb movements. Hum Neurobiol. 1984;2(4):235-44.

Dib, B., Rompre, P.P., Amir, S., and Shizgal, P. (1994). Thermogenesis in brown adipose tissue is activated by electrical stimulation of the rat dorsal raphe nucleus. Brain research 650, 149-152.

Dvorzhak A, Gertler C, Harnack D, Grantyn R. High frequency stimulation of the subthalamic nucleus leads to presynaptic GABA(B)-dependent depression of subthalamo-nigral afferents. PLoS One. 2013 Dec 23;8(12):e82191.

Ekstrand, M.I., Nectow, A.R., Knight, Z.A., Latcha, K.N., Pomeranz, L.E., and Friedman, J.M. (2014). Molecular profiling of neurons based on connectivity. Cell 157, 1230-1242.

Fife KH, Gutierrez-Reed NA, Zell V, Bailly J, Lewis CM, Aron *AR et al. Causal* role for the subthalamic nucleus in interrupting behavior. Elife. 2017 Jul 25;6. pii: e27689.

Follett KA, Weaver FM, Stern M, Hur K, Harris CL, Luo P, *et al.* Pallidal versus subthalamic deep-brain stimulation for Parkinson's disease. N Engl J Med. 2010 Jun 3;362(22):2077-91.

Frank, M., Samanta, J., Moustafa, A. & Sherman, S. Hold Your Horses: Impulsivity, Deep Brain Stimulation, and Medication in Parkinsonism. *Science (80-.).* **1309,** (2007).

Garfield, A.S., Shah, B.P., Burgess, C.R., Li, M.M., Li, C., Steger, J.S., Madara, J.C., Campbell, J.N., Kroeger, D., Scammell, T.E., et al. (2016). Dynamic GABAergic afferent modulation of AgRP neurons. Nature neuroscience 19, 1628-1635.

GENSAT - The Gene Expression Nervous System Atlas Project, NINDS Contracts N01NS02331 & HHSN271200723701C to The Rockefeller University (New York, NY). (GENSAT.org)

Gradinaru V, Mogri M, Thompson KR, Henderson JM, Deisseroth K. Optical deconstruction of parkinsonian neural circuitry. Science. 2009;324(5925):354-9.

Grillner S, Robertson B. The Basal Ganglia Over 500 Million Years. Curr Biol. 2016 Oct 24;26(20):R1088-R1100.

Griscavage, Wilk and Ignarro. (1996) Inhibitors of the proteasome pathway interfere with induction of nitric oxide synthase in macrophages by blocking activation of nuclear factor-kappa B. Proc. Natl. Acad. Sci. USA 93:3308–3312.

Gruetter CA, Barry BK, McNamara DB, Gruetter DY, Kadowitz PJ and Ignarro LJ. Relaxation of bovine coronary artery and activation of coronary arterial guanylate cyclase by nitric oxide, nitroprusside and a carcinogenic nitrosoamine. (1979) J. Cyclic Nucl. Res. 5: 211–224.

Hälbig TD, Tse W, Frisina PG, Baker BR, Hollander E, Shapiro H et al. Subthalamic deep brain stimulation and impulse control in Parkinson's disease. Eur J Neurol. 2009 Apr;16(4):493-7.

Heida T, Marani E, Usunoff KG. (2001). The Subthalamic Nucleus. Part II: Modelling and Simulation of Activity. Springer-Verlag, Berlin Heidelberg (Germany), 2008, pp14-30.

Hemingway, A., Forgrave, P., and Birzis, L. (1954). Shivering Suppression by Hypothalamic Stimulation. Journal of neurophysiology 17, 375-386.

Hillegaart, V. (1991). Effects of local application of 5-HT and 8-OH-DPAT into the dorsal and median raphe nuclei on core temperature in the rat. Psychopharmacology (Berl) 103, 291-296.

Hirtz D, Thurman DJ, Gwinn-Hardy K, Mohamed M, Chaudhuri AR, Zalutsky R. How common are the “common” neurologic disorders? (2007). *Neurology* 68(5): 326-337.

Hori, T., and Harada, Y. (1976). Responses of Midbrain raphe neurons to local temperature. Pflugers Arch 364, 205-207.

Kalueff AV, Stewart AM, Song C, Berridge KC, Graybiel AM, Fentress JC. Neurobiology of rodent self-grooming and its value for translational neuroscience. Nat Rev Neurosci. 2016 Jan;17(1):45-59.

Kandel, E. R., Schwartz, J. H., & Jessell, T. M. (2000). *Principles of neural science*. New York: McGraw-Hill, Health Professions Division.

Karachi C, Grabli D, Baup N, Mounayar S, Tandé D, François C *et al*. Dysfunction of the subthalamic nucleus induces behavioral and movement disorders in monkeys. Mov Disord. 2009;24(8):1183-92.

Karachi C, Yelnik J, Tandé D, Tremblay L, Hirsch EC, François C. The pallidosubthalamic projection: an anatomical substrate for nonmotor functions of the subthalamic nucleus in primates. (2005) Mov Disord. 20(2):172-80.

Kita H, Kitai ST. Efferent projections of the subthalamic nucleus in the rat: light and electron microscopic analysis with the PHA-L method. J Comp Neurol. 1987 Jun 15;260(3):435-52.

Kitai ST, Kita H. Anatomy and physiology of the subthalamic nucleus: a driving force of the basal ganglia. In: Carpenter MB, Jayaraman A, editors. The basal ganglia II-Structure and function: current concepts. Advances in behavioral biology. New York: Plenum Press; 1987. p 357–373.

Klavir O, Flash S, Winter C, Joel D. High frequency stimulation and pharmacological inactivation of the subthalamic nucleus reduces 'compulsive' lever-pressing in rats. Exp Neurol. 2009 Jan;215(1):101-9.

Knight, Z.A., Tan, K., Birsoy, K., Schmidt, S., Garrison, J.L., Wysocki, R.W., Emiliano, A., Ekstrand, M.I., and Friedman, J.M. (2012). Molecular profiling of activated neurons by phosphorylated ribosome capture. Cell 151, 1126-1137.

Kravitz AV, Freeze BS, Parker PR, Kay K, Thwin MT, Deisseroth K, Kreitzer AC. Regulation of parkinsonian motor behaviours by optogenetic control of basal ganglia circuitry. Nature. 2010 Jul 29;466(7306):622-6.

Kringelbach ML, Jenkinson N, Owen SL, Aziz TZ. Translational principles of deep brain stimulation. (2007). Nat Rev Neurosci. 8(8):623-35.

Kuang XL, Zhao XM, Xu HF, Shi YY, Deng JB, Sun GT. Spatio-temporal expression of a novel neuron-derived neurotrophic factor (NDNF) in mouse brains during development. BMC Neurosci. 2010 Oct 25;11:137.

Lambert, C., Zrinzo, L., Nagy, Z., Lutti, A. & Hariz, M. Confirmation of functional zones within the human subthalamic nucleus: Patterns of connectivity and sub-parcellation using diffusion weighted imaging. *Neuroimage* **60,** 83–94 (2012).

Lanciego JL, Luquin N, Obeso JA. Functional Neuroanatomy of the Basal Ganglia. *Cold Spring Harb Perspect Med*. 2012 Dec; 2(12): a009621

Leckman JF. Tourette's syndrome. Lancet. 2002 Nov 16;360(9345):1577-86.

Lein ES, Hawrylycz MJ, Ao N, Ayres M, Bensinger A, Bernard A *et al.* Genome-wide atlas of gene expression in the adult mouse brain. Nature. 2007 Jan 11;445(7124):168-76. (celltypes.brain-map.org)

Lévesque, J.-C. & Parent, A. GABAergic interneurons in human subthalamic nucleus. Mov. Disord. 20, 574–84 (2005).

Madisen, L., Zwingman, T.A., Sunkin, S.M., Oh, S.W., Zariwala, H.A., Gu, H., Ng, L.L., Palmiter, R.D., Hawrylycz, M.J., Jones, A.R., et al. (2010). A robust and high-throughput Cre reporting and characterization system for the whole mouse brain. Nature neuroscience 13, 133-140.

Magoun, H.W., Harrison, F., Brobeck, J.R., and Ranson, S.W. (1938). Activation of heat loss mechanisms by local heating of the brain. Journal of neurophysiology 1, 101-114.

Mallet L, Polosan M, Jaafari N, Baup N, Welter ML, Fontaine D, *et al.* Subthalamic nucleus stimulation in severe obsessive-compulsive disorder. N Engl J Med. 2008 Nov 13;359(20):2121-34.

Mallet L, Schüpbach M, N'Diaye K, Remy P, Bardinet E, Czernecki V, *et al*. Stimulation of subterritories of the subthalamic nucleus reveals its role in the integration of the emotional and motor aspects of behavior. PNAS USA 2007;104(25):10661-6

Marani E, Heida T, Lakke EAJF, Usunoff KG. (2001). The Subthalamic Nucleus. Part I: Development, Cytology, Topography and Connections. Springer-Verlag, Berlin Heidelberg (Germany), 2008, pp14-30.

Martin DM, Skidmore JM, Philips ST, Vieira C, Gage PJ, Condie BG *et al.* PITX2 is required for normal development of neurons in the mouse subthalamic nucleus and midbrain. Dev Biol. 2004 Mar 1;267(1):93-108.

Martínez-Delgado G, Estrada-Mondragón A, Miledi R, Martínez-Torres A. An Update on GABAρ Receptors. Curr Neuropharmacol. 2010 Dec;8(4):422-33.

Milad MR, Rauch SL. Obsessive-compulsive disorder: beyond segregated cortico-striatal pathways. (2012). *Trends Cogn Sci.* 16(1):43-51.

Morrison, S.F., and Nakamura, K. (2011). Central neural pathways for thermoregulation. Front Biosci (Landmark Ed) 16, 74-104.

Munzberg, H., Qualls-Creekmore, E., Berthoud, H.R., Morrison, C.D., and Yu, S. (2016). Neural Control of Energy Expenditure. Handbook of experimental pharmacology 233, 173-194.

Nambu, a, Takada, M., Inase, M. & Tokuno, H. Dual somatotopical representations in the primate subthalamic nucleus: evidence for ordered but reversed body-map transformations from the primary motor cortex and the supplementary motor area. *J. Neurosci.* **16,** 2671–83 (1996).

Nambu, A. A new dynamic model of the cortico-basal ganglia loop. *Prog. Brain Res.* **143,** 461–6 (2004)

Nambu, A., Tokuno, H. & Takada, M. Functional significance of the cortico-subthalamo-pallidal “hyperdirect” pathway. *Neurosci. Res.* **43,** 111–7 (2002).

Nectow, A.R., Ekstrand, M.I., and Friedman, J.M. (2015). Molecular characterization of neuronal cell types based on patterns of projection with Retro-TRAP. Nature protocols 10, 1319-1327.

Nectow, A.R., Moya, M.V., Ekstrand, M.I., Mousa, A., McGuire, K.L., Sferrazza, C.E., Field, B.C., Rabinowitz, G.S., Sawicka, K., Liang, Y., et al. (2017a). Rapid Molecular Profiling of Defined Cell Types Using Viral TRAP. Cell reports 19, 655-667.

Nectow, A.R., Schneeberger, M., Zhang, H., Field, B.C., Renier, N., Azevedo, E., Patel, B., Liang, Y., Mitra, S., Tessier-Lavigne, M., et al. (2017b). Identification of a Brainstem Circuit Controlling Feeding. Cell 170, 429-442 e411.

Nelson AB, Kreitzer AC. Reassessing models of basal ganglia function and dysfunction. Annu Rev Neurosci. 2014;37:117-35.

Nicoletti A, Luca A, Raciti L, Contrafatto D, Bruno E, Dibilio V, Sciacca G, Mostile G, Petralia A, Zappia M. Obsessive compulsive personality disorder and Parkinson's disease. (2013). *PLoS ONE* 8(1):e54822.

Odekerken VJ, van Laar T, Staal MJ, Mosch A, Hoffmann CF, Nijssen PC, *et al.* Subthalamic nucleus versus globus pallidus bilateral deep brain stimulation for advanced Parkinson's disease (NSTAPS study): a randomised controlled trial. Lancet Neurol. 2013 Jan;12(1):37-44.

Parent, A. & Hazrati, L. Functional anatomy of the basal ganglia. I. The cortico-basal ganglia-thalamo-corticalloop Andre. *Brain Res. Rev.* **20,** 91–127 (1995).

Patel NK, Heywood P, O'Sullivan K, McCarter R, Love S, Gill SS. Unilateral subthalamotomy in the treatment of Parkinson's disease. Brain. 2003 May;126(Pt 5):1136-45.

Paul DL, Abramovitch A, Rauch SL, Geller DA. Obsessive-compulsive disorder: an integrative genetic and neurobiological perspective. Nat Rev Neurosci. 2014 Jun;15(6):410-24.

Pomeranz, L.E., Ekstrand, M.I., Latcha, K.N., Smith, G.A., Enquist, L.W., and Friedman, J.M. (2017). Gene expression profiling with Cre-conditional pseudorabies virus reveals a subset of midbrain neurons that participate in reward circuitry. The Journal of neuroscience : the official journal of the Society for Neuroscience.

Pringsheim T, Jette N, Frolkis A, Steeves TD. The prevalence of Parkinson's disease: a systematic review and meta-analysis. Mov Disord. 2014 Nov;29(13):1583-90.

Przewlocka, B., Stala, L., and Scheel-Kruger, J. (1979). Evidence that GABA in the nucleus dorsalis raphe induces stimulation of locomotor activity and eating behavior. Life Sci 25, 937-945.

Rafols J, Fox C. The neurons in the primate subthalamic nucleus: a Golgi and electron microscopic study. *J. Comp. Neurol.* (1976). at

Rajfer, Aronson, Bush, Dorey and Ignarro. (1992) Nitric oxide as a mediator of relaxation of the corpus cavernosum in response to nonadrenergic, noncholinergic neurotransmission. N. Engl. J. Med. 326: 90–94.

Rappel P, Marmor O, Bick AS, Arkadir D, Linetsky E, Castrioto A *et al.* Subthalamic theta activity: a novel human subcortical biomarker for obsessive compulsive disorder. Transl Psychiatry. 2018 Jun 18;8(1):118.

Ren, J., Friedmann, D., Xiong, J., Liu, C.D., Ferguson, B.R., Weerakkody, T., DeLoach, K.E., Ran, C., Pun, A., Sun, Y., et al. (2018). Anatomically Defined and Functionally Distinct Dorsal Raphe Serotonin Sub-systems. Cell 175, 472-487 e420.

Renier N, Wu Z, Simon DJ, Yang J, Ariel P, Tessier-Lavigne M. iDISCO: a simple, rapid method to immunolabel large tissue samples for volume imaging. Cell. 2014;159(4):896-910.

Renier, N., Adams, E.L., Kirst, C., Wu, Z., Azevedo, R., Kohl, J., Autry, A.E., Kadiri, L., Umadevi Venkataraju, K., Zhou, Y., et al. (2016). Mapping of Brain Activity by Automated Volume Analysis of Immediate Early Genes. Cell 165, 1789-1802.

Ring HA, Serra-Mestres J. Neuropsychiatry of the basal ganglia. J Neurol Neurosurg Psychiatry. 2002 Jan;72(1):12-21.

Robbins TW, Vaghi MM, Banca P. Obsessive-Compulsive Disorder: Puzzles and Prospects. Neuron. 2019 Apr 3;102(1):27-47.

Ruscio AM, Stein DJ, Chiu WT, Kessler RC. The epidemiology of obsessive-compulsive disorder in the National Comorbidity Survey Replication. Mol Psychiatry. 2010 Jan;15(1):53-63.

Ryu, V., Garretson, J.T., Liu, Y., Vaughan, C.H., and Bartness, T.J. (2015). Brown adipose tissue has sympathetic-sensory feedback circuits. The Journal of neuroscience : the official journal of the Society for Neuroscience 35, 2181-2190.

Saltzman, E., and Roberts, S.B. (1995). The role of energy expenditure in energy regulation: findings from a decade of research. Nutr Rev 53, 209-220.

Schweizer N, Pupe S, Arvidsson E, Nordenankar K, Smith-Anttila CJ, Mahmoudi S *et al.* Limiting glutamate transmission in a Vglut2-expressing subpopulation of the subthalamic nucleus is sufficient to cause hyperlocomotion. Proc Natl Acad Sci U S A. 2014 May 27;111(21):7837-42.

Schweizer N, Viereckel T, Smith-Anttila CJ, Nordenankar K, Arvidsson E, Mahmoudi S *et al.* Reduced Vglut2/Slc17a6 Gene Expression Levels throughout the Mouse Subthalamic Nucleus Cause Cell Loss and Structural Disorganization Followed by Increased Motor Activity and Decreased Sugar Consumption. eNeuro. 2016 Sep 29;3(5).

Smeding HM, Speelman JD, Koning-Haanstra M, Schuurman PR, Nijssen P, van Laar T *et al*. Neuropsychological effects of bilateral STN stimulation in Parkinson disease: a controlled study. Neurology. 2006 Jun 27;66(12):1830-6.

Smith, B.N., Banfield, B.W., Smeraski, C.A., Wilcox, C.L., Dudek, F.E., Enquist, L.W., and Pickard, G.E. (2000). Pseudorabies virus expressing enhanced green fluorescent protein: A tool for in vitro electrophysiological analysis of transsynaptically labeled neurons in identified central nervous system circuits.

Proceedings of the National Academy of Sciences of the United States of America 97, 9264-9269.

Steculorum, S.M., Ruud, J., Karakasilioti, I., Backes, H., Engstrom Ruud, L., Timper, K., Hess, M.E., Tsaousidou, E., Mauer, J., Vogt, M.C., et al. (2016). AgRP Neurons Control Systemic Insulin Sensitivity via Myostatin Expression in Brown Adipose Tissue. Cell 165, 125-138.

Stephenson-Jones M, Yu K, Ahrens S, Tucciarone JM, van Huijstee AN, Mejia LA *et alx*. A basal ganglia circuit for evaluating action outcomes. Nature. 2016 Nov 10;539(7628):289-293.

Tai CH, Boraud T, Bezard E, Bioulac B, Gross C, Benazzouz A. Electrophysiological and metabolic evidence that high-frequency stimulation of the subthalamic nucleus bridles neuronal activity in the subthalamic nucleus and the substantia nigra reticulata. FASEB J. 2003 Oct;17(13):1820-30.

Tan, C.L., and Knight, Z.A. (2018). Regulation of Body Temperature by the Nervous System. Neuron 98, 31-48.

Tan, C.L., Cooke, E.K., Leib, D.E., Lin, Y.C., Daly, G.E., Zimmerman, C.A., and Knight, Z.A. (2016). Warm-Sensitive Neurons that Control Body Temperature. Cell 167, 47-59 e15.

Ungerstedt U, Arbuthnott GW (1970) Quantitative recording of rotational behaviour in rats after 6-hydroxydopamine lesions of the nigrostriatal dopamine system. Brain Res 24, 485–493.

Uslaner JM, Robinson TE. Subthalamic nucleus lesions increase impulsive action and decrease impulsive choice - mediation by enhanced incentive motivation? Eur J Neurosci. 2006 Oct;24(8):2345-54.

Veasey, S.C., Fornal, C.A., Metzler, C.W., and Jacobs, B.L. (1997). Single-unit responses of serotonergic dorsal raphe neurons to specific motor challenges in freely moving cats. Neuroscience 79, 161-169.

Vertes, R.P. (1991). A PHA-L analysis of ascending projections of the dorsal raphe nucleus in the rat. The Journal of comparative neurology 313, 643-668.

Vertes, R.P., and Kocsis, B. (1994). Projections of the dorsal raphe nucleus to the brainstem: PHA-L analysis in the rat. The Journal of comparative neurology 340, 11-26.

Voon V, Pessiglione M, Brezing C, Gallea C, Fernandez HH, Dolan RJ, Hallett M. Mechanisms underlying dopamine-mediated reward bias in compulsive behaviors. (2010). *Neuron* 65(1):135-42.

Wan Y, Ade KK, Caffall Z, Ilcim Ozlu M, Eroglu C, Feng G *et al.* Circuit-selective striatal synaptic dysfunction in the Sapap3 knockout mouse model of obsessive-compulsive disorder. Biol Psychiatry. 2014 Apr 15;75(8):623-30.

Warden, M.R., Selimbeyoglu, A., Mirzabekov, J.J., Lo, M., Thompson, K.R., Kim, S.Y., Adhikari, A., Tye, K.M., Frank, L.M., and Deisseroth, K. (2012). A prefrontal cortex-brainstem neuronal projection that controls response to behavioural challenge. Nature 492, 428-432.

Waterhouse, B.D., Devilbiss, D., Seiple, S., and Markowitz, R. (2004). Sensorimotor-related discharge of simultaneously recorded, single neurons in the dorsal raphe nucleus of the awake, unrestrained rat. Brain research 1000, 183-191.

Waterson, M.J., and Horvath, T.L. (2015). Neuronal Regulation of Energy Homeostasis: Beyond the Hypothalamus and Feeding. Cell metabolism 22, 962-970.

Weiss, B.L., and Aghajanian, G.K. (1971). Activation of Brain Serotonin Metabolism by Heat - Role of Midbrain Raphe Neurons. Brain research 26, 37-+.

Weissbourd, B., Ren, J., DeLoach, K.E., Guenthner, C.J., Miyamichi, K., and Luo, L. (2014). Presynaptic partners of dorsal raphe serotonergic and GABAergic neurons. Neuron 83, 645-662.

Welch JM, Lu J, Rodriguiz RM, Trotta NC, Peca J, Ding JD, Feliciano C, Chen M, Adams JP, Luo J, Dudek SM, Weinberg RJ, Calakos N, Wetsel WC, Feng G. Cortico-striatal synaptic defects and OCD-like behaviours in Sapap3-mutant mice. Nature. 2007;448(7156):894-900.

Welter ML, Burbaud P, Fernandez-Vidal S, Bardinet E, Coste J, Piallat B *et al.* Basal ganglia dysfunction in OCD: subthalamic neuronal activity correlates with symptoms severity and predicts high-frequency stimulation efficacy. Transl Psychiatry. 2011 May 3;1:e5.

Welter ML, Schüpbach M, Czernecki V, Karachi C, Fernandez-Vidal S, Golmard JL *et al*. Optimal target localization for subthalamic stimulation in patients with Parkinson disease. Neurology. 2014 Apr 15;82(15):1352-61.

Winstanley CA, Baunez C, Theobald DE, Robbins TW. Lesions to the subthalamic nucleus decrease impulsive choice but impair autoshaping in rats: the importance of the basal ganglia in Pavlovian conditioning and impulse control. Eur J Neurosci. 2005 Jun;21(11):3107-16.

Yahiro, T., Kataoka, N., Nakamura, Y., and Nakamura, K. (2017). The lateral parabrachial nucleus, but not the thalamus, mediates thermosensory pathways for behavioural thermoregulation. Sci Rep 7, 5031.

Yelnik J, Bardinet E, Dormont D, Malandain G, Ourselin S, Tandé D, Karachi C, Ayache N, Cornu P, Agid Y. A three-dimensional, histological and deformable atlas of the human basal ganglia. I. Atlas construction based on immunohistochemical and MRI data. Neuroimage. 2007 Jan 15;34(2):618-38.

Yelnik J, Percheron G. Subthalamic neurons in primates: a quantitative and comparative analysis. Neuroscience 4, 1717–43 (1979).

Yelnik J. Functional anatomy of the basal ganglia. Mov Disord. 2002;17 Suppl 3:S15-21.

Zhang X, van den Pol AN. Rapid binge-like eating and body weight gain driven by zona incerta GABA neuron activation. Science. 2017 May 26;356(6340):853-859.

Zhao, Z.D., Yang, W.Z., Gao, C., Fu, X., Zhang, W., Zhou, Q., Chen, W., Ni, X., Lin, J.K., Yang, J., et al. (2017). A hypothalamic circuit that controls body temperature. Proceedings of the National Academy of Sciences of the United States of America.